Reformed Methanol Fuel Cell Systems - and their use in Electric Hybrid Systems

Justesen, Kristian Kjær

Publication date:
2015

Document Version
Publisher's PDF, also known as Version of record

Reformed Methanol Fuel Cell Systems

- and their use in Electric Hybrid Systems

PhD Dissertation

Kristian Kjær Justesen

Dissertation submitted August , 2015

Thesis submitted: August, 2015

PhD Supervisor: Associate Prof. Søren Juhl Andreasen, Aalborg University

PhD Committee: Prof. Daniel Hissel, University of Franche-Comté

Thomas Steenberg, Technical Director, Danish Power Systems ApS

Associate Prof. Henrik Clemmensen Pedersen, Aalborg University

PhD Series: Faculty of Engineering and Science, Aalborg University

ISSN: 2246-1248
ISBN: 978-87-92846-72-3

Published by:
Department of Energy Technology
Pontoppidanstræde 101
DK - 9220 Aalborg East

Printed in Denmark by Uniprint, 2016

Curriculum Vitae

Kristian Kjær Justesen
PhD student - Aalborg University, Department of Energy Technology

Age: 29
e-mail: kkjustes@gmail.com
tel: +45 2963 5660

Education

- **August 2012 – August 2015 Aalborg University, Denmark**
  PhD Student at the Department of Energy Technology at Aalborg University.

- **September 2010 - June 2012 Aalborg University, Denmark**
  Master of Science (M.Sc.), Energy Engineering specializing in Mechatronic Control Engineering.

- **September 2007 – June 2010 Aalborg University, Denmark**
  Bachelor of Science (B.Sc.), Energy Engineering specializing in Mechatronic Control Engineering.

- **2003 – 2006 Silkeborg HTX, Technical College**

Awards and honours

- **Carisma III 2012 2nd Poster Prize**
  Awarded at the Carisma 2012 International Conference in September 2012 in Copenhagen. The award was won with the coauthors John Andersen, Mikkel P. Ehmsen, Søren J. Andreasen, Hamid R. Shaker and Simon L. Sahlin.

- **1st Prize for excellent and innovative project work**
  Awarded by the Energy Sponsor Programme at the Department of Energy Technology, Aalborg University in June 2012 for the best master thesis at the department that year.

- **Best Poster Paper award at the Fuel Cells 2012 Science and Technology Conference in Berlin**
  Together with John Andersen, Mikkel P. Ehmsen, Søren J. Andreasen, Hamid R. Shaker and Simon L. Sahlin.

Publications

- Kristian Kjær Justesen, Søren Juhl Andreasen, Hamid Reza Shaker, Mikkel Præstholm Ehmsen, John Andersen. "Gas composition modeling in a reformed Methanol Fuel Cell system using adaptive Neuro-Fuzzy Inference Systems" published in the *International Journal of Hydrogen Energy* Vol. 38, pp. 10577–10584, 2013.

- Kristian Kjær Justesen, Søren Juhl Andreasen, Hamid Reza Shaker. "Dynamic Modeling of a Reformed Methanol Fuel Cell System Using Empirical Data and Adaptive Neuro-Fuzzy Inference System Models" published in the *Journal of Fuel Cell Science and Technology* Vol. 11, pp. 021004-1–021004-8, 2014.

- Kristian Kjær Justesen, Søren Juhl Andreasen. "Determination of Optimal Reformer Temperature in a Reformed Methanol Fuel Cell System using ANFIS Models and Numerical Optimization Methods" The paper in press in the *International Journal of Hydrogen Energy* Vol 40, pp. 9505–9514, 2015.

Thesis Details

Thesis Title:	Reformed Methanol Fuel Cell Systems: and their use in Electric Hybrid Systems
PhD Student:	Kristian Kjær Justesen
Supervisors:	Assoc. Prof. Søren Juhl Andreasen, Aalborg University

The main body of this thesis consists of the following papers.

[A] Kristian Kjær Justesen, Søren Juhl Andreasen, Hamid Reza Shaker, Mikkel Præstholm Ehmsen, John Andersen, "Gas composition modeling in a reformed Methanol Fuel Cell system using adaptive Neuro-Fuzzy Inference Systems," *International Journal of Hydrogen Energy*, vol. 38, pp. 10577–10584, 2013.

[B] Kristian Kjær Justesen, Søren Juhl Andreasen, Hamid Reza Shaker, "Dynamic Modeling of a Reformed Methanol Fuel Cell System Using Empirical Data and Adaptive Neuro-Fuzzy Inference System Models," *Journal of Fuel Cell Science and Technology*, vol. 11, pp. 021004-1–021004-8, 2014.

[C] Kristian Kjær Justesen, Søren Juhl Andreasen, Dr. Sivakumar Pasupathi, Bruno Pollet, "Modeling and control of the output current of a Reformed Methanol Fuel Cell system," submitted to *International Journal of Hydrogen Energy*, vol. 11, pp. 021004-1–021004-8, 2014.

[D] Kristian Kjær Justesen, Søren Juhl Andreasen, Simon Lennart Sahlin, "Modeling of a HTPEM Fuel Cell using Adaptive Neuro-Fuzzy Inference Systems," submitted to *Special section CARISMA2014, International Journal of Hydrogen Energy*

[E] Kristian Kjær Justesen, Søren Juhl Andreasen, "Determination of Optimal Reformer Temperature in a Reformed Methanol Fuel Cell System using ANFIS Models and Numerical Optimization Methods," *International Journal of Hydrogen Energy*

Paper [B] was first published in the Proceedings of the ASME 2013 11th Fuel Cell Science, Engineering and Technology Conference, FuelCell2013, July 14-19, 2013, Minneapolis, MN, USA. where it was also presented. It was later accepted for publication in the Journal of Fuel Cell Science and Technology after a second peer review.

In addition to the main papers, the PhD Student has been a co-author of chapter 21 of the following book:

- Qingfeng Li, David Aili, Hans Aage Hjuler, Jens Oluf Jensen, "High Temperature Polymer Electrolyte Membrane Fuel Cells, Approaches, Status, and Perspectives" to be published by: *Springer International Publishing* on the 14th of September 2015

In addition to the main papers, the following posters have also been presented at conferences:

[A] Kristian K. Justesen, John Andersen, Mikkel P. Ehmsen, Søren J. Andreasen, Hamid R. Shaker and Simon L. Sahlin, "Control of a methanol reformer system using an Adaptive Neuro-Fuzzy Inference System approach," presented at the *Carisma 2012 Conference* in Copenhagen, Denmark

[B] Kristian Kjær Justesen, "Initial Performance Analysis of a Methanol Steam Reformer," presented at the *European Technical School on Hydrogen and Fuel Cells 2014* in Rethymnon, Greece

[C] Kristian Kjær Justesen, Søren Juhl Andreasen, Simon Lennart Sahlin, "Modeling of a HTPEM Fuel Cell using Adaptive Neuro-Fuzzy Inference Systems," presented at the *Carisma 2014 Conference* in Cape Town, South Africa

This present report combined with the above listed scientific papers has been submitted for assessment in partial fulfilment of the PhD degree. The scientific papers are not included in this version due to copyright issues. Detailed publication information is provided above and the interested reader is referred to the original published papers. As part of the assessment, co-author statements have been made available to the assessment committee and are also available at the Faculty of Engineering and Science, Aalborg University.

Abstract

PEM fuel cells are widely regarded as a promising technology which has the potential to replace more polluting and less efficient internal combustion engines in many applications. They do, however, have the drawback that their hydrogen fuel is cumbersome and energy consuming to store and transport. Alternative system topologies that use a liquid fuel is therefore of great interest. One such topology is the Reformed Methanol Fuel Cell (RMFC) system where a mixture of liquid methanol and water is reformed via the steam reformation process to hydrogen and carbon dioxide. Most of the hydrogen is then used in a fuel cell and the rest is passed to a catalytic burner which supplies the process heat for the reformer. This makes RMFCs complex systems where the different parts of the system affect each other and it makes demands on the way they are integrated with the loads they supply. This PhD study has therefore been concerned with the module's integration in a practical application and the optimization of the operating parameters of the system based on models of the system components.

The chosen application is a street sweeping machine which is a good case because they often operate in fleets with long periods of operation. Both of which are beneficial for the integration of RMFC systems. To analyze if the integration of an RMFC system is a good idea, a dynamic model of a street sweeping machine including approximate models of a battery and a RMFC system is produced. This model, along with a defined drive cycle, is then used in the context of the Outdoor Reliable Application using CLean Energy (ORACLE) project to predict the performance of a RMFC powered street sweeping machine before a prototype is made. After the prototype has been manufactured, the model is updated based on measurements and the performance of the vehicle is reanalyzed. It is concluded that the vehicle can operate for a full 8-hour working day without discharging the drive battery, if the vehicle is fitted with a 10 $[kW]$ RMFC system. In this case 62.13 $[L]$ of methanol is used if the standard hysteresis method is used to control the state of charge (SOC) of the battery. An analysis of the power through the drivetrain shows that most of the energy loss occurs in the RMFC system and that this loss could be minimized if a more constant lower power set point is used for the fuel cell. To achieve this, a SOC control is developed that minimizes fluctuations in the output power of the RMFC system. When this is done, the fuel consumption drops to 46.85 $[L]$, which is a reduction of 24.6%.
It is further concluded that if the power consumption is minimized further it is realistic to reduce the RMFC power to 5 $[kW]$ and the fuel consumption to 42.08 $[L]$.

To be able to achieve the efficiency gain observed in the vehicle model, it

is necessary to develop a controller that can control the output current of the RMFC system instead of the fuel cell current which is the standard procedure. To be able to do this, a model of the output current of an RMFC system is produced. This includes approximate models of the dynamics of the fuel cell and battery as well as the power consumption of the Balance Of Plant (BOP) consumers. The models are fitted on the basis of experiments and used to develop a PI controller with feedforward and anti-windup, which is tested experimentally with success. A model predictive controller is also developed based on the system models and it is tested in the model, but it was not possible to verify its functionality on the experimental setup. It is, however, believed that it could be an effective way to control output current of the module, especially if it is combined with an identification experiment during the startup of the module.

A series of models of the components of an RMFC system was also made to analyze how the operating points of the system affect the system efficiency. The first of these was an Adaptive Neuro-Fuzzy Inference System model of the cell voltage of an HTPEM fuel cell which is trained on an identification experiment spanning the expected operating range. The inputs of the model are the fuel cell temperature, the carbon monoxide content in the anode's supply gas and the current density. Such a model has not been observed in literature before. The Mean Absolute Error (MEA) of the model is 0.94% and is it concluded that it is suitable for use in larger system models or for integration in a dynamic model of the fuel cell.
Subsequently ANFIS models of the carbon monoxide concentration and hydrogen flow in the output gas of the reformer are trained based on identification experiments. The carbon monoxide concentration model has an MAE of 0.323% and the hydrogen flow model has an MAE of 0.074%. These models are then combined with the ANFIS model of an HTPEM fuel cell and their combined efficiency is analyzed for different fuel cell currents and reformer temperatures. It is concluded that the system efficiency can be improved by an average of 1.47 percentage points across fuel cell currents and 4 percentage points at maximum fuel cell current at a fuel cell temperature of 170 $[^{\circ}C]$.
If this efficiency gain is added to the gain achieved through the development of a controller for the battery SOC, the total efficiency gain achieved through modeling and control is increased to 28%.

Dansk resumé

PEM brændselsceller anses for at være en lovende teknologi, der har potentiale til at erstatte mere forurenende og mindre effektive forbrændingsmotorer i mange sammenhænge. De har dog den ulempe, at det brint de bruger som brændstof, er besværligt og energikrævende at opbevare og transportere. Alternative system topologier der bruger et flydende brændstof er derfor af stor interesse. En sådan topologi er reformeret metanol brændselscellesystemer (RMFC), der bruger en blanding af metanol og vand som brændstof. Dette brændstof reformeres i en dampreformer til brint og kuldioxid, der så føres ind i brændselscellen. Her forbruges det meste af brinten og det resterende føres videre til en brænder, der forsyner proces energien til reformeren. Denne opbygning gør RMFC systemer komplekse, da systemets komponenter påvirker hinanden og den last de forsyner. Dette Ph.D. studium har derfor omhandlet integrationen af et RMFC modul i en applikation og optimering af systemets arbejdspunkter baseret på modeller på systemniveau.
Den valgte applikation er en gadefejemaskine, der anses for at være en god applikation, fordi de ofte opererer i store flåder med lange operationstider, noget der taler til RMFC systemers stærke sider. For at analysere om integrationen af RMFC systemer i fejemaskiner er en god ide, fremstilles en dynamisk model af en sådan, inklusiv omtrentlige modeller af batteriet of RMFC systemet. Denne model bruges i sammenspil med en driftscyklus derefter i Outdoor Reliable Application using CLean Energy (ORACLE) projektet, til at forudsige ydelsen på en RMFC drevet fejemaskine før en prototype fremstilles. Efter fremstillingen af prototypen opdateres modellen på baggrund af målinger og ydelsen revurderes. Det konkluderes, at fejemaskinen kan køre en hel arbejdsdag på 8 timer uden at aflade sit batteri, hvis den forsynes med et 10 $[kW]$ RMFC system. I dette tilfælde vil den bruge 62,13 $[L]$ metanol, hvis hysterese metoden bruges til at styre batteriets ladestand, hvilket er almindelig praksis. En analyse af energiforbruget i fejemaskinen viser, at det meste af den energi der går tabt, går tabt i RMFC systemet og at et mere konstant, lavere, effektforbrug vil sænke dette energiforbrug. For at opnå dette udvikles en ladestandsregulator der kan minimere disse udsving. Simuleringer viser, at implementeringen af denne regulator sænker metanolforbruget til 46,85 $[L]$. En sænkelse på 24,6%.
Det konkluderes endvidere, at det, hvis fejemaskinens energiforbrug minimeres yderligere, er realistisk at bruge et 5 $[kW]$ RMFC system i stedet for et på 10 $[kW]$. I dette tilfælde vil metanolforbruget være 42,08 $[L]$.
For at opnå den forbedring af effektiviteten der blev observeret i modellen af fejemaskinen, var det nødvendigt at udvikle en regulator der kan styre udgangsstrømmen i stedet for brændselscellestrømmen, som er standard meto-

den for RMFC systemer. For at gøre dette muligt var det nødvendigt at fremstille en model af udgangsstrømmen fra et RMFC modul. Denne model indeholder dynamiske modeller af brændselscellen og batteriet og effektforbruget af modulets interne forbrugere, som blæsere og varmelegemer. Modellerne fintunes på baggrund af eksperimenter og bruges til at udvikle en PI regulator med feedforward og anti-windup, der kan styre udgangsstrømmen på et RMFC modul. Regulatoren afprøves også eksperimentelt og det konstateres at den fungerer. En såkaldt Model Predictive Controller (MPC) udvikles også på baggrund af de udviklede modeller, men det var desværre ikke muligt at teste denne eksperimentelt. Den menes dog at være en effektiv måde at styre udgangsstrømmen på et RMFC modul, specielt hvis den kombineres med et identifikationseksperiment, der udføres under opstarten af modulet.
En serie af modeller af et RMFC systems komponenter blev også fremstillet, med det formål at analysere hvordan de enkelte komponenters arbejdspunkter påvirker systemet effektivitet. Den første af disse modeller var en Adaptive Neuro-Fuzzy Inference System (ANFIS) model af cellespændingen på en HTPEM brændselscelle, trænet på baggrund af eksperimentelt indsamlet data. Modellens inputs er brændselscelletemperaturen, kulmonooxidsindholdet i brændselscellens anodegas og strømdensiteten. En sådan model er ikke før set i litteraturen. Den gennemsnitlige afvigelse på modellen er 0,94% og det konkluderes, at den er egnet til brug i større systemmodeller og til integration i dynamiske modeller af brændselscellen.
Efterfølgende udvikles ANFIS modeller af koncentrationen af kulmonooxid og brintmasseflowet i reformerens udgangsgas, på baggrund af en serie af identifikations eksperimenter. Modellen af kulmonooxidkoncentrationen har en gennemsnitlig afvigelse på 0,323% og modellen af brintmasseflowet har en afvigelse på 0,074%. Disse modeller kombineres derefter med ANFIS modellen af en HTPEM brændselscelle og deres samlede effektivitet analyseres for forskellige brændselscellestrømme og reformertemperature. Det konkluderes, at systemeffektiviteten kan forbedres med 1,47 procentpoint i gennemsnit på tværs af brændselscellestrømme og med 4 procentpoint ved den maximale brændselscellestrøm. Alt sammen ved en brændselcelletemperatur på 170 $[^{\circ}C]$.
Hvis denne forøgelse i effektiviteten lægges til den der blev opnået igennem udviklingen af en ladestandsregulator, er den totale forbedring af effektiviteten, der er opnået igennem modellering og regulering 28%.

Acknowledgments

It would seem that the end of a three year project has arrived already and here at the end it is time to look back and thank the people who helped me along the way.
First of all I would like to thank my supervisor, Søren Juhl Andreasen, who has helped me along, but also given me the freedom to explore the topics I found interesting. Gratitude is also extended to Søren Knudsen Kær and Jakob Rabjerg Vang for giving valuable feedback on my thesis.

My colleagues at the Department of Energy Technology also deserve thanks for the good times we have had together and specially the lab staff for their help and input on technical matters throughout the project. I would also like to thank my office mates, Simon Sahlin and Christian Jeppesen, for the many good discussions we have had through the years, both scientific and otherwise.

A big thank you is also extended to Dr. Sivakumar Pasupathi for hosting me at HySa System in Cape Town during my stay there. I would also like to thank my temporary colleagues in Cape Town for the great experience, both at the university and outside.

The EUDP program is gratefully acknowledged for providing funding for this project through the Outdoor Reliable Application using CLean Energy (ORACLE) project in the beginning of the project and through the Commercial Breakthrough of Advanced Fuel Cells II (COBRAII) project towards the end. In this connection I would also like to thank the partners in the ORALE project: Nilfisk Outdoor Division, Nilfisk Advance, Serenergy A/S and Danish Power Systems for their input to the project, which has been invaluable.

Finally a big thank you is also extended to my friends and family for the support throughout my studies and especially to my girlfriend who has been a constant and invaluable support.

Nomenclature

Abbreviation	Meaning
H_2	Hydrogen
CO	Carbon monoxide
CO_2	Carbon dioxide
O_2	Oxygen
e^-	Free electron
H_2O	Water
PEM	Polymer electrolyte membrane
GDL	Gas diffusion layer
MEA	Membrane electrode assembly
HTPEM	High temperature polymer electrolyte membrane
LTPEM	Low temperature polymer electrolyte membrane
PBI	Polybenzimidazole
DC	Direct Current
RMFC	Reformed methanol fuel cell
CH_3OH	Methanol
ΔH^0	Enthalpy change
SOFC	Solid Solid Oxide Fuel Cell
DMFC	Direct Methanol Fuel Cell
CFD	Computational Fluid Dynamics
ANFIS	Adaptive Neuro-Fuzzy Inference System
SOC	State Of Charge
ORACLE	Outdoor Reliable Application using CLean Energy
BOP	Balance Of Plant
CAN	Controller area network
MAE	Mean absolute error
PI	Proportional Integral
MPC	Model Predictive Control
$x_{1,2,3}$	Input for ANFIS model
$O_{i,i2}$	Output of layer i rule $i2$
a_i, b_i, c_i	Adaptive premise parameters
w_i	Firing level of rule i
$\bar{w}_i$	Normalized firing level of rule i
o_i, p_i, q_i, r_i	Consequent parameters of rule i
f_i	Output function of rule i
cRIO	Compact Reconfigurable Input Output

Contents

Part I

Thesis

Chapter 1

Introduction

The world's energy system is under pressure from an increasing population with a higher standard of living and the environmental consequences of a high reliance on fossil fuels. Interest in alternative energy sources and more efficient energy consuming devices is therefore high throughout the world, but in Europe in particular [1]. One of the technologies which are being considered is hydrogen fuel cells and they will be described in the next section.

1 Hydrogen fuel cells

The basic concept of H_2 fuel cells was first presented by Grove in 1843 [2] and it is interesting because it can produce electricity continuously at a high efficiency and the hydrogen fuel can be produced in various renewable ways [3]. The most common hydrogen fuel cells are the Polymer Electrolyte Membrane (PEM) type. In such a fuel cell hydrogen and oxygen react to generate water and electricity which can be used for a desired application. A PEM fuel cell consists of two electrodes, the negative anode and the positive cathode. These are split by an PEM which can only conduct positive ions. The hydrogen fuel is added to the anode, where it is distributed by a Gas Diffusion Layer (GDL) and a catalyst facilitates the reaction in Equation 1.1.

$$Anode: \quad H_2 \rightarrow 2H^+ + 2e^- \tag{1.1}$$

The positive hydrogen ions migrate through the electrolyte membrane and the released electrons are conducted to a load through wires. On the cathode side of the membrane, oxygen, either in pure form or in atmospheric air, is added and distributed by a GDL. Facilitated by the cathode catalyst, this

oxygen reacts with the hydrogen ions and electrons from the anode according to Equation 1.2

$$Cathode: \quad \frac{1}{2}O_2 + 2H^+ + 2e^- \rightarrow H_2O \tag{1.2}$$

Figure 1.1 illustrates this concept.

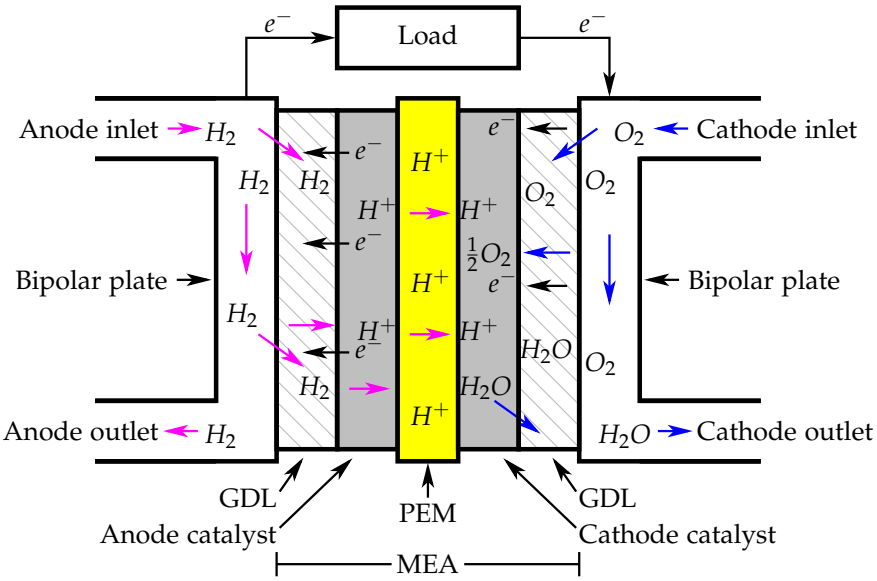

Fig. 1.1: Concept drawing of a fuel cell. The magenta lines signify a hydrogen flow, blue signifies airflow or oxygen.

As the figure shows, the PEM, anode and cathode catalysts and GDLs are combined in a so called Membrane Electrode Assembly (MEA). The MEA is compressed between two bipolar plates which serve as conductors for electrons, but also has a flow field which distributes the reactants over the GDL. Figure 1.2 shows a bipolar plate and an MEA from a fuel cell.

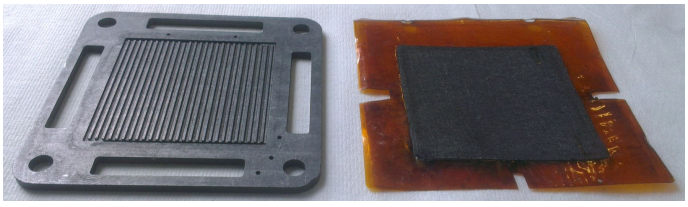

Fig. 1.2: Picture of a bipolar plate and a MEA.

The pictured bipolar plate is made from a graphite-polymer composite, but they can be made from a wide variety of materials [4]. The bipolar plate has a straight flow field, but these can also take many different shapes.
There are two main types of PEM fuel cells, High Temperature PEM (HT-PEM) and Low Temperature PEM (LTPEM) fuel cells. The main difference is that LTPEM fuel cells operate at temperatures below 100 $[^{\circ}C]$ and their membranes, which are typically made from nafion, are humidified by the water that forms in the fuel cell or by an external humidifier. HTPEM fuel cells operate at temperatures above 100 $[^{\circ}C]$ where there is no liquid water present. The membranes, which are often made of Polybenzimidazole (PBI), are generally doped with phosphoric acid [5]. The advantage of HTPEM fuel cells is that they have a higher tolerance to impurities such as CO [6] [7] and waste heat of a higher quality than LTPEM fuel cells. The disadvantages are that they have to be heated to their operating temperature before they can be used and that their efficiency is generally lower [5].

A fuel cell typically has a maximum voltage of around 1 $[V]$ [8] at open circuit conditions, but this decreases when the current density of the fuel cell is increased as illustrated in Figure 1.3.

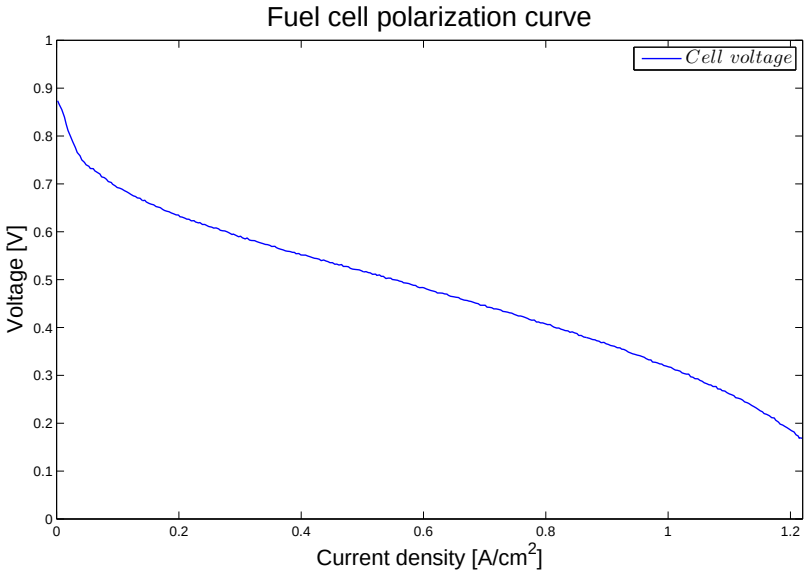

Fig. 1.3: Measured polarization curve of an HTPEM fuel cell.

There is a sharp drop in the fuel cell voltage at low current densities and this is typically called the activation loss. This drop in voltage is followed by a linear region where the losses are ohmic in nature. After the ohmic

losses comes the concentration losses which gives a sharp drop in the fuel cell voltage. If the current is increased too much the voltage drops to zero and the fuel cell cannot produce any power. The current a fuel cell can produce is therefore limited by the area of the cell and it is not practical to increase this area indefinitely. The power rating of a fuel cell system is therefore often increased by connecting several cells in series to form a fuel cell stack. This has the added benefit of yielding a higher output voltage, which is an advantage in most applications, as low voltages and high powers mean high currents and thus large losses.
Figure 1.4 shows a diagram of a typical fuel cell system.

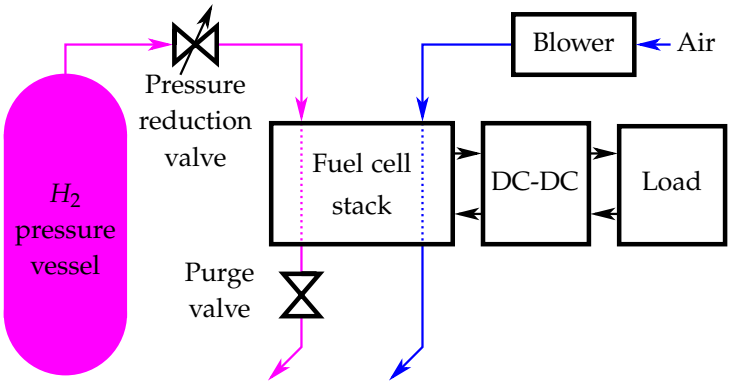

Fig. 1.4: Concept drawing of a typical fuel cell system. The magenta lines signify a hydrogen flow, blue signifies airflow and black is an electric current.

In systems such as this the hydrogen fuel is stored in a pressure vessel at a pressure of above 200 $[bar]$ and often up to 700 $[bar]$ [9]. The pressure is throttled down to the stack operating pressure, which is typically around 0.5 $[bar]$, using a pressure reduction valve. When a fuel cell is operated on pure hydrogen, a closed anode setup is often used. This means that the anode outlet is closed off by a purge valve which can be opened periodically to flush out contaminants and water which has migrated from the cathode [10]. The oxygen for the cathode is supplied in the form of atmospheric air by either a blower or a compressor depending on the demands of the fuel cell. In some fuel cell stacks this blower is also used to control the operating temperature, but most larger systems use a separate liquid cooling system.
The electric current generated by the fuel cell is passed to the load via a DC-DC converter. This is often done to control the fuel cell current and thereby avoid peaks in the fuel cell current and the resulting lowered fuel cell voltage as observed in Figure 1.3.

2 Reformed methanol fuel cell systems

In fuel cell systems like the one in Figure 1.4 that are operated on pure hydrogen, there is a need for a fuel storage system. This can either be under high pressure as in the described system, in liquid form at temperatures below -253 $[^{\circ}C]$ or in a metal hydride [9]. All of these solutions are heavy and take up a lot of space, which is undesirable in mobile application and are energy consuming, which lowers the overall system efficiency. In addition pure hydrogen is difficult to distribute because of its low volumetric energy density.
Fuel cell systems that use a liquid fuel which is easier to store and transport are therefore of interest. One possible fuel is methanol which can be reformed to a hydrogen-rich gas via the following catalyst-reinforced reactions [11]:
Steam reforming:

$$CH_3OH + H_2O \rightarrow 3H_2 + CO_2 \qquad \Delta H^0 = +49.4 \frac{kJ}{mol} \tag{1.3}$$

partial oxidation:

$$CH_3OH + \frac{1}{2}O_2 \rightarrow 2H_2 + CO_2 \qquad \Delta H^0 = -192.2 \frac{kJ}{mol} \tag{1.4}$$

and methanol decomposition:

$$CH_3OH \rightarrow 2H_2 + CO \qquad \Delta H^0 = +128 \frac{kJ}{mol} \tag{1.5}$$

The first two reactions are most desirable for fuel cell applications, because the CO released by the methanol decomposition reaction is harmful to PEM fuel cells.
Some of this CO is removed by the water gas shift reaction which is:

$$CO + H_2O \rightarrow H_2 + CO_2 \qquad \Delta H^0 = -41.1 \frac{kJ}{mol} \tag{1.6}$$

Not all of the CO is removed and a experiments performed in this PhD study shows that a steam reformer typically outputs between 0.2 and 2 % CO depending on the operating point.

In reformers that use steam reforming, 49.4 $\frac{kJ}{mol}$ of heat energy has to be added to the reformer but in reformers that use partial oxidation 192.2 $\frac{kJ}{mol}$ is released. This means that the reformer provides its own reaction energy, but less hydrogen is generated per mole of methanol added.
When a PEM fuel cell is operated on reformed gas, a closed anode setup, like the one in Figure 1.4, cannot be used. This is because the CO_2 released

by the reforming process would build up in the anode preventing H_2 from entering. Instead an open anode must be used, which means that there will be a constant flow of fuel through the fuel cell. When this is the case a higher flow than required by the fuel cell must be passed through the fuel cell to avoid increased concentration losses.
This excess fuel can be used in a burner to provide the necessary heating energy for the reformer. In addition the excess heat produced by the fuel cell can be used to evaporate and preheat the fuel before it reaches the reformer. Figure 1.5 shows a diagram of an integrated Reformed Methanol Fuel Cell (RMFC) system with an air-cooled fuel cell stack.

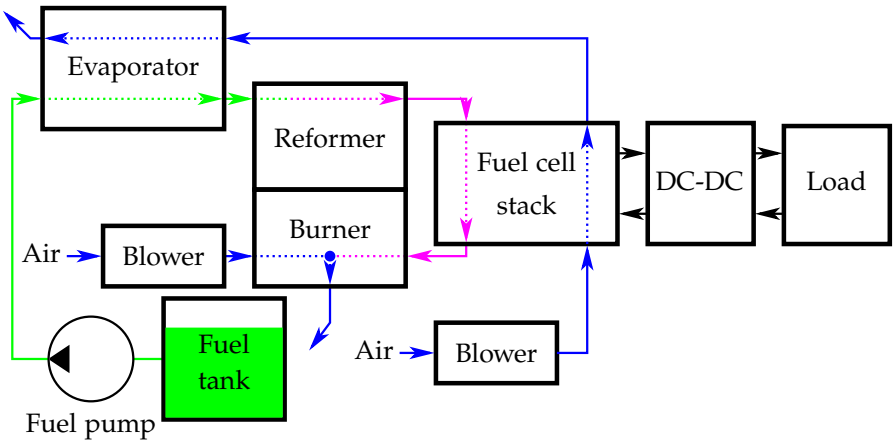

Fig. 1.5: Concept drawing of a reformed methanol fuel cell system. The magenta lines signify a hydrogen rich reformed gas flow, blue signifies airflow, green represents a fuel flow and black is an electric current.

This type of system was first proposed in 1974 by [12] and as it will be described later in the state of the art analysis, these systems are entering commercialization.
In this system the reformed fuel goes directly from the reformer to the fuel cell stack with no gas clean-up or *CO* removal. As mentioned earlier, a reformer typically has a relatively high concentration of *CO* in its output gas. This means that the configuration in Figure 1.5 is only possible if a fuel cell with a high *CO* tolerance, such as an HTPEM fuel cell, is used [13, 14].
In RMFC systems like the one depicted in Figure 1.5, it is important to ensure that the hydrogen flow to the fuel cell matches what is needed to produce the fuel cell current with a specified over-stoichiometry at all times. The hydrogen flow cannot, however, be allowed to be too big, because this would lead to thermal problems in the burner and a reduced system efficiency.
In addition the high degree of system integration means that a thermal equi-

librium has to be reached after every change in fuel cell current and fuel flow. This makes the DC-DC controller between the fuel cell and the load more crucial, because the rate of change of the fuel cell current has to be limited.
This means that if the power delivered to the load is to be controlled, an energy storage device, such as a battery, has to be introduced in the system. Figure 1.6 shows a diagram of this concept.

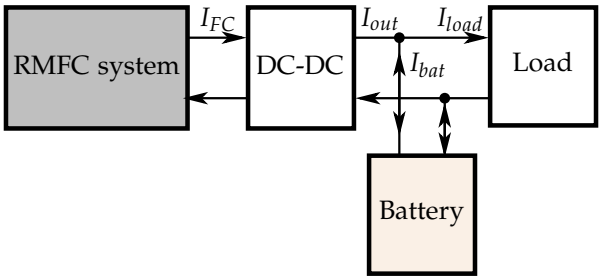

Fig. 1.6: Concept drawing of an RMFC system integrated with a battery in a hybrid system.

As the diagram shows, the battery is connected in parallel with the load and is used as a buffer to supply the load during peak periods.
The battery can also be used to supply the RMFC system with power during start-up and shut-down.

3 State of the art

In this section the state of the art within RMFC systems will be described as well as some of the modeling methods which are used to analyze these systems. This includes models the reformer and fuel cell, both separately and together as a system.
Afterwards a possible application for RMFC systems is described, namely street sweeping machines which provide a promising case.

3.1 Liquid fueled fuel cell technologies

Compared with other kinds of fuel cell systems which can run on liquid fuels, RMFC systems have a relatively low operating temperature, about 165 $[°C]$ for the fuel cell and below 300 $[°C]$ for the reformer. This reformer temperature is low compared with that which is necessary in ethanol reformers, often above 600 $[°C]$ [15]. In addition the process heat for steam reforming of ethanol is 347.4 $[kJ/mol]$, which means that it takes 3.5 times more energy to

create the same amount of H_2.
Solid Oxide Fuel Cells (SOFCs), which as the name suggests has a solid oxide or ceramic electrolyte, can run on liquid methanol directly, but has an operating temperature of around 800 $[^{\circ}C]$ [16]. The drawback of the high operating temperature of the SOFC is that it extends the warmup time and costs energy to perform.
Another fuel cell technology which can convert methanol directly is Direct Methanol Fuel Cells (DMFCs), which perform the fuel reforming inside the fuel cell. The advantage of this technology is that it works at room temperature, but it has a lower efficiency and is mainly being considered for low power applications such as chargers for mobile phones or laptop computers [17]. RMFC systems are therefore an interesting technology which will be described further in the next section.

3.2 Reformed methanol fuel cell systems

RMFC systems were suggested as early as 1974 by [12] but the technology has only recently approached a commercial breakthrough. Table 1.1 shows a list of RMFC products which are more or less commercially available.

Producer	Product	Power $[W]$	Weight $[kg]$	Power density $[W/kg]$
Serenergy	H3 350	350	13.7	25.5
	H3 5000	5k	75	66.7
Ultracell	XX55	50	3	16.7
Ballard	ElectraGen	2.5k - 5k	295	16.9
Protonex	M300	300	16	18.8

Table 1.1: Commercially available Reformed methanol fuel cell systems [18–21] .

The modules produced by Serenergy A/S are based on an HTPEM fuel cell fed directly by a steam reformer [18] and are suitable for both mobile and stationary applications. Ultracell produces RMFC modules for portable military applications such as charging of communication equipment in the field [19]. Ballard's RMFC systems are for telecommunication backup power and are based on their LTPEM fuel cells with a gas clean-up between the steam reformer and fuel cell [20]. The Protonex RMFC system is an integrated unit for Auxiliary power generation in military applications [21] and uses an LTPEM fuel cell and a steam reformer with gas purification.
In this work most of the experimental work has been carried out using an

H3 350 module from Serenergy A/S. Figure 1.7 shows a picture of such a module and Figure 1.8 shows a diagram of its components.

Fig. 1.7: H3 350 reformed methanol fuel cell module produced by Serenergy A/S.

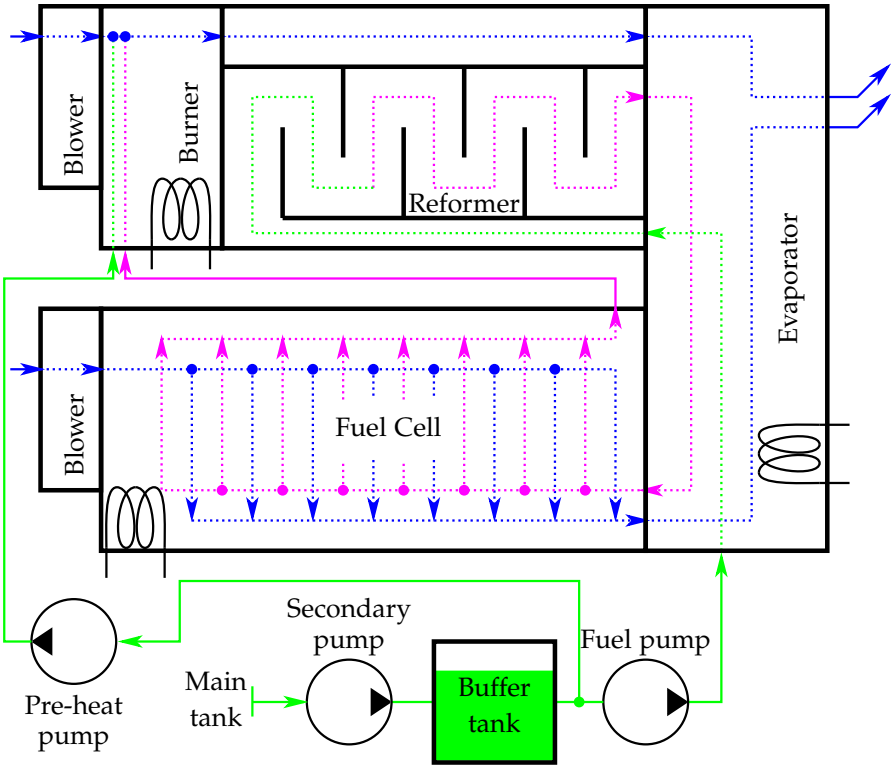

Fig. 1.8: Concept drawing of an H3 350 module. The magenta lines signify a hydrogen-rich reformed gas flow, blue signifies a flow which is predominantly atmospheric air and green represents a fuel flow. Fuel and air filters are not included and the coils in the figure represent electric heaters.

The module uses an air cooled HTPEM fuel cell with 45 cells and a cell area of 45.16 $[cm^2]$. It has a steam reformer which gets its process heat from a burner supplied by the excess hydrogen from the fuel cell anode exhaust. Before it enters the reformer, the fuel passes through an evaporator which is powered by the cathode air of the fuel cell. The module is highly integrated and uses its evaporator as a manifold to transfer the flow between the reformer and the fuel cell. The actuators of the system are controlled by an onboard processor which measures the temperature of the fuel cell at two points, of the reformer at four points along the reformer bed and of the evaporator at one point. The DSP also receives a signal from sensors measuring the level of fuel in the internal buffer tank of the module and activates the secondary pump accordingly.
The module has three electric heating elements for start-up. One in the burner one in the evaporator and one in the fuel cell. It also has a preheating pump which pumps fuel into the burner after an initial preheating to bring the burner and reformer up to operating temperature.
When the module is in normal operation it uses the burner blower to control the temperature of the reformer and the fuel cell blower to control the fuel cell temperature.
The larger H3 5000 module, which has an output power of 5 $[kW]$, is pictured in Figure 1.9

Fig. 1.9: H3 5000 reformed methanol fuel cell module produced by Serenergy A/S.

The module uses the same basic setup as the H3 350, but has a 120 cell, 163.5 $[cm^2]$ liquid-cooled fuel cell and transfers the evaporation heat from the fuel cell to the evaporator via its cooling oil. As opposed to the H3 350 module, which has integrated electric heaters, the H3 5000 uses a methanol powered heater in its cooling oil circuit to warm up the evaporator and fuel cell. Figure 1.10 shows a diagram of an H3 5000 system.

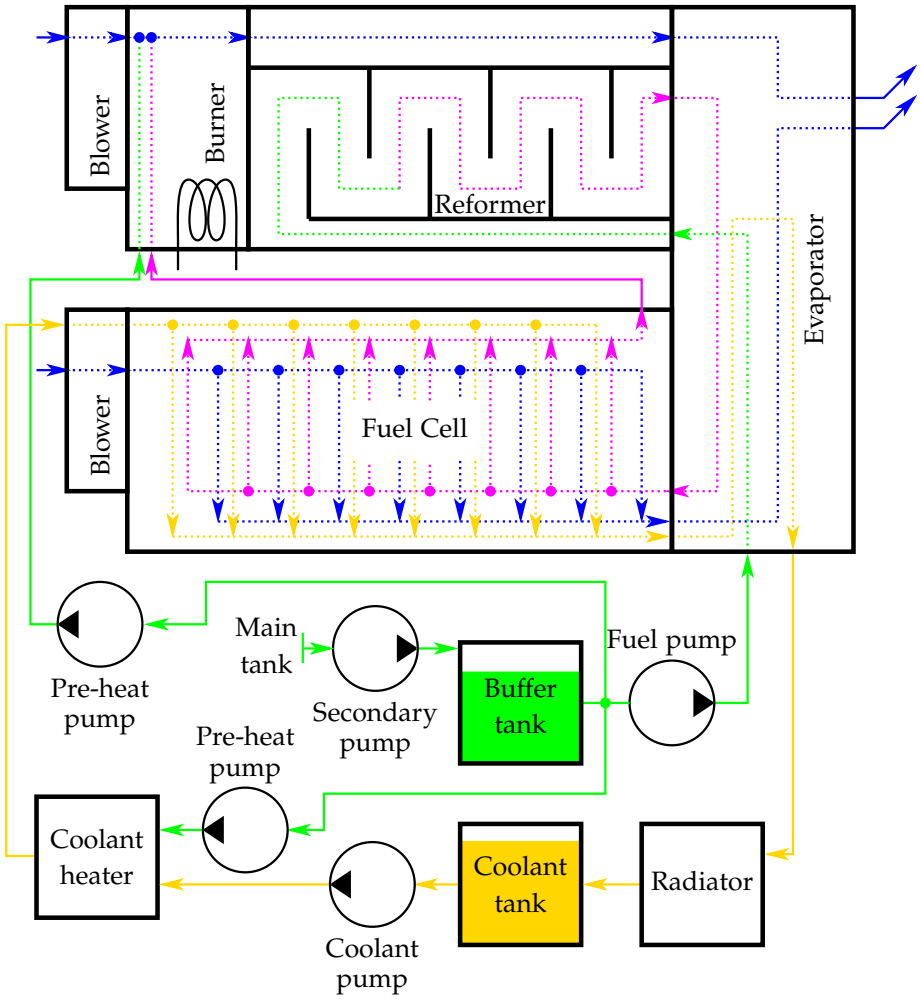

Fig. 1.10: Concept drawing of an H3 5000 module. The magenta lines signify a hydrogen-rich reformed gas flow, blue signifies a flow which is predominantly atmospheric air, green represents a fuel flow and gold represents a cooling oil flow. Fuel and air filters are not included and the coil in the figure represents an electric heater.

As mentioned earlier the transport of heat from the fuel cell to the evaporator is performed with an oil cooling circuit, and the pre-heating of the burner is performed using an electric heater. During normal operation the temperature of the oil circuit, and thus the fuel cell, is controlled using a radiator or by transferring heat energy to an external unit which exploits it for heating. This can for example be in a combined heat and power application.

3.3 Reformed methanol fuel cell system models

There are several disciplines involved in modeling RMFC systems and the systems can be modeled at many different levels, depending on the purpose of the models. If the purpose of the model is to predict the performance of a new reformer design, a combination of kinetic modeling and Computational Fluid Dynamics (CFD) can be used as in [22], which describes the design and test of a micro methanol reformer, or as in [23], which describes an integrated methanol reformer and burner. These models are typically used to analyze and optimize the steady state performance of the reformer as they would be too computationally heavy to use for dynamic modeling at a system level or for integration in the control system of the RMFC system.

If the purpose of the model is to evaluate the thermal dynamics of the system, a model of each component in the system has to be made. This includes thermal models of the fuel cell, reformer and evaporator. Models of the electrochemical reaction in the fuel cell have to be made to predict the heating power in the fuel cell, as well as models of the reforming process to predict the output gas composition of the reformer and the energy consumed by the reforming process.
Paper **[B]** describes such a model of an H3 350 module which is an earlier design than the one in Figure 1.8. The basis for this model was developed in a master project prior to the start of this PhD study [24], but the paper describes an updated version of the model. The model uses lumped thermal masses for the major components of the system and empirical models of the heat transfer between the components and into the flows through them. The fuel cell model used is a modified version of the one from [13] which has the cathode and anode stoichiometry, carbon monoxide concentration, fuel cell current and temperature as inputs and has the fuel cell voltage as output. The output gas composition of the reformer is calculated using the Adaptive Neuro-Fuzzy Inference System (ANFIS) models described in paper **[A]**. These are neuro-fuzzy models that can be trained to imitate the behavior of a real system and they are very useful when physical information such as the actual reformer bed temperature, active catalyst area and the fuel flow temperature is not available.
In this work the concept of using ANFIS models for reformer output gas modeling is extended and an ANFIS model of an HTPEM fuel cell is developed. ANFIS models of LTPEM fuel cells have been presented before for a cell during changes in anode and cathode supply temperatures and backpressure in [25] and dynamically in [26]. But ANFIS models of HTPEM fuel cells are not found in literature and nor are ANFIS models of PEM fuel cells under the influence of CO in the anode supply gas. Such a model is presented in this work in paper **[D]**.

Models such as these are not suitable for component design optimization, but they are suitable for integration in dynamic system models or for analyzing the operating parameters, such as reformer and fuel cell temperature, of a system.
Models for optimizing the operating parameters of a RMFC system are not present in literature, but [27] describes a multilevel optimization approach for the efficiency of an LTPEM system powered by natural gas which has been reformed and passed through a gas clean-up system. [28] describes how physical system models of a Solid Oxide Fuel Cell (SOFC) can be used to find optimal operating conditions and [29] describes how parameters such as temperature, pressure ratios and reactant stoichiometries can be optimized for an LTPEM fuel cell system. Paper **[E]** therefore presents a method for calculating and optimizing the efficiency of an RMFC system using ANFIS models of the reformer and fuel cell.

If the purpose of the modeling is to analyze how the electrical output of an RMFC system interacts with the other components in a hybrid system such as the one in Figure 1.5, a model of the gas composition will not be necessary. Here a model of the output current dynamics of the system will be sufficient.
For a traditional fuel cell system like the one presented in Figure 1.4 integrated in an automobile, [30] presents a model and uses it to develop a model predictive control that minimizes the energy consumption of the drive train, while respecting limits for the battery State Of Charge (SOC) and power ratings. Other control methods and models have been presented but none which are concerned with the challenges which are specific to RMFC systems, namely the highly limited rate of change of the fuel cell current. In this work a model of the output current of an RMFC module has been made and is presented in paper **[C]**. In this connection an analysis has also been made of what can be gained by controlling the state of charge of the battery in the hybrid system.

For a technology like RMFCs to become widespread, cases that demonstrate their usefulness have to be presented. In this work their possible introduction in street sweeping machines, which are normally powered by diesel engines, is analyzed and the next section therefore presents the current state of the art in alternatively fueled street sweeping machines.

3.4 Street sweeping machines - A possible application for RMFC systems

In the analysis presented in [31], street sweeping machines are identified as a possible early market for hydrogen fuel cells. This is because it is an applica-

tion where many vehicles are often operated in a fleet with a central staging area where the refueling infrastructure and maintenance personnel can be based. The same reference also concludes that street sweeping machines are a good case for green technologies with increased cost, because the municipal respondents in their market survey state that they are willing to incur extra costs to have green technologies in their city centers.
This, and the fact that they often run full days without long periods of inactivity, also makes street sweeping machines a good application for RMFC systems.
Endeavors have been made to design street sweeping machines that run on alternative energy. On the commercial market the Tennant 500ze electric street sweeping machine can be mentioned. It is an all electric machine which is powered by replaceable Li-ion batteries. The advantage of this design is that there are no on-site emissions. The disadvantage is that the vehicles carrying capacity has been reduced to minimize the power consumption of the vehicle and make battery operation viable. The vehicle still has to perform battery changes during an 8 $[h]$ working day to extend its range. Figure 1.11a shows a picture of a Tennant 500ze.
Another concept which has been explored is a H_2 fuel cell powered street sweeper constructed in the Swiss Hy.muve project. The test vehicle produced in this project was a full sized street sweeping machine with a 350 $[Bar]$ compressed H_2 storage. This means that a costum infrastructure has to be made for them.
The company Plug Power, which supplies hydrogen fuel cells and refueling stations, specifies that a fleet of at least 40 forklift trucks is necessary to make their systems viable [32]. A similar number can be expected to be the case for H_2 powered fuel cell street sweepers because they are similarly sized machines. Figure 1.11b shows a picture of the Hy.muve prototype.

(a) **(b)**

Fig. 1.11: (a) The Tennant 500ze [33] and **(b)** The Hy.muve prototype vehicle [34].

An RMFC system could be a viable solution to the problems of the presented machines, namely limited range and difficult fuel handling and storage. The Outdoor Reliable Application using CLean Energy (ORACLE) project, which this PhD project has been a part of, is therefore concerned with the development of a RMFC powered street sweeping machine which can serve as a proof of concept. This project is described in the following chapter.

Chapter 2

Applying reformed methanol fuel cell systems

In the previous section street sweeping machines where identified as a possible application for RMFC systems. The Outdoor Reliable Application using CLean Energy (ORACLE) project is a research and development project where 5 companies and institutions cooperate to develop such a machine. The 5 project partners are:

- Nilfisk Outdoor Division: Company that makes traditional diesel powered tool carriers, such as street sweeping machines. Their task was to develop an electric version of one of their street sweeping machines and prepare it for the integration of an RMFC module.
- Nilfisk Advance: Company that develops and produces floor cleaning equipment. Their job was to optimize the suction unit of the street sweeper to minimize its power consumption.
- Serenergy A/S: Company that develops and produces HTPEM fuel cell systems and RMFC systems. Their job was to develop an RMFC system which was suitable for integration in a electric street sweeping machine and to help Nilfisk Outdoor Division with its integration in the vehicle.
- Danish Power Systems: Company which is working on developing and producing HTPEM MEAs. In the context of the ORACLE project they have worked on the durability of their MEAs and their integration in Serenergy's fuel cell stacks.
- Aalborg University Department of Energy Technology: Scientific and educational institution. Their job was to analyze the expected per-

formance of the RMFC-powered street sweeping machine via dynamic modeling of the vehicle's drive-train and to analyze and optimize the performance of the RMFC systems in the vehicle.

Based on a market analysis performed by Nilfisk Outdoor Division, a drive cycle was determined based on expected costumer behavior. This drive cycle has been used throughout the project to calculate the expected performance of the ORACLE test vehicle.
This drive cycle consists of an 8 $[h]$ working day interrupted by 7, 2000 $[m]$ trips to an emptying station and a 100 $[s]$ stop at a simulated red light every 10 $[min]$. During the transportation to and from the cleaning site, the speed of the vehicle is 21 $[km/h]$ and during the cleaning it is 5 $[km/h]$. An Eco-mode, which turns the fan down to 60%, is planned to be in operation for 50 $[s]$ followed by 10 $[s]$ at full power. Figure 2.1 shows a plot of the speed of the vehicle during an 8 $[h]$ drive cycle.

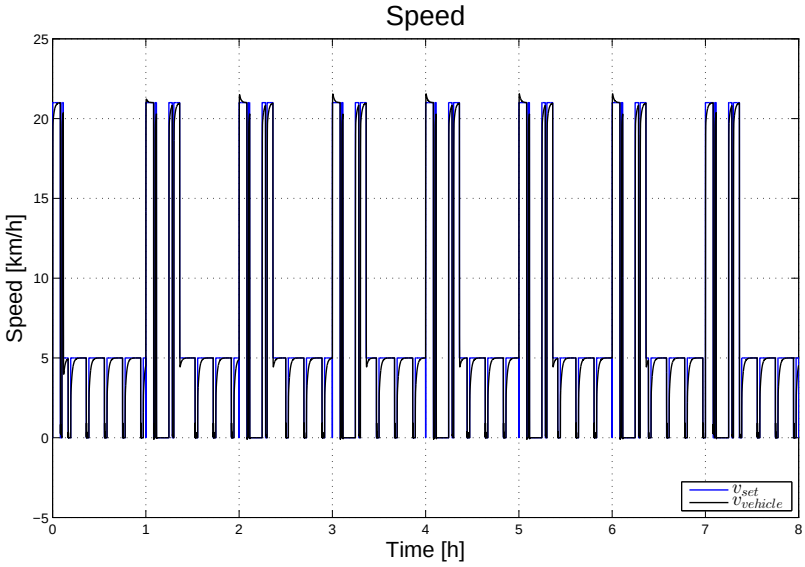

Fig. 2.1: Plot of the speed of the vehicle during the specified drive-cycle.

The distance which is cleaned is 20.8 $[km]$ and the transport distance is 30.3 $[km]$.

The focus of the project was originally the City Ranger 2250 model seen in Figure 2.2a. It was, however, chosen to shift focus to the larger City Ranger 3500 model in Figure 2.2b, because it provided better space for the integration of the RMFC system.

(a) **(b)**

Fig. 2.2: (a) Picture of a City Ranger 2250 and **(b)** a City Ranger 3500 from Nilfisk Outdoor [35].

Both models are powered by a diesel engine which drives a series of hydraulic pumps. Figure 2.3 shows a diagram of the drive-train of the City Ranger 3500.

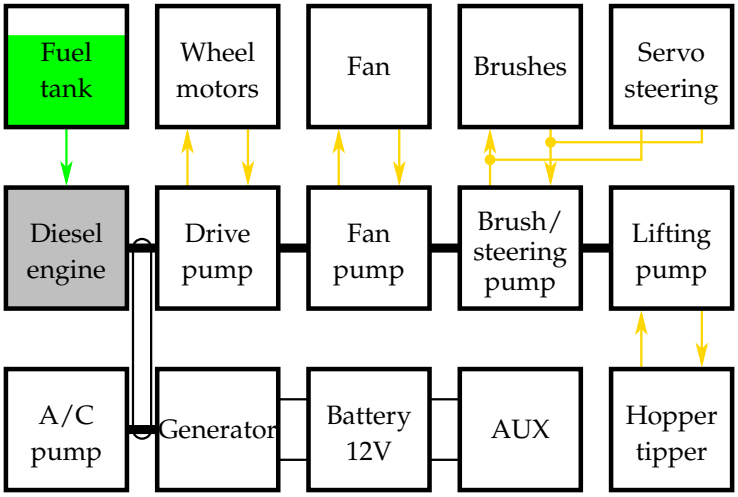

Fig. 2.3: Diagram of the power train of a City Ranger 3500.

As the figure shows, four hydraulic pumps are connected in series to the drive shaft of the engine. The first pump drives the hydraulic hub motors in the wheels, the second drives the suction fan of the vehicle, the third the brushes and servo steering and the last pump powers the tipping mechanism for the collection hopper of the vehicle. The engine also drives an air-conditioning pump and a 12 $[V]$ generator for the auxiliary systems of the vehicle via a belt.

The electrification of the vehicle could have been done by replacing the diesel engine with an equally sized electric motor, but this would have been an inefficient solution, as it introduces an extra conversion from electric to hydraulic power. It was therefore chosen to convert as much as practically possible of the drive-train of the vehicle to electrical power. Figure 2.4 shows the layout of converted drive-train.

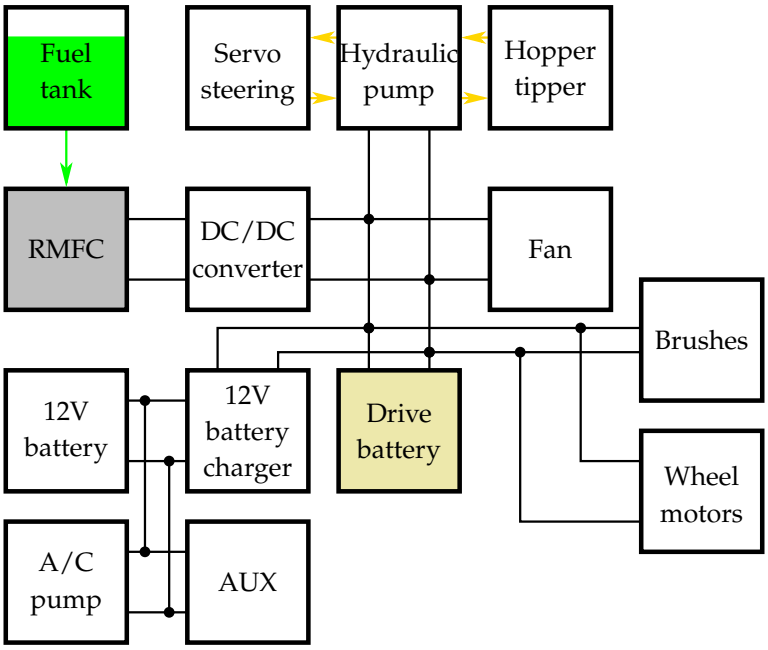

Fig. 2.4: Diagram of the power train of a the converted City Ranger 3500.

As the figure shows, the hybrid structure presented in Figure 1.6 is used. This means that a battery is connected in parallel with the RMFC system and the consumers. This is done to be able to supply the instantaneous power demand of the load. A review of the available motors and control electronics led to the choice of a 48 $[V]$ drive battery.
The hydraulic hub motors are replaced with electric motors. As are the motors for the brushes and the fan. The 12 $[V]$ battery is now charged by a charger powered by the drive battery and the auxiliary systems are kept as is. An air-conditioning pump is added to the 12 $[V]$ circuit as well.
The relatively low power consumption of the power steering pump and the hopper tipper means that they have not been replaced, but are instead powered by an electrohydraulic pump.
Figure 2.5a, b and c show pictures of the finished ORACLE vehicle.

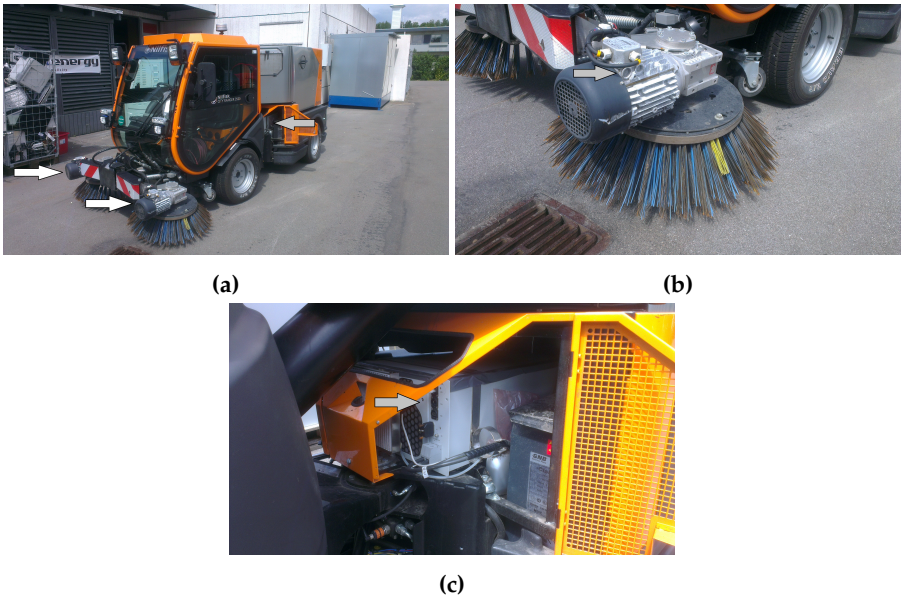

(a) **(b)**

(c)

Fig. 2.5: Picture of the ORACLE vehicle **(a)**, a close-up of the implementation of the electric brush motors **(b)** and an RMFC system implemented in the vehicle **(c)**. The white arrows indicate where the brush motors are mounted and the gray arrows indicate where the single H3 5000 RMFC system is mounted.

1 Vehicle modeling

To be able to predict the range and energy consumption of the vehicle, as well as the consequence of using different sizes of RMFC systems and batteries, it is necessary to develop a model of the consumers of the vehicle, battery and RMFC system. Such a model will be a powerful tool when it comes to choosing the relative sizes of the RMFC system and battery, as well as for designing a strategy for sharing the load between them to minimize the fuel consumption and deciding what size the fuel tank should have. In this project an approximate model of each of the consumers has been made, as well as models of the battery and RMFC system and these have been combined into one model. Figure 2.6 shows the structure of the model implemented in MATLAB Simulink.

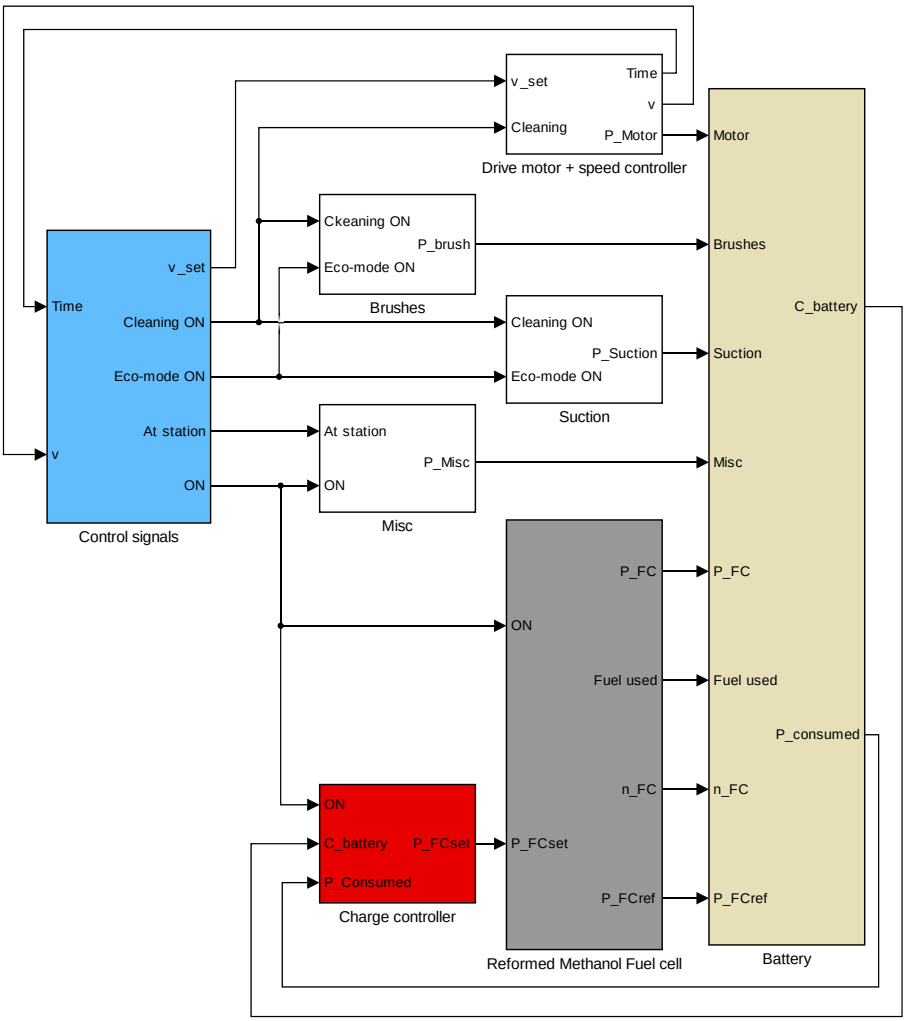

Fig. 2.6: Block diagram of the MATLAB Simulink model of a street sweeper powered by an RMFC system.

In the following the content of each of the submodels seen in the figure will be described.

Control signals

In this submodel the drive-cycle is generated. This is done by a series of logic circuits that switch the states of the vehicle. The states of the vehicle are:

- **ON:** Is the vehicle on?

- **Eco-mode:** Is Eco-mode on or off? This is alternately on for 50 $[s]$ and off for 10 $[s]$ as specified in the drive-cycle.
- **Cleaning ON:** Is the vehicle cleaning? This mode is on when the vehicle is at the cleaning site and moving, i.e. not stationary at a red light. This mode turns the suction fan and brushes of the vehicle on and switches the speed set point to the cleaning speed.
- **Transport:** Is the vehicle in transport mode? This is the case when the vehicle is moving to and from the emptying station. When this mode is on, the speed set point is set to the transport speed.

The switching process can be controlled by setting fx. the interval between trips to the emptying station, the distance to the station and the time it takes to empty the hopper. The outputs of the submodel is the vehicle modes and the speed set point.

Drive motor + speed controller

This submodel contains a calculation of the power consumption of the motor. It is not the purpose of this model to design speed controllers or assess the performance of different motor systems relative to each other. The model is therefore a simple estimation based on Newtons 3rd law assuming that all loss terms can be collected in a Coulomb friction term:

$$\begin{aligned} m_{vehicle} \cdot a_{vehicle} &= f_{motor} - f_{fric} \\ v_{vehicle} &= \frac{1}{m_{vehicle}} \int \left(f_{motor} - f_{fric} \right) \cdot dt \end{aligned} \tag{2.1}$$

where:

$$f_{fric} = m_{vehicle} \cdot g \cdot k_{fric} \tag{2.2}$$

Here g is the gravitational constant and k_{fric} is a friction constant which is determined based on the expected power consumption of the vehicle. The power consumption is then calculated at any given moment to be:

$$P_{motor} = f_{motor} \cdot v_{motor} \tag{2.3}$$

In this submodel, the speed is controlled by a PI-controller and the inputs to the submodel are a speed set point and the ON/OFF set point of the cleaning mode of the vehicle. The latter is only relevant for the logging and data analysis.

Brushes

The consumption of the brushes is modeled as a constant contribution when the vehicle is in cleaning mode. Otherwise it is 0.

Suction

The consumption of the suction fan of the vehicle is modeled as a constant contribution when the vehicle is in cleaning mode and Eco-mode is switched off. When Eco-mode is on, the power consumption is reduced to 60%. Otherwise it is 0.

Misc

This model covers consumers such as the power steering, hopper tipper, air-condition and auxiliary consumption. Whenever the vehicle is ON, this consumer is set to a constant value.

Reformed Methanol Fuel Cell

This submodel contains a model of the RMFC system in the vehicle. This model has the fuel cell power set point and the ON signal as inputs and the fuel cell power, accumulated fuel consumption, the momentary fuel cell efficiency and the fuel cell power set point as outputs.
The first components of the model are a rate limiter which limits the rate of change of the fuel cell power and a saturation function which limits the magnitude of the fuel cell power. The rate of change is limited to 15 minutes for a change corresponding to the full RMFC power. A model of the efficiency of an H3 350 unit is made based on experiments and normalized with respect to its maximum power. The efficiency of the RMFC system in the vehicle is then assumed to be proportional to this. The top plot in Figure 2.7 shows a plot of this model.

Battery

In the battery model, the contributions of the consumer models and the output power of the RMFC system is summed to give the battery power according to the following equation:

$$P_{bat} = P_{FC} - P_{Motor} - P_{Suction} - P_{Brushes} - P_{Misc} \tag{2.4}$$

This power is then reduced by a battery efficiency model if it is positive, i.e. going into the battery, or increased if it is negative, i.e. going out of the battery before it is integrated to give the battery SOC. The battery efficiency

model used, which can be seen in the bottom plot in Figure 2.7, is from the datasheet of the GNB EPzV lead acid battery used in the ORACLE test vehicle.

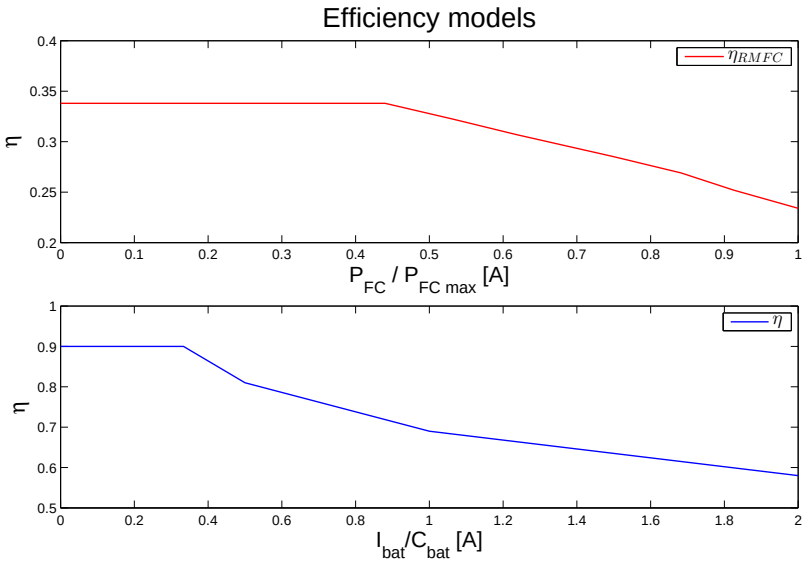

Fig. 2.7: Plot of the RMFC and battery efficiencies used in the model.

Charge controller

This submodel contains the controllers for the fuel cell power. The inputs for the submodel are the ON signal, the battery state of charge and the instantaneous power consumption of the vehicle and the output is the fuel cell power set point.

1.1 Initial simulations

In the planning phase of the ORACLE project, the vehicle model was used to predict the expected range of the test vehicle with different battery and fuel cell combinations. This was done to ensure that the vehicle would have a long enough range for testing the concept of an RMFC powered street sweeping machine. The consumer constants where estimated at conservatively high values based on measurements made on the original diesel-powered vehicle. Table 2.1 shows the consumer constants used for the initial simulations.

Parameter	Value %
$P_{Suction}$	8.6 $[kW]$
$P_{Brushes}$	4.9 $[kW]$
P_{Misc}	1 $[kW]$
C_{fric}	0.05 $[-]$

Table 2.1: Initial consumer constants.

The weight of the vehicle is set to 2600 $[kg]$, the energy density of the battery is set to 41.46 $[kg/kWh]$ and the power density of the RMFC system is set to 15 $[kg/kW]$. The total weight of the vehicle is then calculated as the sum of these contributions. Figure 2.8 shows the power consumption of the consumers of the vehicle during a 8 $[h]$ working day.

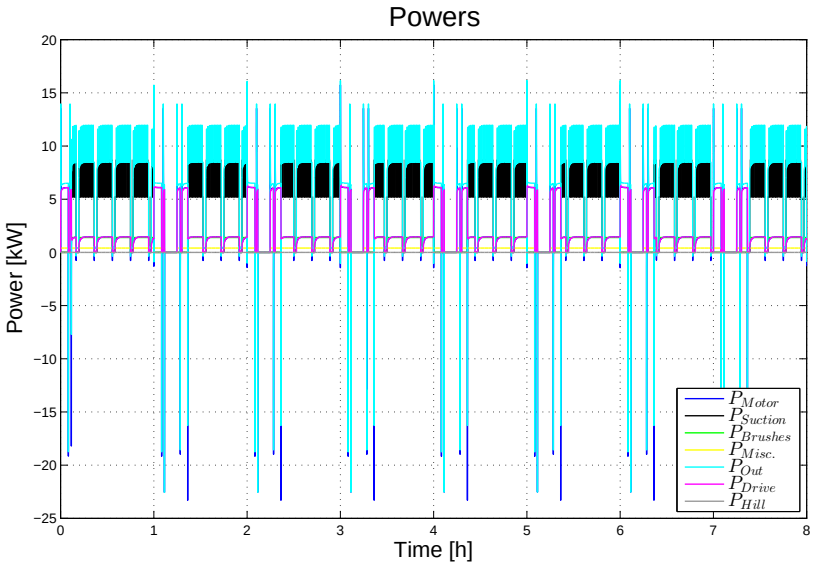

Fig. 2.8: Plot of the vehicles power consumption during the specified drive-cycle.

As the figure shows the motor power is negative during decelerations. This is because it is assumed that the drive motors of the vehicle are used to recover brake energy.
A 19.2 $[kWh]$ GNB EPzV battery was identified as a possible drive battery for the test vehicle, and Figure 2.9 shows the State Of Charge (SOC) of the battery with no fuel cell and with 5 and 10 $[kW]$ fuel cells, corresponding to 1 and 2 H3 5000 units.

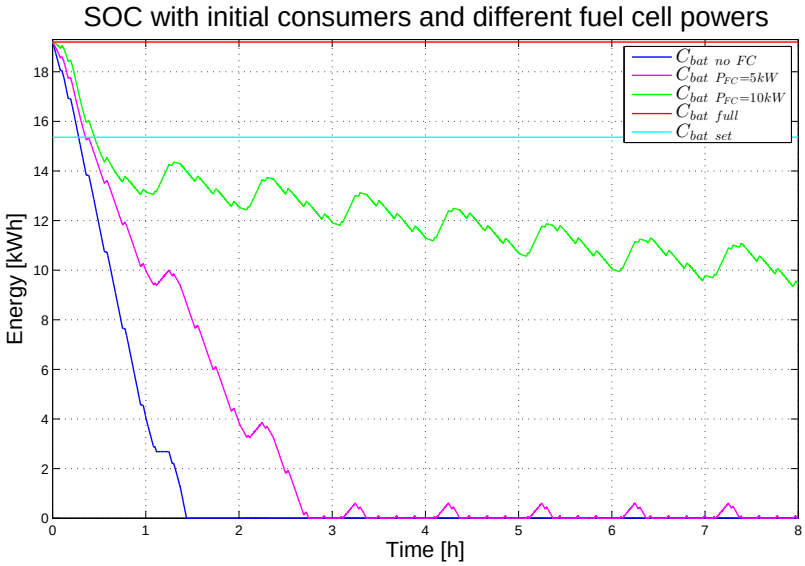

Fig. 2.9: Plot of the state of charge of the battery of the vehicle during the specified drive cycle with the initially estimated consumers and different fuel cell sizes.

The vehicle can run 1.5 hours without an RMFC system, 2.75 hours with a 5 $[kW]$ RMFC system and all day with a 10 $[kW]$ RMFC system. The average fuel cell power is 9.6 $[kW]$ and the methanol consumption is 88.37 $[L]$, which is not quite enough to sustain the battery state of charge.
On the basis of these simulations, it was concluded that a battery size of 19.2 $[kWh]$ will be sufficient to demonstrate the functionality of the electrified vehicle without a RMFC system and that an RMFC powered street sweeper can function.
To demonstrate that adding an RMFC system to the vehicle makes sense, the battery size was increased in a series of simulations until it was large enough to power the vehicle during a full drive cycle. Figure 2.10 shows a plot of the battery SOC during the final simulation.

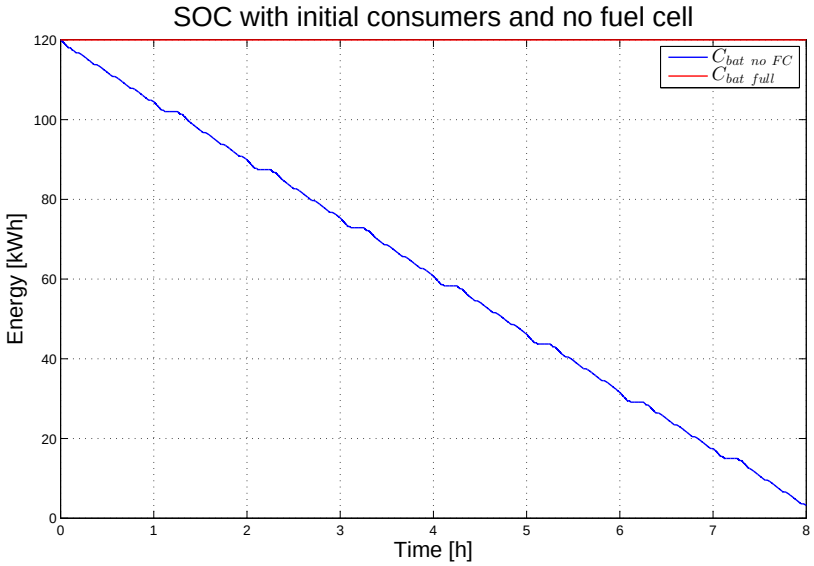

Fig. 2.10: Plot of the state of charge of the vehicles battery during the specified drive cycle with no fuel cell and sufficient battery capacity.

As the figure shows, a battery size of 120 $[kWh]$ is necessary. This is not practically possible because this battery would weigh 4974 $[kg]$ which is more than twice the vehicle weight.

1.2 Updated simulations

Nilfisk Outdoor Division and Nilfisk Advance have worked on the efficiency of the consumers of the street sweeping machine. The consumer constants achieved by the end of the project appear from table 2.2.

Parameter	Value %
$P_{Suction}$	8.7 $[kW]$
$P_{Brushes}$	1.4 $[kW]$
P_{Misc}	0.41 $[kW]$
C_{fric}	0.03 $[-]$

Table 2.2: Updated consumer constants.

When compared to the numbers in Table 2.1, the suction power ended up close to the initial estimate but the power for the brushes, miscellaneous consumers and the friction losses where all reduced. Figure 2.11 shows a plot of a simulation conducted with updated consumer constants.

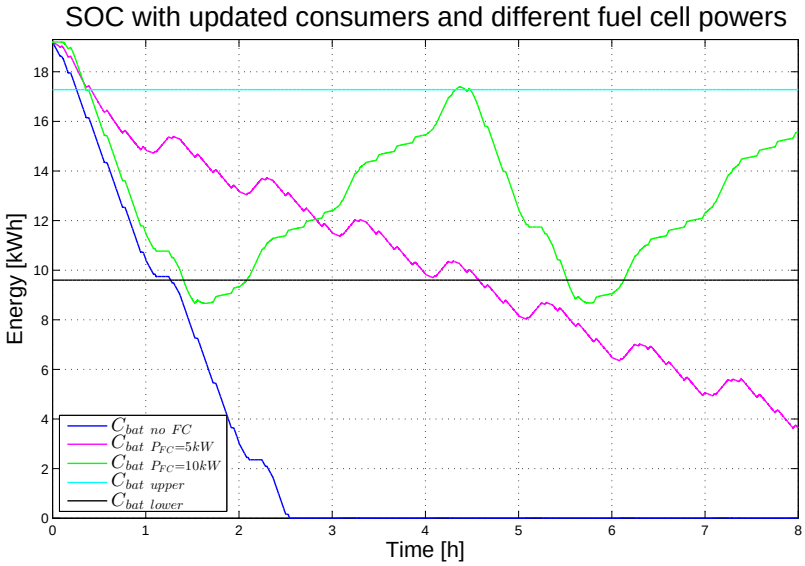

Fig. 2.11: Plot of the batteries state of charge during the specified drive cycle with the updated consumers and different fuel cell sizes.

As the figure shows, the output current of the RMFC system is controlled using the hysteresis method, where the module is turned on with a constant fuel cell current when the battery SOC is below 50% and then back off when the SOC is above 90%. This is the standard control method for RMFC systems. The figure also shows that the vehicle can run 2.5 hours with no RMFC system. With a 5 $[kW]$ RMFC system the battery is drained during the drive cycle but it can run for 8 $[h]$ with a methanol consumption of 43.84 $[L]$. With a 10 $[kW]$ RMFC system it can maintain the SOC during the day. The average fuel cell power is 6.28 $[kW]$ and the methanol consumption is 62.13 $[L]$.

An investigation of the accumulated power losses in the vehicle shows that the loss in the RMFC system is 226.7 $[kWh]$ and the loss in the battery is 6.5 $[kWh]$. This means that the dominating power loss in the hybrid system is that of the RMFC system. It is therefore relevant to minimize this loss via proper control if it is possible. The following section will therefore present a method to do this.

1.3 Charge control

It is observed in the simulation performed with the updated consumers in Figure 2.11 that using the standard method of hysteresis control, the RMFC system always runs on full power where it has its lowest efficiency. The

constant difference between the RMFC power output and the load power demand also means that a lot of power is moving in and out of the battery, further decreasing the overall efficience.
It is also noted that the RMFC system is switched of and then back on again during the drive cycle leading to extra fuel cell degradation as observed in [36].
A SOC control is therefore developed in this project to see if the fuel consumption of the vehicle can be decreased by running a more constant RMFC power and if the start/stop operation can be eliminated.
The controller developed is a PI-controller with an added feedforward of an average of the power consumption of the load and anti-windup. Figure 2.12 shows a diagram of the controller.

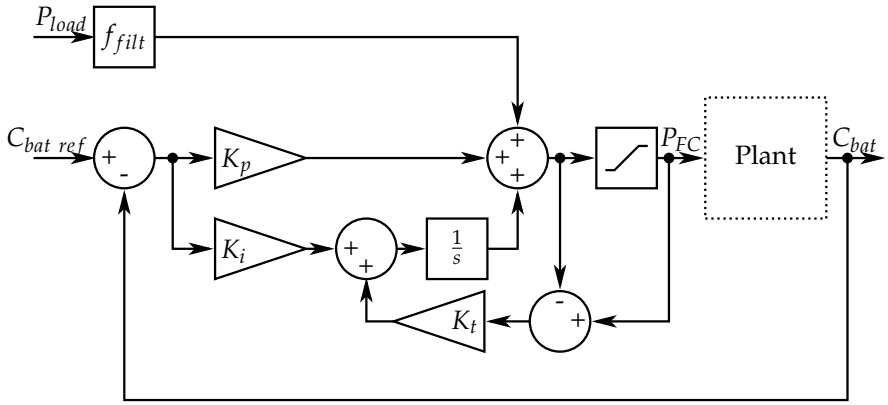

Fig. 2.12: Diagram of the implemented power controller.

K_p is set to 2, K_i to 0.001 and K_i is set to 0.00025 using an iterative training approach. The feedforward signal is averaged over a period of 5000 $[s]$ because this was found to have a good smoothing effect on the RMFC power set point.
To compare the SOC level controller with the standard hysteresis controller, the two are plotted together in Figure 2.13.

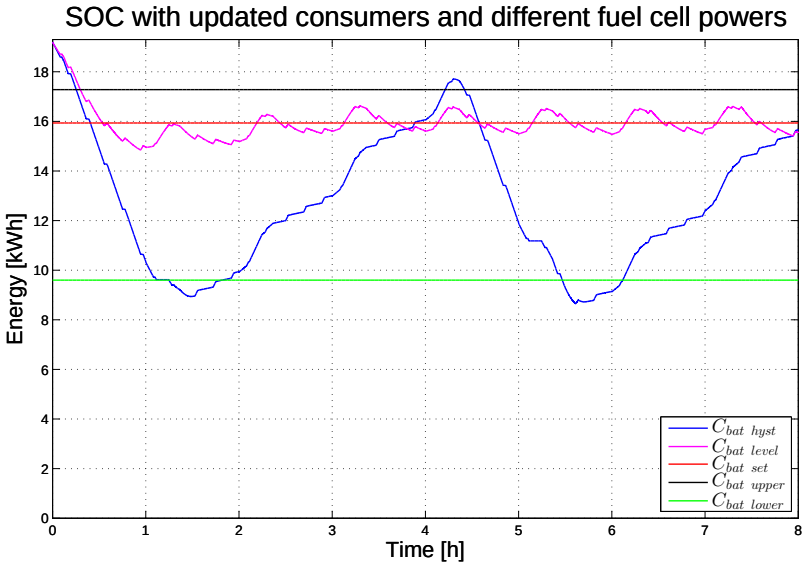

Fig. 2.13: Plot of the state of charge of the batteries during the specified drive cycle with hysteresis and level state of charge control.

The set point for the level controller is chosen to give the same SOC at the end of operation as the hysteresis control. With this set point, 83% SOC, the average fuel cell power is 6.3 $[kW]$ and the fuel consumption is 46.85 $[L]$.
With the hysteresis control the average fuel cell power is 6.72 $[kW]$ and methanol consumption is 62.13 $[L]$ including the 0.4 $[L]$ which is used for each module heat-up. This means that using the state of charge level controller instead of the standard hysteresis control saves 15.28 $[L]$ of methanol corresponding to 24.6% of the fuel consumption. In addition a start stop operation which is can lower the lifetime of the fuel cell is eliminated, but the operation time is increased by 2.37 $[h]$.
When the power loss in the RMFC system is analyzed again, it is found that it is now reduced to 170.3 $[kWh]$ and the loss in the battery is reduced to 3.2 $[kWh]$. This means that the reduced fuel consumption is mainly due to improved RMFC efficiency at achieved via the more constant RMFC output power.

1.4 Future prospects

The project partners believe that there are further possibilities for optimization of the vehicles consumers. This is especially the case for the suction power which it is believed can be reduced to 6 $[kW]$ via changes to the design of the suction unit. It is also believed that the power consumption of the

brushes can be reduced to 1 $[kW]$. It is also the plan to replace the lead acid battery of the test vehicle with a lighter, more efficient Li-ion battery.
To give an impression of how this vehicle could perform, a simulation with a 10 $[kWh]$ Winston WB-LYP400AHA Li-ion battery with an energy density of 10.88 $[kg/kWh]$ is made. Efficiency data for this battery is not available and 5% efficiency is added throughout the range of the battery.
Figure 2.14 shows a plot of the battery SOC during a simulation performed with these constants and a 5 $[kW]$ RMFC system.

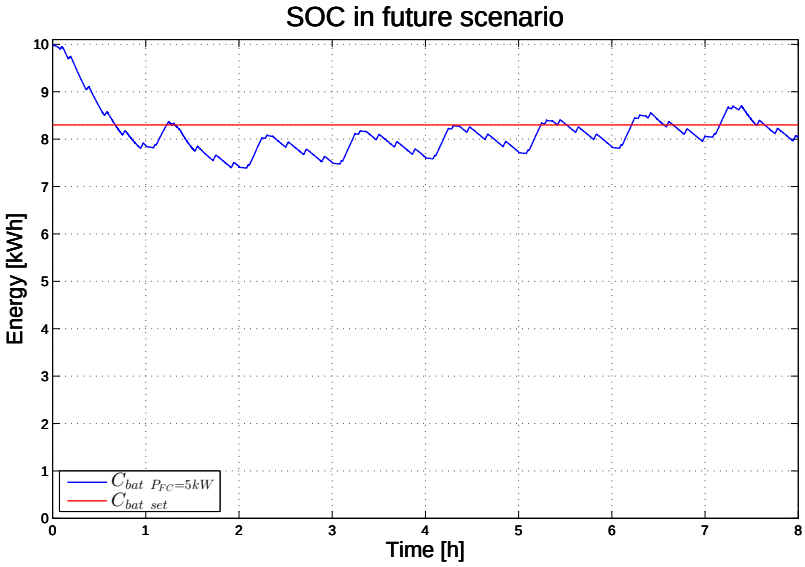

Fig. 2.14: Plot of the state of charge of the vehicles battery during the specified drive cycle with hysteresis and level state of charge control.

In this scenario, a 5 $[kW]$ RMFC system is enough to sustain the SOC of the battery, and the methanol consumption is 42.08 $[L]$. This is a further 10.2% reduction of the fuel consumption.

1.5 Conclusion

In this section a model of the ORACLE test vehicle was presented. The model has proved to be a powerful tool for predicting the performance of the vehicle and optimizing it based on simulations. The model was used to analyze the expected performance of the test vehicle after its electrification. After the realization of the test vehicle, the model was used to analyze the effect of implementing a charge controller and it was found that this could lower the fuel consumption by 24.6% and eliminate a start/stop operation. This happens at

the cost of a 2.37 $[h]$ extension of the operation time.
A simulation of a possible future scenario where the consumers of the vehicle are optimized further, shows that it is realistic to run an RMFC powered street sweeping machine on one 5 $[kW]$ H3 5000 module.
It is, however, worth noting that this type of controller is not directly implementable in the H3 5000 RMFC control systems of the module. This is because the controllable parameter in these systems is the fuel cell current and not the output power or current of the module. In the following chapter a proposal for a solution to this problem will be given, along with other suggestions on how to optimize the efficiency of RMFC systems based on system models.

Chapter 3

Reformed methanol fuel cell modeling and optimization

RMFC systems are a relatively new technology and there is therefore a great potential for optimization of the operating parameters and control systems of the system through modeling.
This chapter presents a series of models at a system level which can be used to analyze and optimize the operation of an RMFC system. First a model of the relationship between the fuel cell current and output current of an H3 350 module from Serenergy is presented. This model is then used to develop an output current controller which can be used to control the SOC of a battery to achieve the efficiency gains described in the previous chapter. This model is described in detail in paper **[C]**.
Next the efficiency of an H3 350 system is analyzed using a series of empirical models. First an Adaptive Neuro-Fuzzy Inference System (ANFIS) model of the HTPEM fuel cell is presented. More information on this model can be found in paper **[D]**. Next ANFIS models of the composition of the reformers output gas are constructed and used with the model of the fuel cell to calculate the system efficiency under the influence of changes in fuel cell current and reformer temperature. This procedure is described in more detail in paper **[E]**.

1 Output current control

As mentioned earlier, the controllable parameter in a RMFC system is the fuel cell current but it would be advantageous to be able to control the output current instead. This is because it makes it possible to control the state of charge of the battery in a hybrid system with an increase in system efficiency

as a result.
Figure 3.1 illustrates the difference between the fuel current and the output current of the module during a series of changes in fuel cell current for an H3 350 module.

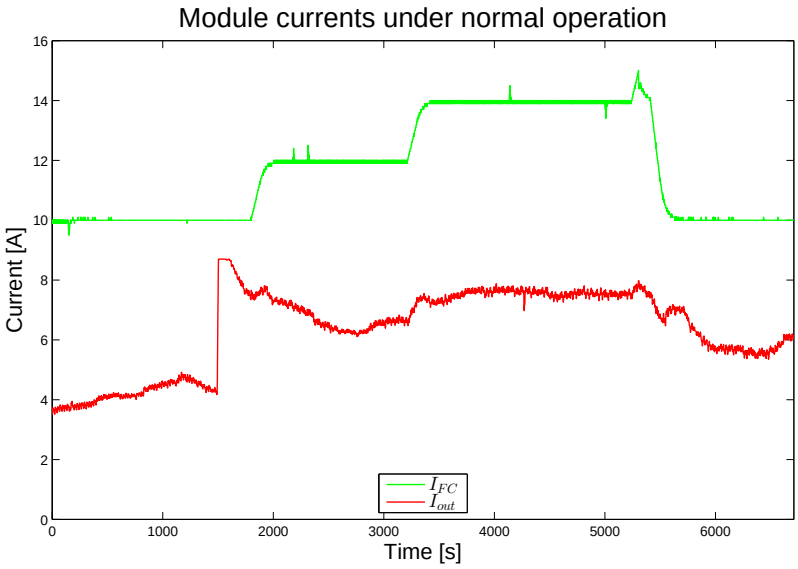

Fig. 3.1: Plot of the fuel cell and battery current during a series of steps in the fuel cell current of an H3 350 module.

There are several reasons for the difference between the two currents. First of all, some of the power produced by the fuel cell is used to power the RMFC systems Balance Of Plant (BOP) components, such as blowers, control electronics, fuel pumps and electric heating elements. Another reason is that the fuel cell and battery have different voltages and the DC-DC converter between the two bucks or boosts the current accordingly.
The fluctuation in the battery current which can be observed in the plot is due to changes in the BOP consumption.
To be able to design a controller for the output current of the module, models of the fuel cell and battery voltages have to be made as well as a model of the BOP consumption of the system. A detailed description of how these models are derived can be found in paper **[C]**. A block diagram of how the models are implemented in MATLAB Simulink can be seen in Figure 3.2.

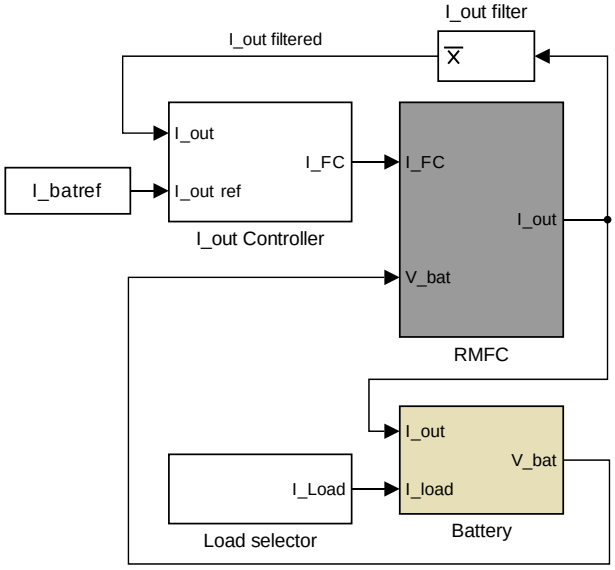

Fig. 3.2: Block diagram of the MATLAB Simulink model of the output current of the module.

A series of experiments have been performed to fit the parameters of the individual models. The experiments where performed on a scaled down version of the drive train of the street sweeping machine described in Section 2 of Chapter 2 and Figure 3.3 shows a diagram of this test setup.

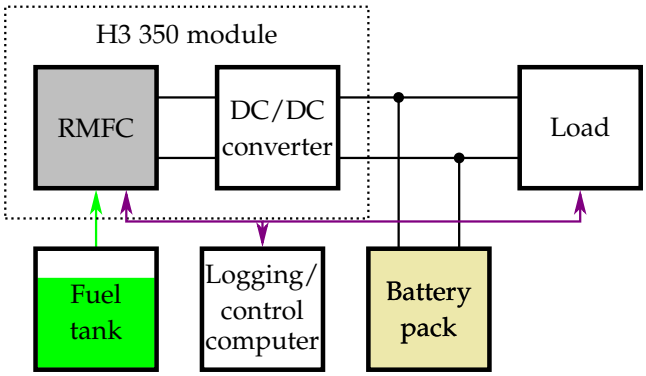

Fig. 3.3: Diagram of the test setup used in the experiments. Green lines indicate a fuel flow, purple lines indicate a communication bus and black lines indicate an electric current.

As the figure shows, the H3 350 module is connected in parallel to a battery pack and a programmable load module. The setup is controlled

by a computer which communicates with the H3 350 module and the programmable load module via CAN bus. The developed controller is implemented in a LabVIEW program which can override the controllers in the H3 350 module, making it possible to experiment with new types of control strategies for the system.

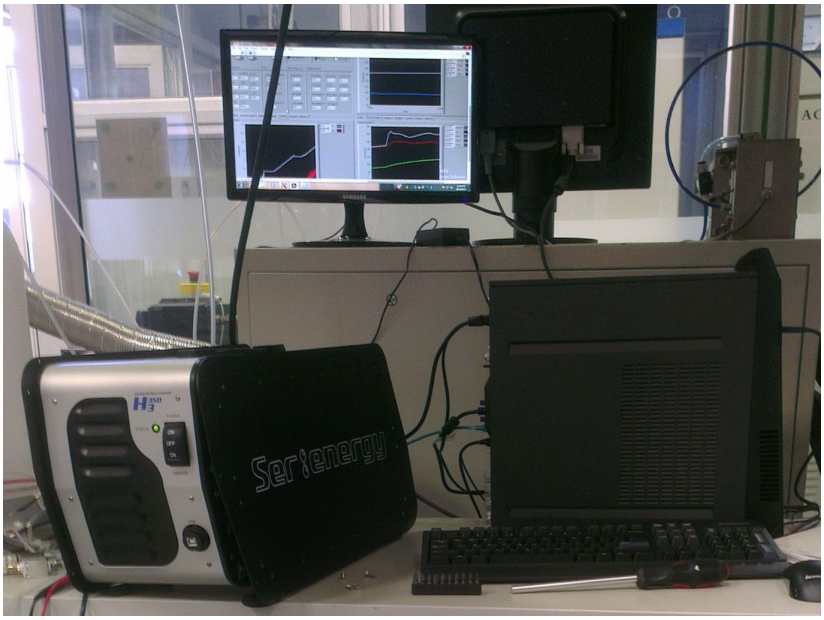

Fig. 3.4: Picture of the test setup used in the experiments. The batteries are stored under the table.

The fitting process is described in detail in paper **[C]** but here a few plots of the model fits are shown along with the model equations. The model of the battery consists of a constant open circuit voltage source and an equivalent circuit model consisting of a series resistor and a parallel resistor and capacitor. The transfer function of the equivalent circuit model can be seen in Equation 3.1.

$$V_{imp} = \frac{R_s \cdot R_p \cdot C_p \cdot s + R_p + R_s}{R_p \cdot C_p \cdot s + 1} \cdot I_{bat} \tag{3.1}$$

The fit of the model of the battery voltage during a step in the the battery current, which has been normalized around the initial voltage, is shown in Figure 3.5.

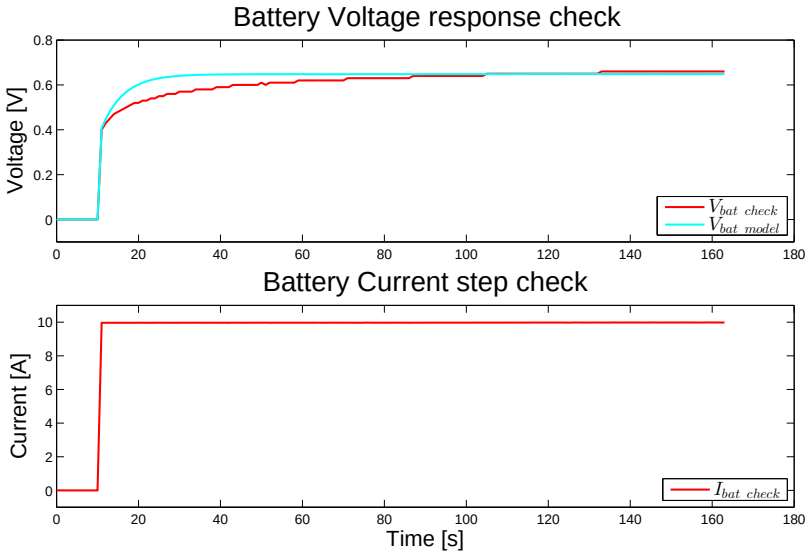

Fig. 3.5: Plot of the normalized battery current and voltage during the current step used to check the model fit during the fitting process of the battery model.

When the model is fitted on a separate data set, the fit is exact and the Mean Absolute Error (MAE) is 1.2% but during the checking experiment which is plotted in the figure, the MAE is 4.15%. The dynamics during the two steps are different and it is therefore not possible to make it fit in both cases. The steady state response does, however, fit in both cases and the model is considered valid for its intended purpose.
The fuel cell model consists of a look-up table containing a polarization curve and a first order system, which provides the fuel cell dynamics. The transfer function of the model is seen in Equation 3.2.

$$V_{FC} = \frac{1}{\tau \cdot s + 1} \cdot V_{FC\ RAW} \tag{3.2}$$

Because of the limits imposed on the rate of change of the fuel cell current by its integration in an RMFC system, it is not possible to make a step in the fuel cell current. Figure 3.6 therefore shows the fit of the model of the fuel cell dynamics during a ramped change in fuel cell current. Both voltage and current have been normalized around their initial conditions.

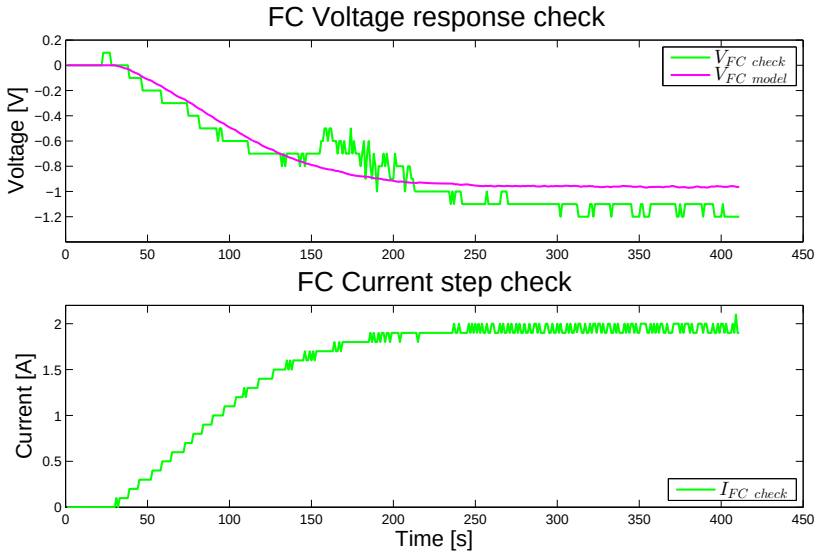

Fig. 3.6: Plot of the fuel cell current and voltage during the current step used to check the model fit during the fitting process of the fuel cell model.

The MAE of the model to the fitting data is 11.8% and the fit to the checking data is 14.9%. The magnitude of this error may seem high at first glance, but it is worth noting that it is primarily caused by a thermal phenomena in the reformer which changes the gas composition during the transition. The fit of the model can therefore not be improved without increasing the model complexity considerable, which would be very computationally heavy. Another factor which makes the error high is the normalization of the experimental data. If the error was calculated around the actual fuel cell voltage of $\approx 24\ [V]$ the error becomes 0.5%. The model is therefore considered to be valid for its purpose in the system model. The developed model also includes a model of the BOP consumer of the system. More details of these models can be found in paper **[C]**.
The controller which was developed in this work to control the output current of the RMFC system is a PI-controller with anti-windup and a feedforward in the form of the reference + a constant. Figure 3.7 shows a diagram of this controller.

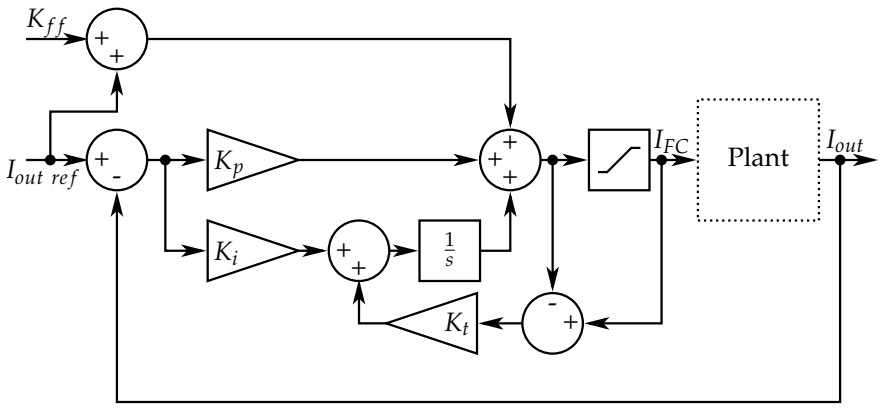

Fig. 3.7: Diagram of the developed output current controller.

Based on observations of the system, K_{ff} is set to 3 $[A]$. Based on an iterative approach K_p is set to 0.024 and K_i to 0.0192. The tracking time constant, K_t is set to the same value as K_i.
Figure 3.8 shows the response of the output current of the RMFC system to a series of steps in its set point as well as the raw controller output and the actual fuel cell current after the rate limiter.

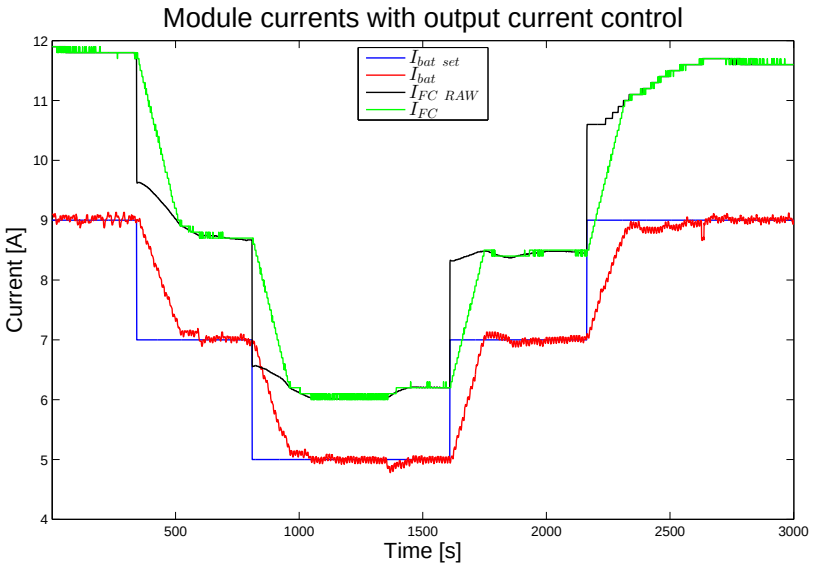

Fig. 3.8: Plot of the fuel cell and battery current during a series of steps in battery current set point using the developed controller.

As the figure shows, the controller is able to control the output current of the H3 350 module as intended and that it can compensate for fluctuations in the BOP consumption and changes in the battery voltage.

1.1 Integration of the output current controller in the vehicle model

To analyze if the developed output current controller can be used to achieve the efficiency gains described in Section 1.3 of Chapter 2, the fuel cell power set point from the vehicle model simulation is converted to a current. This is done by dividing the RMFC power from the simulation with the maximum RMFC power rating and multiplying it by the maximum output current rating of the modeled system. Figure 3.9 shows a plot of how the output current controller handles this current reference.

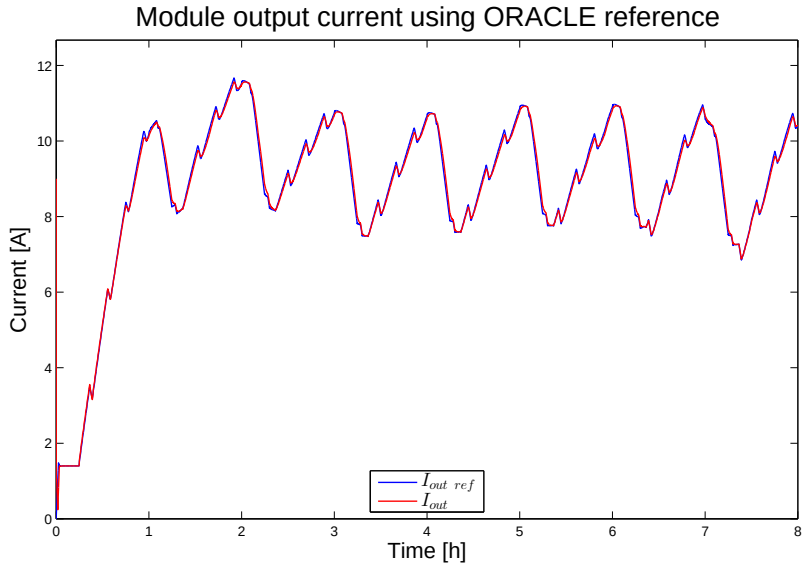

Fig. 3.9: Plot of the output current of the module and the output current reference generated from the ORACLE vehicle model.

As the figure shows, the controller is able to follow the output current reference and it is concluded that it is realistic to achieve the efficiency gains described in Section 1.3 of Chapter 2.

1.2 Model predictive control of the output current of the module

Because of the many disturbances affecting the output current of the module that were observed in the experiments, a more advanced controller structure which could actively compensate for them was considered. This is especially interesting as many of the disturbances, such as the changing power consumptions of the electric heaters and blowers in the system, are measurable. This is also the case for the load current which also affects the output current of the RMFC module by affecting the battery voltage.
The availability of linear models of the system gave rise to the idea of implementing them in a Model Predictive Controller (MPC) which can control a system by calculating the future optimal control signal based on model simulations. This has the added advantage that if a component of the system, such as the battery, is changed, the models can be updated and the controller will still work as intended. This could also be combined with an identification procedure, such as the one presented in paper **[C]**, which runs automatically at start-up. This would be ideal because the activation of the electric heaters of the module constitutes a step in the battery current. In this work the MPC control structure available in MATLAB has been used and it is as such not a new structure and more details can be found in [37]; only a general description of the structure is given here.
The basis for any model predictive control is a model of the system. The MPC used in this work uses a modified version of the state space models developed in the previous section. Here a model of a measured disturbance is added as an extra power consumption from the BOP of the RMFC system. The state space model is used in the MPC to calculate the system states and again in the quadratic optimization that calculates the optimal future control signal. The optimization is conducted over a prediction horizon of 10 samples and the control horizon is 2 samples. The sample time of the controller is 1 $[s]$ as this is the sample time used in the model. The optimization process can be made subject to constraints on the model states such as the range of the control variable and its derivative. This makes it ideal for the application at hand, because the rate of change of the control variable, which is the fuel cell current, must be constrained as described in Section 2 of Chapter 1. This means that there is no risk of encountering a wind-up phenomena in the controller and no modifications, such as anti-windup, needs to be implemented. The model structure used in the MPC can be seen in Figure 3.10.

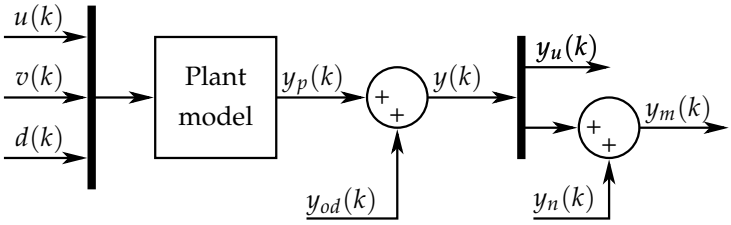

Fig. 3.10: Diagram of the model structure employed in the MPC controller used in this work.

Here $u(k)$ is the manipulated variable, in this case the fuel cell current, $v(k)$ is the measured disturbance, in this case a measured change in the BOP consumers and $d(k)$ is the unmeasured disturbances which is left blank in this initial implementation as is the unmeasured output disturbance $y_{od}(k)$ and the measurement noise $y_u(k)$. $y_u(k)$ is the unmeasured output and $y_m(k)$ is the measured output, in this case the module's output current.
Figure 3.11 shows a plot of a series of steps in the output current set point performed in the model using the PI controller presented in the previous section and the MPC controller presented in this section. A series of steps in a measured disturbance input is also performed in the simulation.

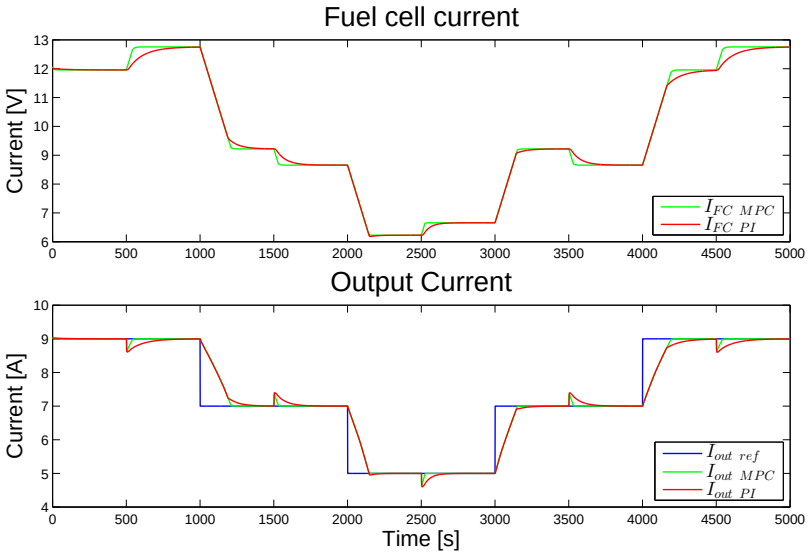

Fig. 3.11: Plot of a simulation of the output current of the module being controlled by PI and MPC controllers.

As the figure shows, both of the controllers are able to control the out-

put current of the H3 350 RMFC module both during the steps in set point and during disturbances. The MPC controller, however, performs the task faster with no added instability. As an example the peak in the output current caused by the disturbance at 1500 $[s]$ has a peak of 0.35 $[A]$ using the MPC controller compared to 0.4 $[A]$ using the PI controller. The error in the output current is below 0.1 $[A]$ in 24 $[s]$ using the MPC compared to 101 $[s]$ using the PI controller. It is therefore concluded that using an MPC controller to control the output current of an RMFC system could be beneficial. The controller was implemented in the LabVIEW program, which controls the test setup depicted in Figure 3.3. It was, however not possible to test the controller because of an unrelated firmware breakdown in the module. It is therefore concluded that MPC is a promising control algorithm for the output current control in RMFC systems, but further work is necessary to verify the effectiveness of the MPC in practice.

1.3 Conclusion

In this section a model of the output current of an RMFC system which has the fuel cell current of the system as input has been described. The model includes a model of the polarization curve of the fuel cell and an approximation of its dynamics, a model of the battery connected to the RMFC system and the BOP consumers of the system. This model was used to design a PI controller with feedforward and anti-windup which can control the output current of the RMFC system. The functionality of the controller was verified experimentally. The controller was tested in the model with a current reference matching the load profile experienced in the ORACLE vehicle model presented in Chapter 2 and it is concluded that the developed controller will make it possible to achieve the 24.6% efficiency increase observed in Section 1.3 of Chapter 2.
A model predictive controller for the output current controller was also developed based on the linear system models presented earlier in this chapter. The functionality of the controller was verified in the model, but it was not possible to test it in the experimental setup due to a hardware problem. The advantage of the MPC control is that it can compensate better for measured disturbances, such as changes in the BOP consumers or changes in the load current. If the MPC controller is combined with an automatic identification experiment at start-up, the MPC controller could become a useful part of the control system of the module.

2 Modeling of HTPEM fuel cells using ANFIS models

To further analyze the performance of the H3 350 module, it is necessary to construct models of the system components. In this section an Adaptive Neuro-Fuzzy Inference System (ANFIS) model of an HTPEM fuel cell under the influence of *CO* in the anode gas, changes in the fuel cell temperature and changes in the current density will be presented. First the modeling structure will be described and then the experiments performed to acquire training data and the training process itself will be described. More details of this model can be found in paper **D**.

2.1 Modeling structure

In this work the ANFIS modeling structure first presented in [38] is used. It is, as the name suggests a mixture of fuzzy logic and neural networks where the model parameters are adjusted on the basis of experimental data. This means that model structure leans from experience and imitates human reasoning in that regard. Figure 3.12 shows a diagram of this ANFIS structure with 3 input variables and 2 membership functions. Here $x_{1,2,3}$ are the input variables and y is the output of the model.
Layer (1) one in the modeling structure is the fuzzification layer where the crisp inputs are turned into fuzzy variables, i.e. numbers between 0 and 1 indicating the degree of membership of the variable to a fuzzy set. In a model with two membership functions, this can be interpreted as "to which degree is the input high" and "to which degree is the input low". Membership functions can take many different shapes, but in this case bell-shaped membership functions of the following form are used:

$$O_{1,1} = \mu_{A_1}(x_1) = \frac{1}{1 + \left|\frac{x_1 - c_1}{a_1}\right|^{2b_1}} \tag{3.3}$$

Here $O_{1,1}$ is the degree of membership of the first input variable x_1 to the fuzzy set "low" and a_1, b_1 and c_1 are adaptive premise parameters which determine the shape of the membership function. The premise parameters are subject to optimization during the training process.
In layer (2) the rule base of the model is established and there is one rule for each combination of membership functions. This explanation will follow the calculation of the contribution of the first rule to the output of the model. The path of this rule is marked in red on Figure 3.12. In layer (2) the firing level, or level of activity, of each rule is calculated using the Fuzzy AND according to Equation 3.4:

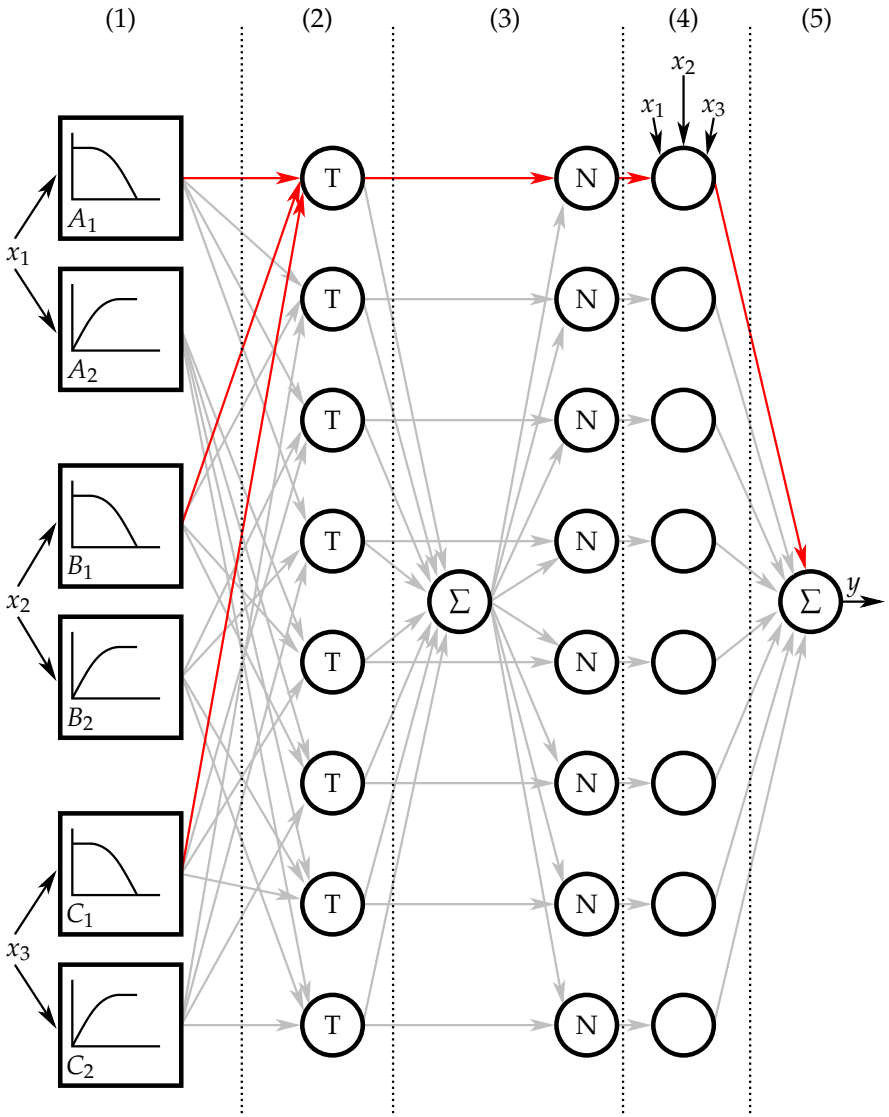

Fig. 3.12: ANFIS modeling structure.

$$O_{2,1} = w_1 = \mu_{A_1}(x_1) \cdot \mu_{B_1}(x_2) \cdot \mu_{C_1}(x_3) \tag{3.4}$$

Where w_1 is the firing level of rule 1 which can be interpreted as "to which degree are x_1 AND x_2 AND x_3 low?".
In layer (3) the firing levels of the rules are normalized. This means that their sum will be 1 after this layer:

$$O_{3,1} = \bar{w}_1 = \frac{w_1}{\sum_{i=1}^{n} w_i} \tag{3.5}$$

Here n is the number of rules in the rule base and $\bar{w}_1$ is the normalized firing level of rule 1.
In layer (4) the contribution of each rule to the output of the ANFIS model is calculated according to:

$$O_{4,1} = \bar{w}_1 \cdot f_1 = \bar{w}_1 \cdot (o_1 \cdot x_1 + p_1 \cdot x_2 + q_1 \cdot x_3 + r_1) \tag{3.6}$$

Where f_1 is the output function of rule 1 and is a linear combination of the inputs of the model and the consequent parameters o_1, p_1, q_1 and r_1. The consequent parameters are subject to optimization during the training process.
In the final layer, the output of the model is calculated as the sum of the contributions of each rule:

$$O_5 = \sum_{i=1}^{n} O_{4,i} \tag{3.7}$$

For the models to imitate a physical system they have to be trained accordingly. The following section describes how this is done.

2.2 Training process

When a training data set which represents the entire operating range of the system which is to be modeled is produced, the training process can begin. The process is performed over either a predefined number of iterations or until a certain precision demand is meet.
Before the training starts, the membership functions are initialized with values that split the ranges of the input variables in the training data set in equal parts. Then the first part of the training iteration, the forward pass, where the model is evaluated up to layer (4) for each point in the training data set is performed. This is illustrated in Figure 3.13 for a model with 2 inputs and 2 membership functions.

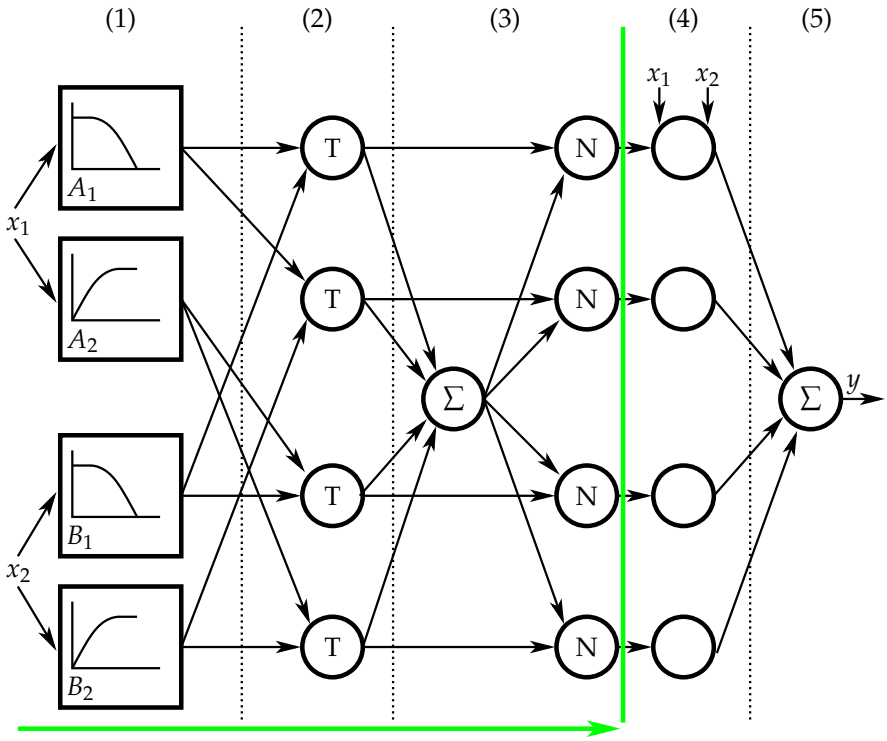

Fig. 3.13: ANFIS modeling structure during the forward pass of the training process.

The adaptive consequent parameters in layer (4) are then updated using least squares regression.
The second part of the training iteration is the backward pass, illustrated in Figure 3.14, where the premise parameters are updated using gradient descent methods using the premise parameters calculated in the forward pass.

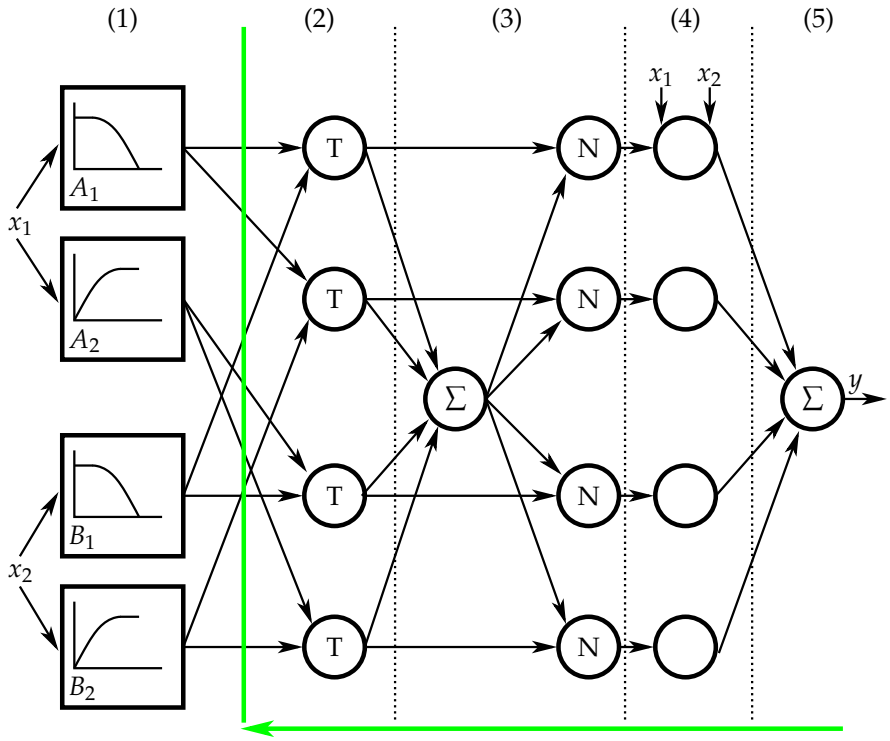

Fig. 3.14: ANFIS modeling structure during the backward pass of the training process.

This process is repeated for the specified number of iterations or until the precision demand has been achieved.

2.3 Identification experiment

For the ANFIS model to give an accurate representation of the performance of the fuel cell at all operating points, an experiment which spans the entire operating range of the system should be performed.
Experiments with the reformer in an H3 350 unit show that CO concentrations between 0.2 and 1.9% can be expected, and the identification experiment is therefore performed at 8 equally spaced points in this range. The typical operating temperature of the HTPEM fuel cell is 160 to 170 $[°C]$ and the identification experiment is repeated at temperatures of 160, 165 and 170 $[°C]$. At each of the 24 points that is formed by these variables, a polarization curve is made for the fuel cell. The maximum rated current density of the fuel cell is 0.6 $[A/m^2]$ and the minimum cell voltage allowed is 0.4 $[V]$. Each polarization curve will therefore start at 0 $[A/m^2]$ and be ramped up to the level where the first of these conditions.

This identification experiment is performed on the HTPEM fuel cell stack pictured in Figure 3.15.

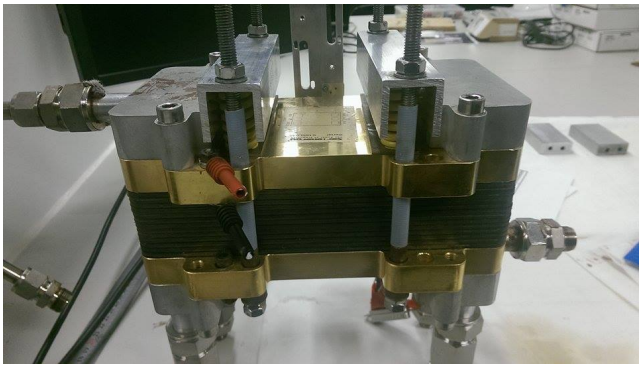

Fig. 3.15: Fuel cell short stack used in the identification experiment.

The fuel cell stack is a 14-cell version of the one in an H3 5000 RMFC system and uses the same type of membrane as the fuel cell in an H3 350 system and its performance when compensated by the cell area is expected to be representative of both.
Figure 3.16 shows a plot of the data from the identification experiment performed at 170 $[^{\circ}C]$.

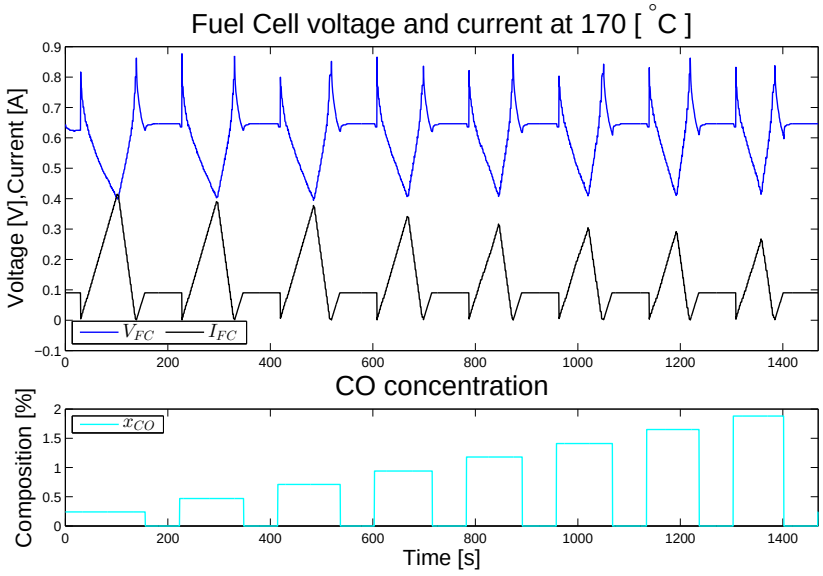

Fig. 3.16: Plot of the fuel cell voltage, current and anode *CO* concentration during the experiment.

As the figure shows, the stop condition for all operating points has been the minimum fuel cell voltage of 0.4 $[V]$. This is because the fuel cell was in an advanced state of degradation when the experiment was performed. This means that the developed models will only be valid for a fuel cell in this state of degradation but the results are, nevertheless, suitable for a proof of concept for the modeling procedure.

To better visualize the results of the experiment, each polarization curve read with 0.01 $[A/cm^2]$ intervals and arranged into three matrices. One for each temperature. These matrices are plotted in the contour plot of Figure 3.17.

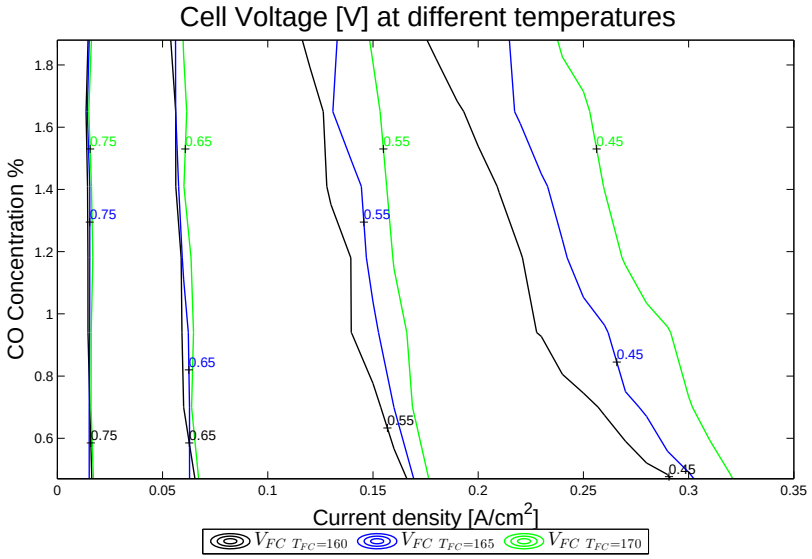

Fig. 3.17: Fuel cell voltage at T_{FC} of 160, 165 and 170 $[°C]$.

As the figure shows, the addition of *CO* to the anode gas has little influence at low current densities, but as the current density increases, the detrimental effects of *CO* increase as well. The fuel cell temperature also has little effect on the fuel cell voltage at low current densities, but at higher temperatures the fuel cell voltage is generally higher and the addition of *CO* to the anode gas has a less influence. This is in accordance with what is observed in literature [39] [40].

In paper **[D]** models with different numbers of membership functions are constructed and their precision, training time and evaluation time is evaluated. It is concluded that going beyond 2 membership functions yields little

reward and increases the training and evaluation time considerably. Figure 3.18 shows the response of the model with two membership functions.

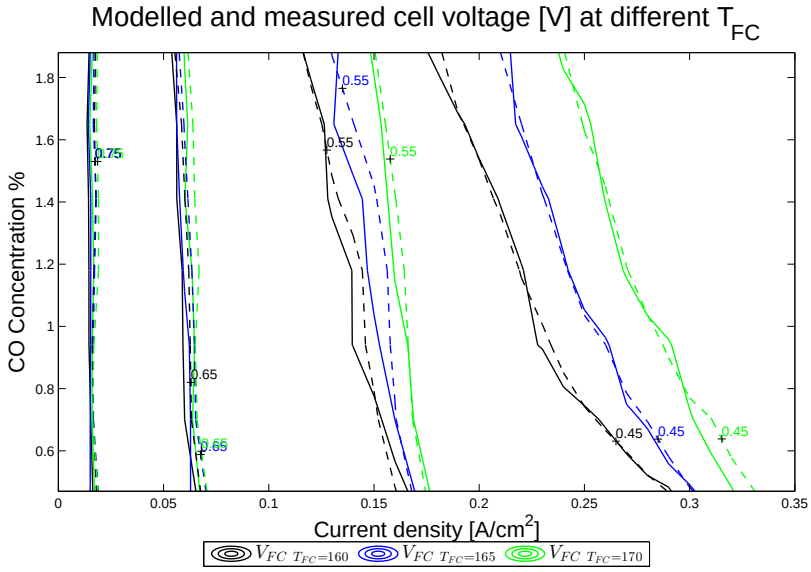

Fig. 3.18: Contour plot of the fuel cell voltage in experiment and model at T_{FC} of 160, 165 and 170 $[^{\circ}C]$. The solid lines show the measured values and the dashed lines show the model response.

An analysis of the model performance shows that it has a MAE of 0.94%. To illustrate how the model works, the membership functions are plotted in Figure 3.19. This shows when the models consider each variable high or low. Figure 3.20 shows the normalized firing level of rule 1, marked in red on Figure 3.12 for a fuel cell temperature of 160 $[^{\circ}C]$.

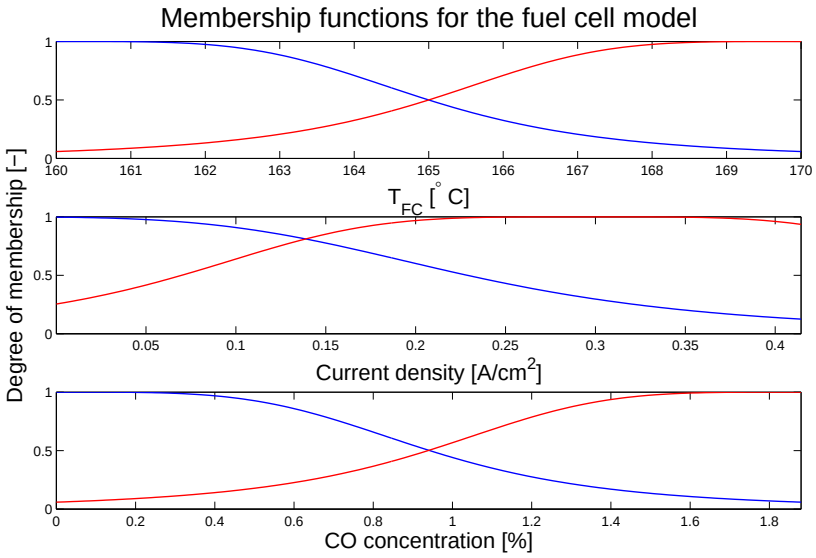

Fig. 3.19: Plots of the membership functions of the developed ANFIS models. The red lines represent the membership function of the fuzzy set "high" and the blue lines represent the set "low".

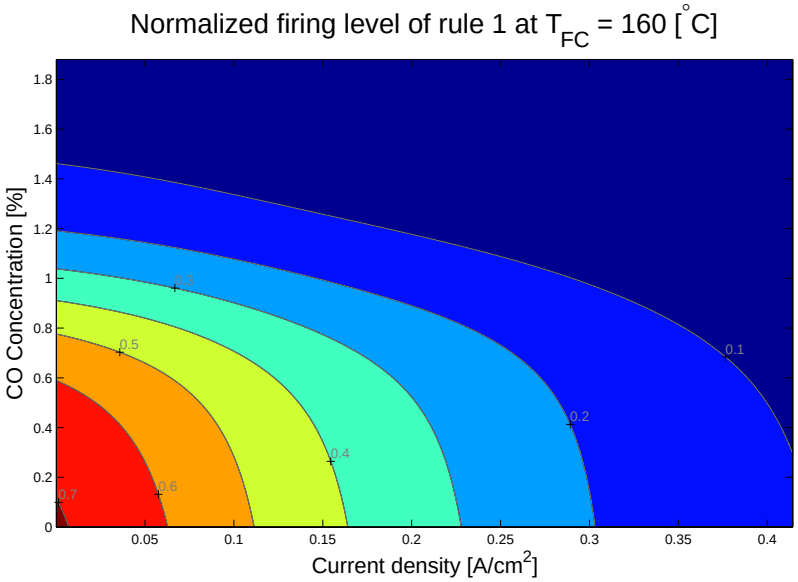

Fig. 3.20: Contour plot of the normalized firing level of rule 1 at $T_{FC} = 160\ [^{\circ}C]$.

As Figure 3.19 shows, there is an overlap between the fuzzy set "high" and "low". This means that all the rules contribute to the output of the model at all times. This is further illustrated by the normalized firing level of rule 1 in Figure 3.20. As would be expected, the firing level is highest when the current density and *CO* concentration are low. This is because rule 1 is associated with the fuzzy variable "low" for all its inputs. The output of rule 1 can now be calculated by multiplying the firing level by the output function of the rule. The output function of rule 1, f_1 in equation 3.6, is plotted in Figure 3.21 for a fuel cell temperature of 160 $[°C]$.

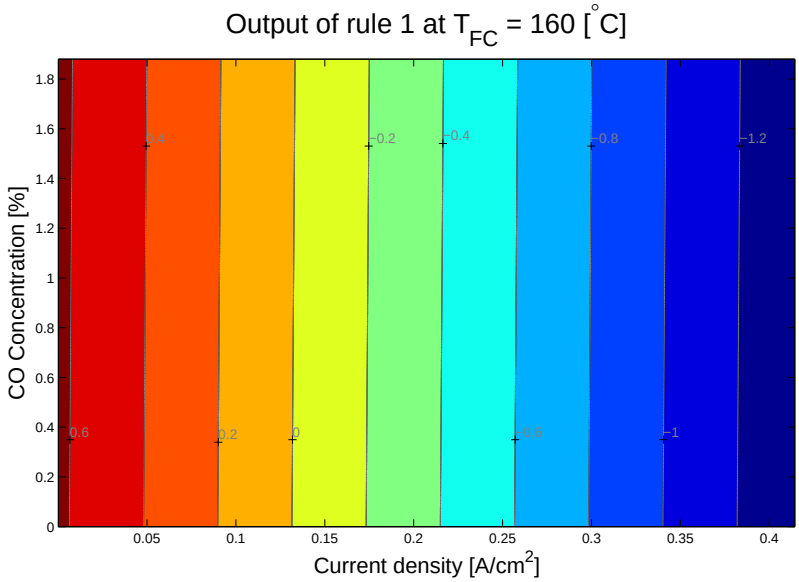

Fig. 3.21: Contour plot of the output function of rule 1 at T_{FC} = 160 $[°C]$.

As the figure shows, the values of f_1 are largest at low current densities and they are influenced relatively little by changes in *CO* concentration. This is what can be expected when observing the measurements in Figure 3.17 where *CO* has little effect at low current densities. To know how big the contribution of rule 1 is to the output, it has to be multiplied by the normalized firing level of the rule. This is plotted in Figure 3.22

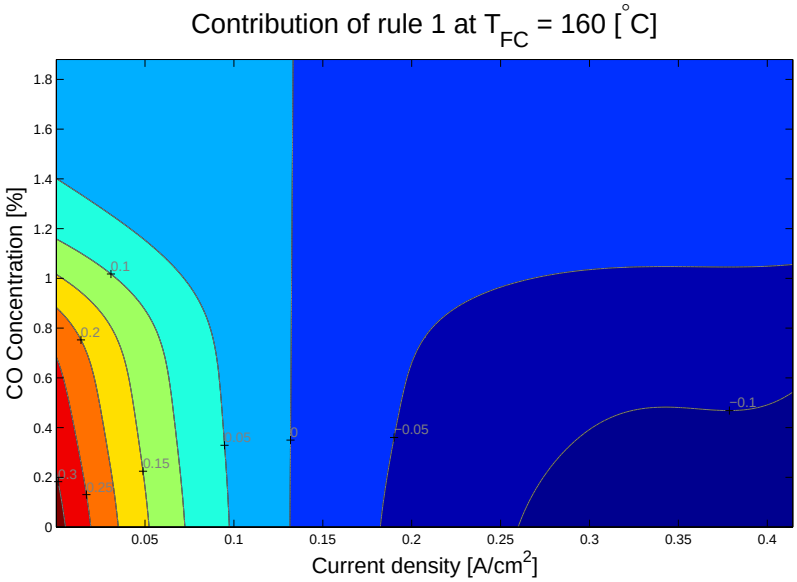

Fig. 3.22: Contour plot of the output contribution of rule 1 at $T_{FC} = 160\ [^{\circ}C]$.

As the figure shows, rule 1 has the largest effect at low current densities and low *CO* concentrations and relatively little influence elsewhere.

2.4 Conclusion

In this section an experiment where an HTPEM fuel cell, of the same type as that used in an H3 350 or H3 5000 system, was operated at different temperatures, anode gas compositions and current densities spanning the expected operating range. An ANFIS model of the cell voltage in the fuel cell stack was then trained using the fuel cell temperature, anode *CO* concentration and current density as inputs. It was concluded that increasing the number of membership functions beyond 2 does not add any additional accuracy but increases the training and evaluation time of the model unnecessarily. The developed ANFIS model has a MAE of 0.94% and it is concluded to be valid for a steady state performance analysis of the fuel cell alone, or integrated in an RMFC system. The model could also be combined with a model of its dynamic behavior to analyze its dynamic performance. More details on the developed model can be found in paper **[D]** of this PhD thesis.
The developed model will be integrated with models of the output gas of the reformer to analyze the performance of an H3 350 system in the next section.

3 Optimal reformer operation

In an integrated system, such as an RMFC system, the operating conditions of one part of the system can influence other parts of the system. This is the case with the reformer temperature of an RMFC system, because it influences the reforming efficiency and the *CO* concentration in the anode gas supply of the fuel cell. This section presents a method for finding the optimal temperature for an H3 350 module based on ANFIS models of the fuel cell and the reformer output gas composition. Paper **E** describes this method in detail.

3.1 Reformer output gas modeling

To construct ANFIS models of the output gas of the reformer a series of identification experiments has to be performed. For this purpose a test setup where the fuel cell of an H3 350 module is replaced with a gas analyzer is made. Figure 3.23 shows a diagram of this test setup.

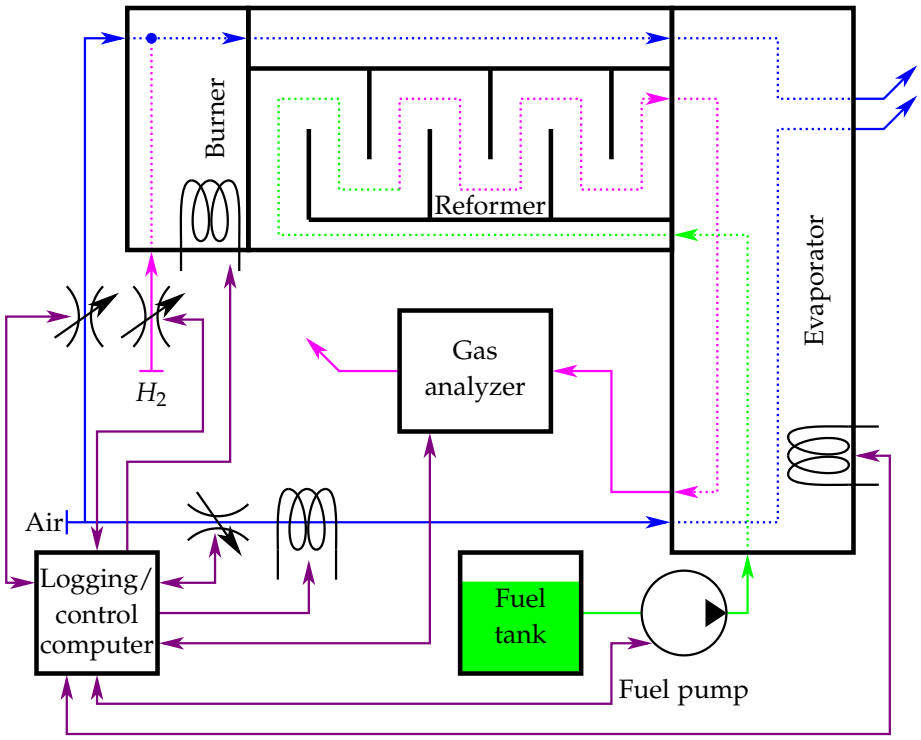

Fig. 3.23: Diagram of the test setup used in the reformer identification experiments. The magenta lines signify a hydrogen-rich reformed gas flow, blue signifies a flow which is predominantly atmospheric air, green represents a fuel flow and purple is a control or logging signal.

In this setup, the hot cathode exhaust air of the fuel cell is replaced by a mass flow controller and an electric heater. The H_2 rich anode waste gas of the fuel cell is replaced by a mass flow controller that matches the H_2 flow to the fuel flow. All the actuators of the system are controlled by a custom made control program which is implemented in a National Instruments cRIO controller. The reformer temperature controller used in the test setup is of the cascade type described in [41] and the setup is programmed to change operating point automatically.
Figure 3.24 shows a picture of this test setup.

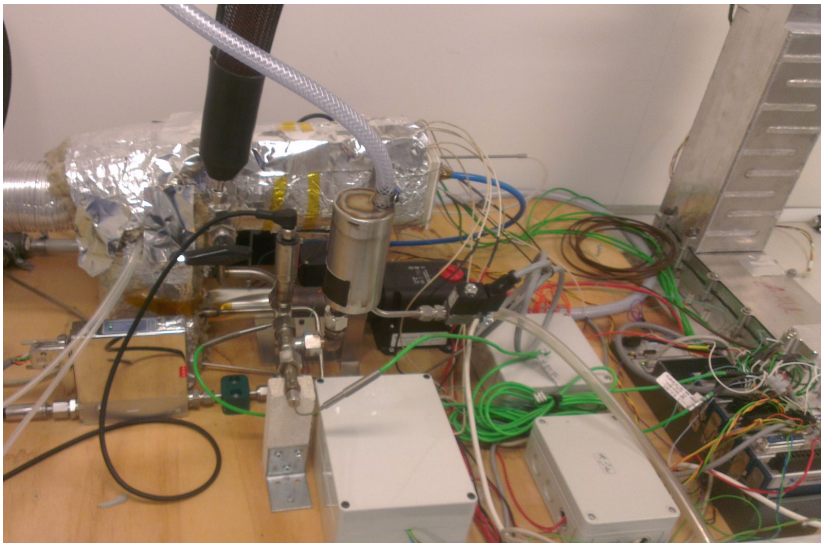

Fig. 3.24: Picture of the reformer test setup.

The reformer identification experiment is performed at 5 $[°C]$ intervals between 235 and 290 $[°C]$. At each temperature 5 equally spaced fuel flows corresponding to fuel cell currents between 5 and 18 $[A]$ with an anode stoichiometry of 1.35 are tested. Steady state conditions are achieved for 20 $[min]$ for each operating point. This experiment takes 28 $[h]$ and Figure 3.25 shows a plot of the temperatures of the reformer and burner measured during the experiment and Figure 3.26 shows a plot of the measured gas composition.

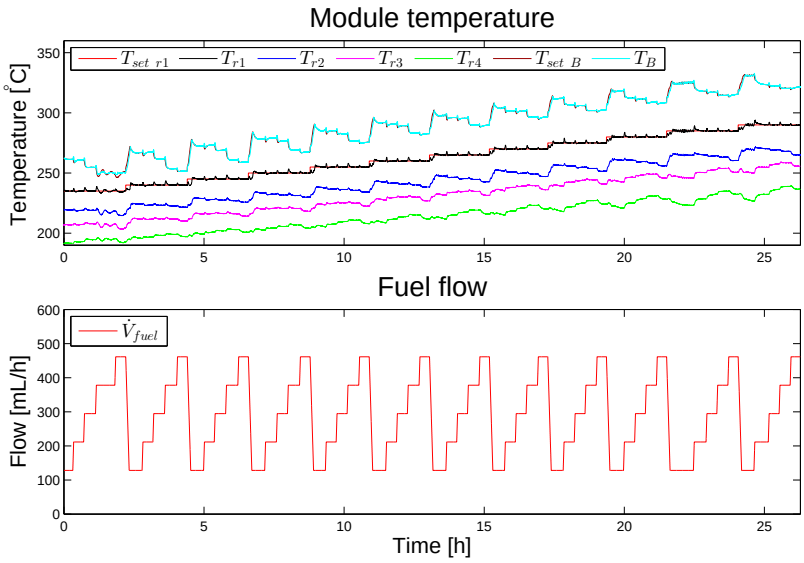

Fig. 3.25: Plot of the reformer and burner temperatures measured during a 28 $[h]$ identification experiment.

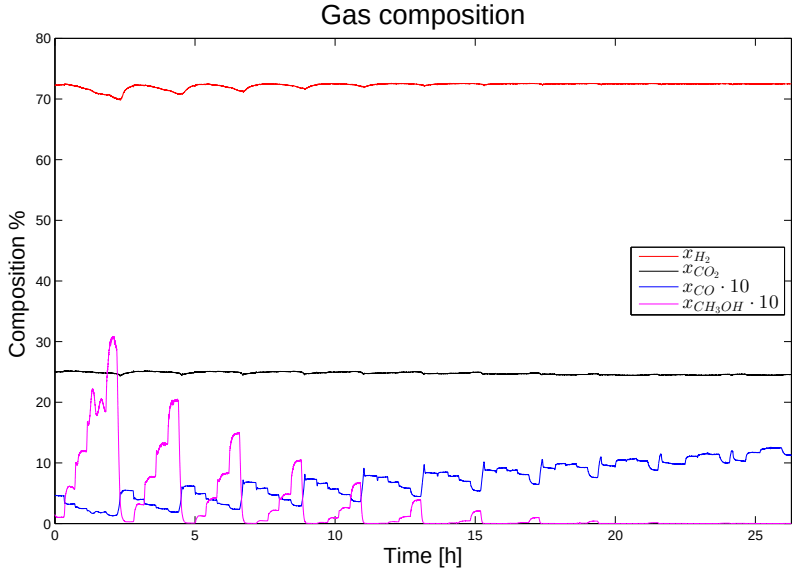

Fig. 3.26: Plot of the gas composition measured during a 28 $[h]$ identification experiment.

The plots show that the temperature of the reformer is controlled as in-

tended and that the reformer temperature and fuel flow have an effect on the gas composition as stated in Section 2 of Chapter 1. To evaluate this effect, the average values of the H_2 flow and CO concentration for each operating point is calculated and arranged into result matrices. Figure 3.27 shows the result matrix for the CO concentration.

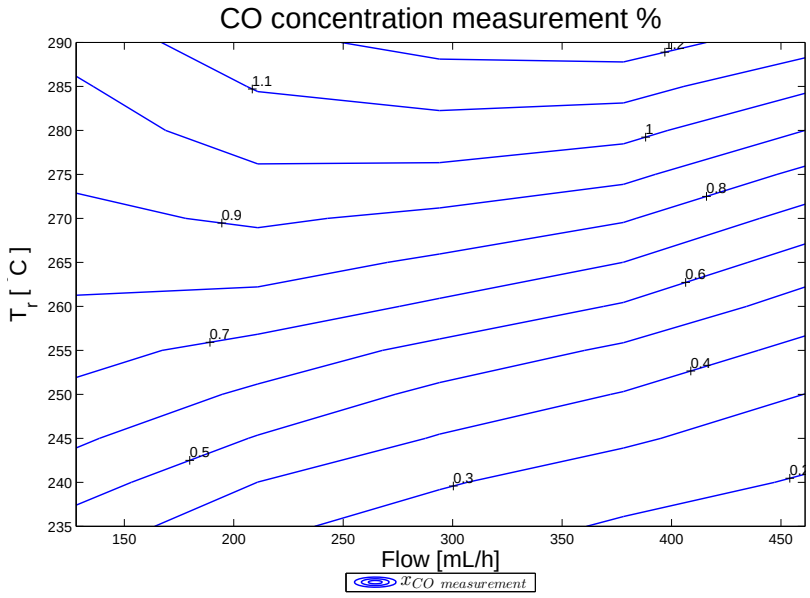

Fig. 3.27: Countour plot of the CO concentration measured in the identification experiment.

The x-axis of the contour plot shows the fuel flow into the reformer and The y-axis shows the temperature at the beginning of the reformer bed. The lines in the contour plot represent constant CO concentrations measured as a percentage of the molar flow in the output gas of the reformer. As literature would suggest, higher reformer temperature means higher CO concentration [42, 43]. At high fuel flows the CO concentration is generally lower than at low flows. This is most likely due to the cooling effect of the higher flow on the reformer bed and the higher space velocity of the fuel. Figure 3.28 shows a contour plot of the hydrogen flow matrix as well as the theoretical maximum achievable hydrogen flow.

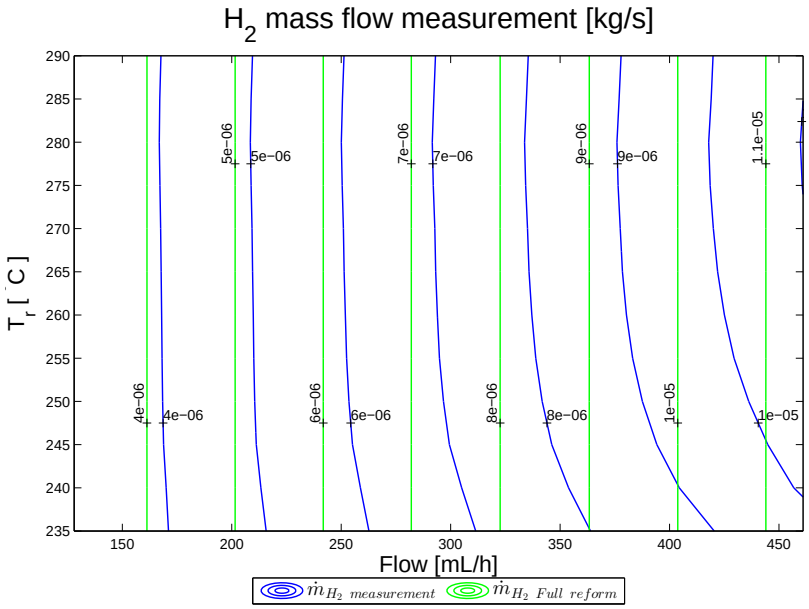

Fig. 3.28: Countour plot of the H_2 flow measured in the identification experiment.

Again the x-axis of the contour plot shows the fuel flow into the reformer and the y-axis shows the temperature at the beginning of the reformer bed. The green lines in the plot represent the mass flow of H_2 out of the reformer if the only reaction that took place in the reformer was the steam reforming reaction in Equation 1.3. The blue lines represent the actual H_2 flow measured in the experiment. As the figure shows, the reformer temperature has little influence at lower fuel flows and the measured H_2 flow is close to the theoretical max flow. However, at higher fuel flows, lower temperatures mean that the difference between the measured and theoretical max flow is increased. It is worth noting that even at low reformer temperatures and low fuel flows where the methanol slip is minimal, the maximum H_2 flow is not achieved. This is because the fact that CO is produced indicates that the methanol decomposition reaction in Equation 1.5 takes place which produces less hydrogen than the steam reforming reaction in Equation 1.3

The highly nonlinear behavior of both the CO concentration and H_2 flow of the reformer, and the lack of information about the factors which are causing them, it is chosen to use the ANFIS modeling structure described in Section 2.1 of this chapter again.
As opposed to the bell-shaped membership functions used in the ANFIS models of an HTPEM fuel cell presented in the previous section, triangular membership functions of the following form is used in the models of the

reformer output gas:

$$O_{1,1} = \mu_{A_1}(x_1) = max\left(min\left(\frac{x_1 - a_1}{b_1 - a_1}, \frac{c_1 - x_1}{c_1 - b_1}\right), 0\right) \tag{3.8}$$

Figure 3.29 shows a contour plot of the fit of the *CO* concentration model.

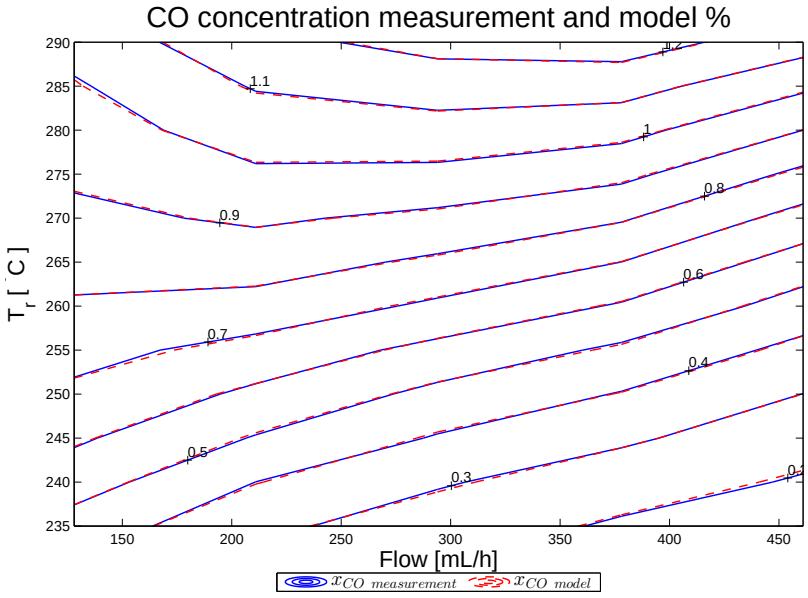

Fig. 3.29: Countour plot of the *CO* concentration measured in the identification experiment and the output of the developed ANFIS model.

Experiments show that using three membership functions gives the best compromise between model complexity and accuracy, and the MAE the model is 0.323%. It is concluded that the model is suitable for use in the optimization of the operating point of the reformer. Figure 3.30 shows a plot of the fit of the H_2 flow model.

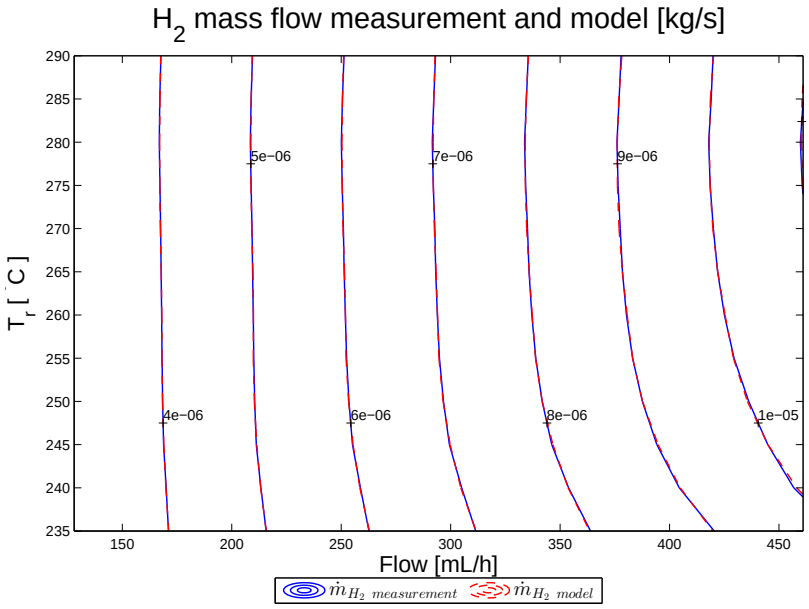

Fig. 3.30: Countour plot of the H_2 flow measured in the identification experiment and the output of the developed ANFIS model.

Again three membership functions result in the best compromise between performance and complexity and the MAE is 0.074% and it is concluded that it is also suitable for use in the optimization of the operating point of the reformer.

3.2 Calculation of system efficiency

To ensure that the desired anode stoichiometry is achieved at all times, a matrix of the necessary fuel flow at different reformer temperatures and fuel cell currents is needed. This is achieved using the developed ANFIS model of the hydrogen mass flow in the output gas of the reformer. This was done by calculating the necessary H_2 flow using the following equation:

$$\dot{m}_{H_2\ need} = \frac{\lambda_{H_2} \cdot N_{cell} M_{H_2}}{2 \cdot F} \cdot I_{FC} \tag{3.9}$$

Where λ_{H_2} is the desired stoichimetry of the fuel cell anode, N_{cell} is the number of cells in the fuel cell, M_{H_2} is the molar mass of H_2 and F is Faraday's constant.
The fuel flow which was necessary to yield this H_2 flow was then found using an iterative method and the ANFIS model described in the previous section. Figure 3.31 shows a plot of the necessary fuel flow matrix.

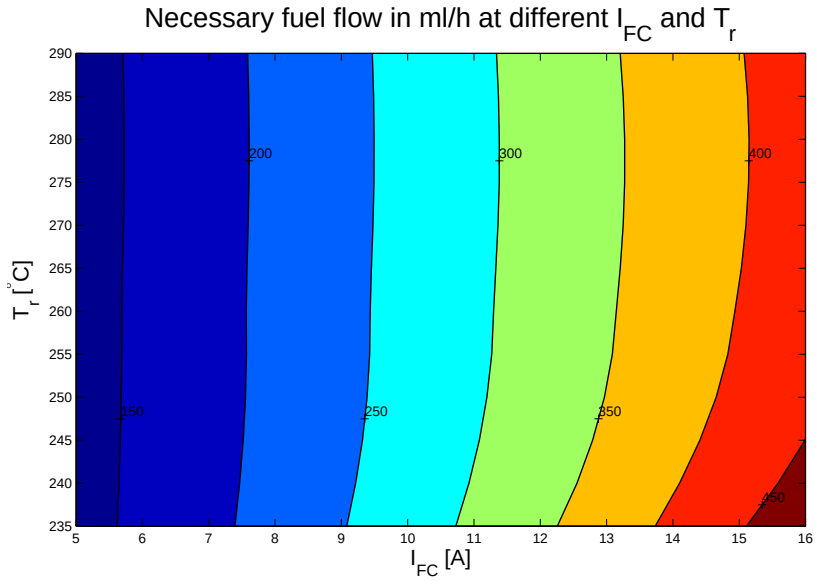

Fig. 3.31: Plot of the calculated necessary fuel flow at different fuel cell currents and reformer temperatures.

As expected on the basis of the plot of the H_2 mass flow in Figure 3.28, the necessary fuel flow is highly dependent on the reformer temperature, especially at higher fuel cell currents. This fuel flow matrix is not only useful in this optimization, but can also ensure that the H3 350 unit is operated with a sufficient H_2 supply at all times, if it is incorporated in the modules controllers.
The calculated fuel flow matrix is then used as an input for the *CO* model presented in the previous section to calculate the *CO* concentration of the anode supply gas at each operating point. Figure 3.32 shows the resulting *CO* content matrix.
The *CO* content matrix is then used as an input for the fuel cell model presented in Section 2 of this chapter. Figure 3.33 shows the resulting fuel cell voltage matrix, after the cell voltage has been multiplied by 45 which is the number of cells in the fuel cell stack of an H3 350 system.

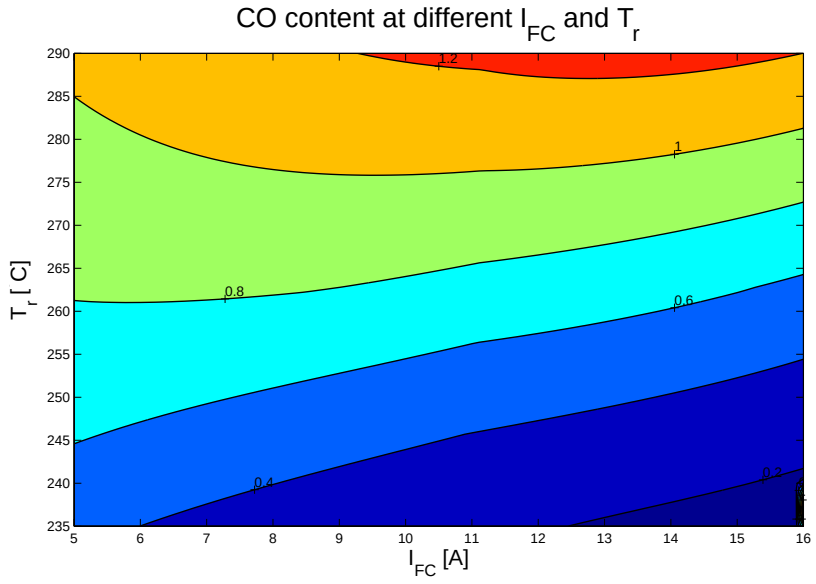

Fig. 3.32: Contour plot of the *CO* concentration at different fuel cell currents and reformer temperatures using the calculated fuel flow matrix.

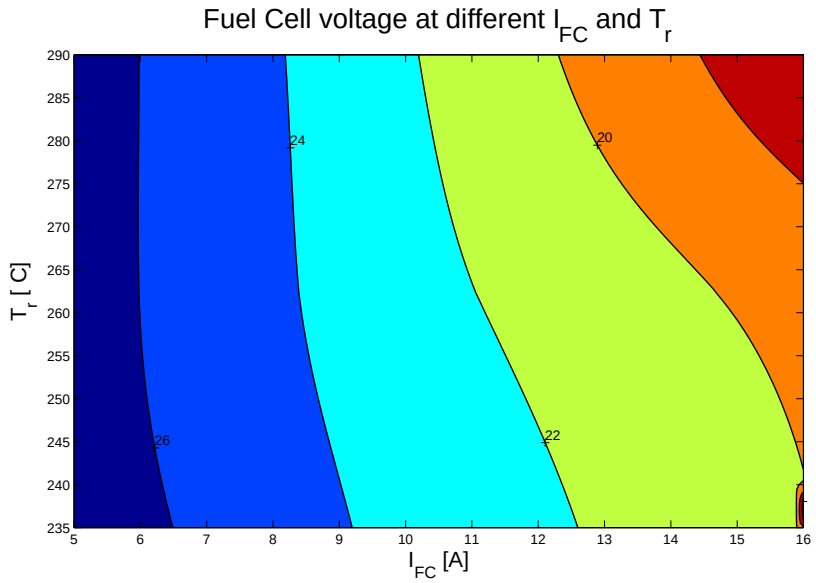

Fig. 3.33: Contour plot of the fuel cell voltage at different fuel cell currents and reformer temperatures using the calculated fuel flow matrix.

As the figure shows, the increasing *CO* concentration at higher reformer temperatures lowers the fuel cell voltage considerably as the fuel cell current is increased. This means that the output power of the system decreases when the reformer temperature is increased. This is illustrated in the contour plot of Figure 3.34.

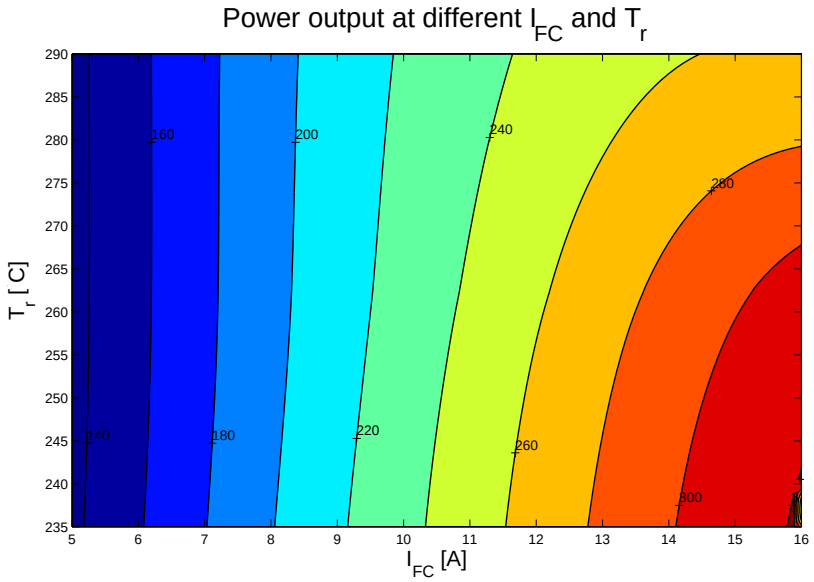

Fig. 3.34: Contour plot of the output power at different fuel cell currents and reformer temperatures using the calculated fuel flow matrix.

This figure seems to indicate that a low reformer temperature is good for the system efficiency. But as Figure 3.31 indicates, lower reformer temperatures lead to a higher necessary fuel flow and therefore a higher input power as illustrated in Figure 3.35.
This means that a compromise between low fuel flow and low *CO* concentration in the fuel must be reached. To find this optimum the system efficiency is plotted in the contour plot in Figure 3.36 along with a line indicating the optimal reformer temperature, a lower optimal temperature that eliminates nonlinear changes in reformer temperature, the optimal constant reformer temperature and the H3 350 modules standard reformer temperature of 290 $[^{\circ}C]$.

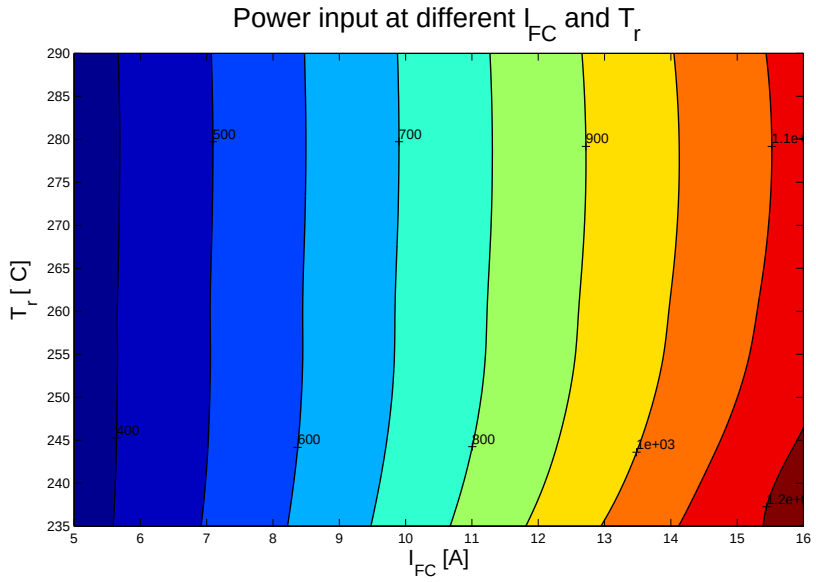

Fig. 3.35: Contour plot of the necessary input power at different fuel cell currents and reformer temperatures using the calculated fuel flow matrix.

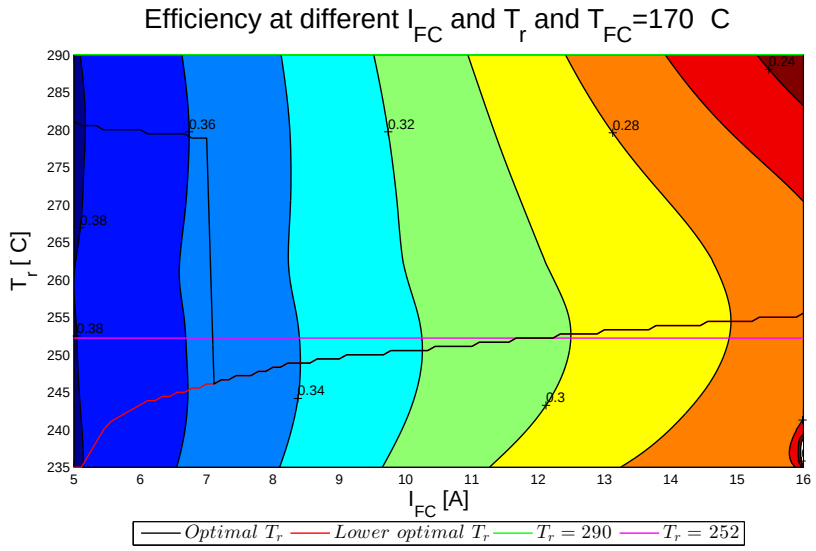

Fig. 3.36: Contour plot of the system efficiency and different reformer temperature control strategies at different fuel cell currents and reformer temperatures using the calculated fuel flow matrix.

To compare the efficiency of each of these reformer temperature control strategies, they are plotted in the top plot of Figure 3.37 and the efficiency deficit of each strategy to the optimal strategy is plotted in the bottom plot of the same figure.

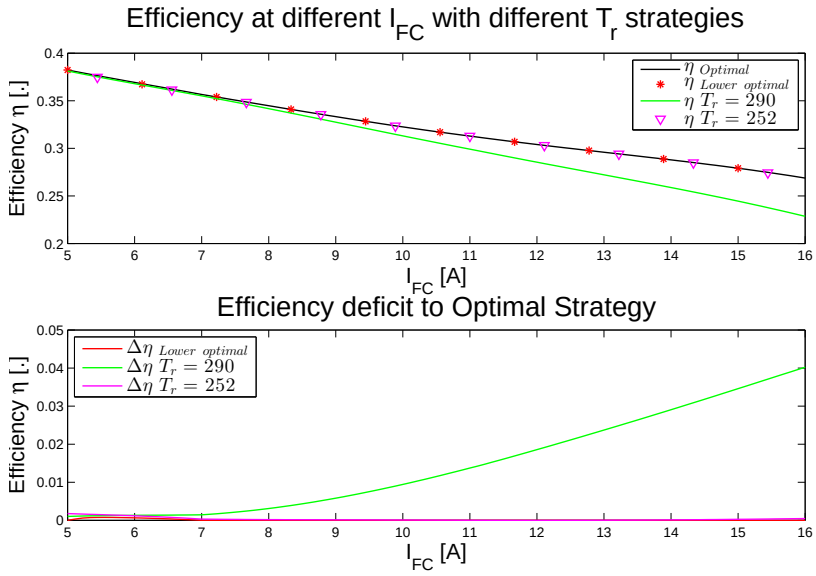

Fig. 3.37: Plot of the efficiency of the possible reformer temperature control strategies and the difference between them.

As the figure shows, the difference in performance of the three control strategies presented in paper **E** is relatively small, but the average gain compared to the standard reformer temperature is 1.47 percentage points and the gain at a fuel cell current of 16 $[A]$ is 4 percentage points.
The optimization described in this section was repeated with fuel cell temperatures of 160 and 165 $[^{\circ}C]$ and the average gain in efficiency that can be achieved is increased to 4.25 and 2.39 percentage points, respectively. This means that there is a significant performance gain to be had by lowering the reformer temperature from the present 290 to 252 $[^{\circ}C]$ and this is can be recommended, provided that this does not introduce any thermal stability problems in the reformer. In the experiments performed in the context of this PhD project no such problems where experienced.

3.3 Consequence for vehicle performance

It is assumed that the same efficiency optimization can be achieved for the RMFC module in the street sweeping machine described in Chapter 2. The efficiency gain is therefore normalized with respect to the output power and added to the RMFC efficiency model of Figure 2.7. The resulting efficiency curve can be seen in Figure 3.38.

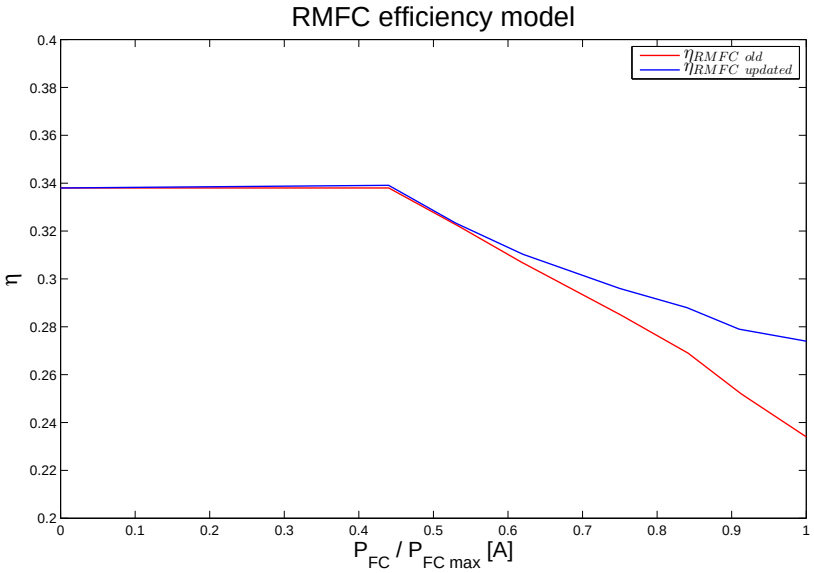

Fig. 3.38: Plot of the RMFC and battery efficiencies used in the model.

Using this updated efficiency curve, the methanol consumption is reduced to 44.7 $[L]$, a 2.15 $[L]$ reduction corresponding to a 4.6% reduction in the methanol consumption when the SOC controller developed in Section 1.3 of Chapter 2 is used. When the consumption is compared to that which is achieved using the standard hysteresis control, the total reduction in methanol consumption is 17.43 $[L]$ or 28%.

3.4 Conclusion

In this section ANFIS models of the reformers output gas were presented. They consist of a model of the *CO* concentration which has a MAE of 0.323% and a model of the H_2 mass flow which has an MAE of 0.074%. These models were combined with the ANFIS model of an HTPEM fuel cell presented in Section 2 of this chapter to give a matrix of the module efficiency with different fuel cell currents and reformer temperatures. It is concluded that

the efficiency of the system can be improved by an average of 1.47 percentage points across fuel cell currents and a gain of 4 percentage points at maximum fuel cell current.
If the gain in efficiency is normalized with respect to the fuel cell power and added to the RMFC efficiency model presented in Chapter 1, the methanol consumption of the RMFC powered street sweeper, which has been used as a case study in this work, can be reduced by 4.6%.
The matrix of the necessary fuel flow constructed in this section can also be used to ensure that the module has the correct H_2 supply at all fuel cell currents and reformer temperatures.

Chapter 4

Conclusion

In this chapter the results achieved in this PhD project will be summarized. This includes both the results of the modeling of a reformed methanol fuel cell powered street sweeping machine and the efficiency gains achieved using it, the modeling and control of the output current of an reformed methanol fuel cell module and the analysis of the efficiency of the module under changes in reformer temperature and fuel cell current.

1 Conclusion

In the context of the Outdoor Reliable Application using CLean Energy (ORACLE) project, a model of the power consumers of a street sweeping machine has been made. This includes approximate models of the drive-train, suction fan, brushes and miscellaneous small power consumers. This model was used to predict the effective operating range of the street sweeping machine, using conservatively high consumer constants, with different battery and fuel cell combinations before the prototype vehicle was constructed. It was concluded that a battery size of 19.2 $[kWh]$ would guarantee 1.5 $[h]$ of operation with no Reformed Methanol Fuel Cell (RMFC) system. This is extended to 2.75 $[h]$ with a 5 $[kW]$ RMFC system and a whole working day of 8 $[h]$ with a 10 $[kW]$ system. This was judged to be enough for a proof of concept. It was also calculated that a 120 $[kWh]$ battery weighing 4974 $[kg]$ would be necessary to power the vehicle on batteries alone, which justified further investigation into the concept of an RMFC powered street sweeping machine.
After the construction of the ORACLE test vehicle by the project partners, the model was updated with the measured constants and the performance of the vehicle was reassessed. The vehicles range was extended to 2.5 $[h]$ with no RMFC system, a full working day, resulting in a drained battery, with a 5 $[kW]$ RMFC system and a full working day with a 10 $[kW]$ RMFC system with

a maintained battery State Of Charge (SOC). The expected fuel consumption of the RMFC system is 62.13 $[L]$ using the standard hysteresis SOC control of the RMFC modules.
Based on observations of the power losses in the vehicle model, a SOC controller for the drive battery of the vehicle was developed. Using this controller, the fuel consumption was lowered to 46.85 $[L]$, a reduction of 15.28 $[L]$, or 24.6%.

The controller developed in the vehicle model works on a $[kWh]$ basis and does not include the dynamics of the battery or the RMFC system. The controllable parameter in the H3 5000 and H3 350 systems which are used in this project, and in RMFC systems in general, is the fuel cell current and not the output power or current of the system. Most battery SOC predictors and controllers work in $[Ah]$. This means that if the prospective efficiency gains are to be realized, a controller which can control the output current of an RMFC system had to be developed. For this purpose a dynamic model of the relationship between the fuel cell current and output current of an H3 350 system is made, along with an equivalent circuit model of a lead acid battery which is scaled appropriately.
Model parameters where identified experimentally and a PI controller with feedforward and anti-windup which is capable of controlling the output current of the RMFC system was developed and tested in an experimental setup. It is concluded that it is possible to control the SOC of a battery using an RMFC system and thus achieve the related efficiency gains. A similar controller has not been observed in literature for an RMFC system.
In addition to the PI controller a Model Predictive Controller (MPC) was developed which was able control the output current better during steps in reference and during measured disturbances. It was not possible to test the MPC controller in the test setup, but based on simulations it is concluded that the MPC control structure could be a valuable addition to an RMFC system. This is especially the case if the system model is updated through an identification experiment during the start-up of the module.

A study was also made of the efficiency of an H3 350 system based on Adaptive Neuro-Fuzzy Inference System (ANFIS) models of the HTPEM fuel cell and the output gas of the reformer, all based on identification experiments. The inputs of the developed fuel cell model are the fuel cell temperature, anode CO concentration and current density and has an MAE of 0.94%. A similar model has not been observed in literature for a PEM fuel cell. The models of the H_2 mass flow model and the CO concentration has the fuel flow into the reformer and reformer temperature as inputs and MAEs of 0.074% and 0.0323%, respectively.
The subsequent analysis of the system efficiency showed that changing the reformer temperature from the present 290 to 252 $[^{\circ}C]$ improves the system efficiency by an average of 1.47 percentage points across fuel cell currents

and 4 percentage points at the maximum rated current. If this efficiency gain is added to the RMFC efficiency model in the developed model of a street sweeping machine, the fuel consumption of the vehicle is reduced by 4.6%. This brings the efficiency gain achieved in this project up to 28%.

2 Future Work

As with most other scientific investigations, the results of this PhD study leaves new opportunities for investigation. This section will describe some of them.

The ORACLE project has proven that an RMFC-powered street sweeping machine is technically feasible and that it has advantages compared with both the conventional diesel powered and the previously existing alternatively fueled street sweeping machines. If the advantages of the RMFC powered street sweeping machine is to be realized, more work has to be done on the energy optimization of the electrified vehicle, and the control system of the RMFC module has to be integrated with that of the street sweeping machine. The model developed in this work can be helpful in this regard.

The PI controller developed to controlled the output current has not been implemented in the ORACLE test vehicle and this still has to be done to test if the efficiency gains calculated in the vehicle model are actually achievable.

The fuel cell used in the identification experiments in Section 2 of Chapter 3 was in an advanced state of degradation, which affects the results of the modeling. This gives rise to the idea of including the state of degradation of the fuel cell as an input for the ANFIS model. This could either be as a number of operating hours or as the amount of energy that has been delivered in its lifetime.

The degradation of the reformer catalyst could be modeled in a similar fashion and the operating point optimization presented in Section 3 can be repeated and the recommendation for the optimal reformer temperature can be made degradation-dependent.

References

[1] M. J. Horowitz, P. Bertoldi, A harmonized calculation model for transforming {EU} bottom-up energy efficiency indicators into empirical estimates of policy impacts, Energy Economics 51 (2015) 135 – 148. doi:10.1016/j.eneco.2015.05.020.

[2] W. R. Grove, On the gas voltaic battery. experiments made with a view of ascertaining the rationale of its action and its application to eudiometry, Philosophical Transactions of the Royal Society of London.

[3] S. Dutta, A review on production, storage of hydrogen and its utilization as an energy resource, Journal of Industrial and Engineering Chemistry 20 (4) (2014) 1148 – 1156. doi:10.1016/j.jiec.2013.07.037.

[4] R. A. Antunes, M. C. de Oliveira, G. Ett, V. Ett, Carbon materials in composite bipolar plates for polymer electrolyte membrane fuel cells: A review of the main challenges to improve electrical performance, Journal of Power Sources 196 (6) (2011) 2945 – 2961. doi:10.1016/j.jpowsour.2010.12.041.

[5] A. Chandan, M. Hattenberger, A. El-kharouf, S. Du, A. Dhir, V. Self, B. G. Pollet, A. Ingram, W. Bujalski, High temperature (ht) polymer electrolyte membrane fuel cells (pemfc) – a review, Journal of Power Sources 231 (2013) 264 – 278. doi:10.1016/j.jpowsour.2012.11.126.

[6] J. Zhang, Z. Xie, J. Zhang, Y. Tang, C. Songa, T. Navessin, Z. Shi, D. Song, H. Wang, D. P. Wilkinson, Z.-S. Liu, S. Holdcroft, High temperature pem fuel cells, Journal of Power Sources 160 (2006) 872–891. doi:10.1016/j.jpowsour.2006.05.034.

[7] S. J. Andreasen, J. R. Vang, S. K. Kær, High temperature pem fuel cell performance characterisation with co and co2 using electrochemical impedance spectroscopy, International Journal of Hydrogen Energy 36 (2011) 9815–9830. doi:10.1016/j.ijhydene.2011.04.06.

[8] D. Chu, R. Jiang, Comparative studies of polymer electrolyte membrane fuel cell stack and single cell, Journal of Power Sources 80 (1–2) (1999) 226 – 234. doi:10.1016/S0378-7753(98)00263-8.

[9] D. Durbin, C. Malardier-Jugroot, Review of hydrogen storage techniques for on board vehicle applications, International Journal of Hydrogen Energy 38 (34) (2013) 14595 – 14617. doi:10.1016/j.ijhydene.2013.07.058.

[10] S. S. Kocha, J. Deliang Yang, J. S. Yi, Characterization of gas crossover and its implications in pem fuel cells, AIChE Journal 52 (5) (2006) 1916–1925. doi:10.1002/aic.10780.

[11] S. Yong, C. Ooi, S. Chai, X. Wu, Review of methanol reforming-cu-based catalysts, surface reaction mechanisms, and reaction schemes, International Journal of Hydrogen Energy 38 (22) (2013) 9541 – 9552. doi:10.1016/j.ijhydene.2013.03.023.

[12] S. S. Kurpit, 1.5 and 3kw indirect methanol-air fuel cell power plants, in: Energy 10; Annual Intersociety Energy Conversion and Engineering Conference, 1975.
URL http://adsabs.harvard.edu/abs/1975iece.conf..222K

[13] A. R. Korsgaard, M. A. P. Nielsen, M. Bang, S. K. Kær, Modeling of co influence in pbi electrolyte pem fuel cells, ASME 2006 4th International Conference on Fuel Cell Science, Engineering and Technologydoi:10.1115/FUELCELL2006-97214.

[14] S. J. Andreasen, S. K. K. Kær, Dynamic model of the high temperature proton exchange membrane fuel cell stack temperature, J. Fuel Cell Sci. Technol. – November 2009 – Volume 6, Issue 4, 041006 (8 pages).

[15] J. Contreras, J. Salmones, J. Colín-Luna, L. Nuño, B. Quintana, I. Córdova, B. Zeifert, C. Tapia, G. Fuentes, Catalysts for {H2} production using the ethanol steam reforming (a review), International Journal of Hydrogen Energy 39 (33) (2014) 18835 – 18853. doi:10.1016/j.ijhydene.2014.08.072.

[16] M. L. Faro, A. Stassi, V. Antonucci, V. Modafferi, P. Frontera, P. Antonucci, A. S. Aricò, Direct utilization of methanol in solid oxide fuel cells: An electrochemical and catalytic study, International Journal of Hydrogen Energy 36 (16) (2011) 9977 – 9986, european Fuel Cell 2009. doi:10.1016/j.ijhydene.2011.05.053.

[17] X. Li, A. Faghri, Review and advances of direct methanol fuel cells (dmfcs) part i: Design, fabrication, and testing with high concentration methanol solutions, Journal of Power Sources 226 (2013) 223 – 240. doi:10.1016/j.jpowsour.2012.10.061.

[18] Serenergy a/s home page,
http://www.serenergy.com/ (July 2015).

[19] Ultrahome llc homepage,
http://www.serenergy.com/ (July 2015).

[20] Ballard telecom backup power, http://www.ballard.com/fuel-cell-applications/backup-power.aspx (July 2015).

[21] Protonex homepage, http://www.protonex.com/products/m300/ (July 2015).

[22] T. Kim, Micro methanol reformer combined with a catalytic combustor for a {PEM} fuel cell, International Journal of Hydrogen Energy 34 (16) (2009) 6790 – 6798, 4th Dubrovnik Conference4th Dubrovnik Conference. doi:10.1016/j.ijhydene.2009.06.024.

[23] G. Arzamendi, P. Diéguez, M. Montes, M. Centeno, J. Odriozola, L. Gandía, Integration of methanol steam reforming and combustion in a microchannel reactor for {H2} production: A {CFD} simulation study, Catalysis Today 143 (1–2) (2009) 25 – 31, international Symposium on Catalysis for Clean Energy and Sustainable Chemistry, on occasion of the 60th birthday of Prof. Jose L.G. Fierro. doi:10.1016/j.cattod.2008.09.034.

[24] J. Andersen, M. P. Ehmsen, K. K. Justesen, Feedforward control for a reformed methanol fuel cell system, Master thesis, Aalborg University (2012).

[25] Y. Vural, D. B. Ingham, M. Pourkashanian, Performance prediction of a proton exchange membrane fuel cell using the anfis model, International journal of hydrogen energy 34 (2009) 9181–9187. doi:10.1016/j.ijhydene.2009.08.096.

[26] R. Silva, R. Gouriveau, S. Jemei, D. Hissel, L. Boulon, K. Agbossou, N. Y. Steiner, Proton exchange membrane fuel cell degradation prediction based on adaptive neuro-fuzzy inference systems, International Journal of Hydrogen Energy 39 (21) (2014) 11128 – 11144. doi:10.1016/j.ijhydene.2014.05.005.

[27] K. Kim, M. R. von Spakovsky, M. Wang, D. J. Nelson, A hybrid multilevel optimization approach for the dynamic synthesis/design and operation/control under uncertainty of a fuel cell system, Energy 36 (6) (2011) 3933 – 3943, {ECOS} 2009. doi:10.1016/j.energy.2010.08.024.

[28] H. Cao, X. Li, Z. Deng, J. Li, Y. Qin, Thermal management oriented steady state analysis and optimization of a kw scale solid oxide fuel cell stand-alone system for maximum system efficiency, International Journal of Hydrogen Energy 38 (28) (2013) 12404 – 12417. doi:10.1016/j.ijhydene.2013.07.052.

[29] J. Wishart, Z. Dong, M. Secanell, Optimization of a {PEM} fuel cell system based on empirical data and a generalized electrochemical semi-empirical model, Journal of Power Sources 161 (2) (2006) 1041 – 1055. doi:10.1016/j.jpowsour.2006.05.056.

[30] C. Bordons, M. A. Ridao, A. Perez, A. Arce, D. Marcos, Model predictive control for power management in hybrid fuel cell vehicles, Vehicle Power and Propulsion Conference IEEEdoi:10.1109/VPPC.2010.5729119.

[31] S. Walter, S. Ulli-Beer, A. Wokaun, Assessing customer preferences for hydrogen-powered street sweepers: A choice experiment, International Journal of Hydrogen Energy 37 (16) (2012) 12003 – 12014. doi:10.1016/j.ijhydene.2012.05.026.

[32] P. Power, Plug power home page, http://www.plugpower.com/Customers.aspx (2012).

[33] Tennant, Tennant home page, http://www.tennantco.com/apac-en/pages/ProductDetails.aspx?item=500ze (2012).

[34] P. Schlienger, C. B. F. Büchi, Hydrogen driven municipal vehicle (hy.muve) vehicle concept demonstration and field testing in switzerland, 18th World Hydrogen Energy Conference 2010 - WHEC 2010 Parallel Sessions Book 6: Stationary Applications / Transportation Applications Proceedings of the WHEC, May 16.-21. 2010, Essen Schriften des Forschungszentrums J"ulich / Energy & Environment, 78-6 (2010) 126–131.

[35] Nilfisk, Nilfisk outdoor division home page, http://www.nilfisk-outdoor.com/ (2015).

[36] T. J. Schmidt, J. Baurmeister, Properties of high-temperature pefc celtec-p 1000 meas in start/stop operation mode, Journal of Power Sources 176 (2) (2008) 428 – 434, selected Papers presented at the10th {ULM} ElectroChemical Days W. Tillmetz, J. Lindenmayer 10th Ulm ElectroChemical Days. doi:10.1016/j.jpowsour.2007.08.055.

[37] MathWorks, Model Predictive Control Toolbox (July 2015). URL http://se.mathworks.com/help/mpc/

[38] J.-S. R. Jang, Anfis: Adaptive-network-based fuzzy inference system, IEEE Transactions on Systems, Man, and Cybernetics 23 (1993) 665–685. doi:10.1109/21.256541.

[39] J. Zhang, Z. Xie, J. Zhang, Y. Tang, C. Song, T. Navessin, Z. Shi, D. Song, H. Wang, D. P. Wilkinson, Z.-S. Liu, S. Holdcroft, High temperature pem fuel cells, Journal of Power Sources 160 (2) (2006) 872 – 891, special issue

including selected papers presented at the International Workshop on Molten Carbonate Fuel Cells and Related Science and Technology 2005 together with regular papers. doi:10.1016/j.jpowsour.2006.05.034.

[40] S. K. Das, A. Reis, K. Berry, Experimental evaluation of {CO} poisoning on the performance of a high temperature proton exchange membrane fuel cell, Journal of Power Sources 193 (2) (2009) 691 – 698. doi:10.1016/j.jpowsour.2009.04.021.

[41] S. J. Andreasen, S. K. Kær, S. L. Sahlin, Control and experimental characterization of a methanol reformer for a 350 w high temperature polymer electrolyte membrane fuel cell system, International Journal of Hydrogen Energy 38 (3) (2013) 1676 – 1684, 2011 Zing International Hydrogen and Fuel Cells Conference: from Nanomaterials to Demonstrators. doi:10.1016/j.ijhydene.2012.09.032.

[42] D. Hammoud, C. Gennequin, A. Aboukais, E. A. Aad, Steam reforming of methanol over xPreparation by adopting memory effect of hydrotalcite and behavior evaluation, International Journal of Hydrogen Energy 40 (2) (2015) 1283 – 1297. doi:10.1016/j.ijhydene.2014.09.080.

[43] R. Dagle, A. Platon, D. Palo, A. Datye, J. Vohs, Y. Wang, Pdznal catalysts for the reactions of water-gas-shift, methanol steam reforming, and reverse-water-gas-shift, Applied Catalysis A: General 342 (1 - 2) (2008) 63 – 68. doi:10.1016/j.apcata.2008.03.005.

Part II

Papers

Paper A

Gas composition modeling in a reformed Methanol Fuel Cell system using adaptive Neuro-Fuzzy Inference Systems

Kristian Kjær Justesen, Søren Juhl Andreasen,
Hamid Reza Shaker, Mikkel Præstholm Ehmsen,
John Andersen

The paper has been published in the
International Journal of Hydrogen Energy Vol. 38, pp. 10577–10584, 2013.

Paper B

Dynamic Modeling of a Reformed Methanol Fuel Cell System Using Empirical Data and Adaptive Neuro-Fuzzy Inference System Models

Kristian Kjær Justesen, Søren Juhl Andreasen,
Hamid Reza Shaker

The paper has been published in the
Journal of Fuel Cell Science and Technology Vol. 11 pp. 021004-1–021004-8, 2014.

Paper C

Modeling and control of the output current of a Reformed Methanol Fuel Cell system

Kristian Kjær Justesen, Søren Juhl Andreasen,
Sivakumar Pasupathi, Bruno G. Pollet

The paper has been published in the
International Journal of Hydrogen Energy

Paper D

Modeling of a HTPEM Fuel Cell using Adaptive Neuro-Fuzzy Inference Systems

Kristian Kjær Justesen, Søren Juhl Andreasen,
Simon Lennart Sahlin

The paper has been published in the
Special section CARISMA2014, International Journal of Hydrogen Energy

Paper E

Determination of Optimal Reformer Temperature in a Reformed Methanol Fuel Cell System using ANFIS Models and Numerical Optimization Methods

Kristian Kjær Justesen, Søren Juhl Andreasen

The paper is published in the
International Journal of Hydrogen Energy Vol. 40, pp. 9505–9514, 2015.

Part III

Posters

Poster A

Control of a methanol reformer system using an Adaptive Neuro-Fuzzy Inference System approach

Kristian K. Justesen, John Andersen, Mikkel P. Ehmsen, Søren J. Andreasen, Hamid R. Shaker and Simon L. Sahlin

The poster has been presented at the
Carisma 2012 Conference in Copenhagen
where it won the 2nd Poster Prize

Control of a methanol reformer system using an Adaptive Neuro-Fuzzy Inference System approach

Kristian K. Justesen*, John Andersen, Mikkel P. Ehmsen, Søren J. Andreasen, Hamid R. Shaker and Simon L. Sahlin

Department of Energy Technology, Aalborg University, Pontoppidanstræde 101, 9220 Aalborg East, Denmark

Introduction

This work presents a stoichiometry control strategy for a reformed methanol fuel cell system, which uses a reformer to produce hydrogen for an HTPEM fuel cell. One such system is the Serenus H3-350 battery charger developed by the Danish company Serenegy® which this work is based on. Figure 1 shows a picture of the system.

Figure 1: The Serenus H3-350 Reformed Methanol Fuel Cell system produced by Serenergy®.

Figure 2 shows a block diagram of the layout of the system.

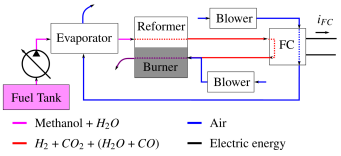

Figure 2: Diagram of the Serenus H3-350 Reformed Methanol Fuel Cell system produced by Serenergy®.

To avoid starving the fuel cell of hydrogen, it is important to know how much hydrogen is produced at any given time.
It is not practical to measure the hydrogen production online and the standard control system of the H3-350 system assumes full reformation. However, the degree of reformation varies with the reformer temperature and the fuel flow. The stoichiometry set point is therefore set to 1.5, which is a safe distance from the recommended minimum of 1.15. This means that more methanol than necessary is consumed in some operating points and the stoichiometry approaches the minimum limit in others.
The reformed gas composition can be calculated with some accuracy if the temperature of the reformer bed is known exactly. This is, however, not the case here as the temperature measurement in the reformer is placed in the bulk material next to the bed and not in the bed itself. Figure 3 shows an illustration of this issue.

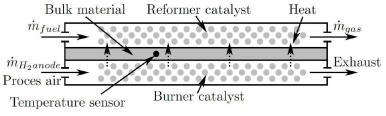

Figure 3: Concept drawing of the reformer and burner of the Serenus H3-350.

This means that as the flow is increased, the reformer bed is cooled, the temperature gradient between the burner and the reformer bed becomes steeper, and the temperature measurement becomes unreliable.

Modeling

This work proposes a method which uses Adaptive Neuro-Fuzzy Inference Systems, ANFIS, trained on experimental data to predict the reformed gas composition. ANFIS is a neuro-fuzzy modeling approach which uses linguistic variables and parameters which are trained using a neural network to mimic the behavior of a physical system. Arbitrary precision can be achieved by increasing the complexity of the models. The ANFIS function in MATLAB is used to train the ANFIS models in this work. Figure 4 shows the ANFIS structure.

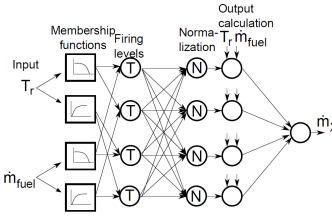

Figure 4: ANFIS model structure with two membership functions. T marks the use of a T-norm and N marks the normalization of the firing levels.

Models of the H_2, CO_2, CO and methanol slip have been developed but here only the hydrogen model is of interest.
The identification experiments have been performed on a test setup where the fuel cell is replaced with a gas analyzer. Figure 5 shows the temperatures and pump flows used in the identification experiment as well as the resulting hydrogen mass flow and the ANFIS model fit.

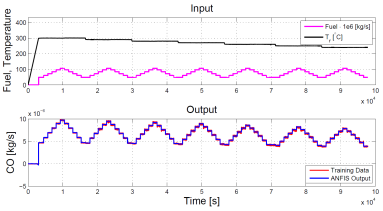

Figure 5: Output of the ANFIS model for the hydrogen content in the reformed gas. Inputs are reformer temperature, T_r, and the fuel flow.

The ANFIS model shows good correlation with the measurements and the model is therefore deemed to be valid. Figure 6 shows the stoichiometry calculated using full reformation and the ANFIS model during a series of load changes.

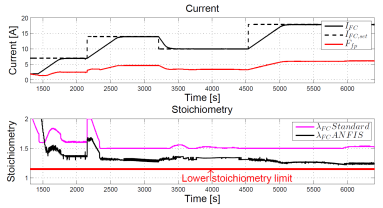

Figure 6: Observed fuel cell stoichiometry during a series of load changes.

The actual stoichiometry is very different from the one which is assumed using full reformation and approaches the lower stoichiometry at higher currents.

Control

The method proposed in this work is based on an ANFIS model which is the reverse of the one in Figure 5. This means that it is trained with the hydrogen production and the reformer temperature as inputs and the fuel flow as output.
The necessary hydrogen production at a certain fuel cell current and stoichiometry set point is calculated online and fed to the ANFIS model as illustrated in Figure 7.

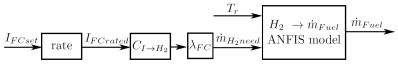

Figure 7: Block diagram of the ANFIS fuel predictor. *rate* is a rate limiter which ensures time for the reformed gas to spread in the system. λ_{FC} is the desired fuel cell stoichiometry and $C_{I\to H_2}$ converts the fuel cell current set point to an equivalent hydrogen mass flow.

This algorithm is implemented in a LabVIEW program and tested on a Serenus H3-350 module. The load pattern used in the experiment is shown in Figure 8 together with the stoichiometry measured during the experiment.
The stoichiometry set point is 1.25 during the experiment, which is a safe distance from the lower limit of 1.15.
The stoichiometry is kept constant during the load changes but the measurement is subject to noise from the temperature measurement.

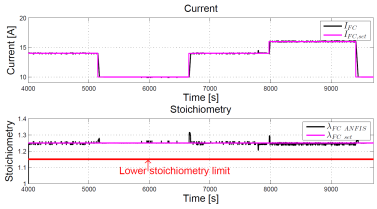

Figure 8: Observed fuel cell stoichiometry during a series of load changes.

The stoichiometry shown in figure 8 is calculated using an ANFIS model which is based on the same data as the predictor. This is a general problem in this kind of system. To give another indication of the validity of the method, the fuel cell voltage during a load change is plotted in Figure 9.

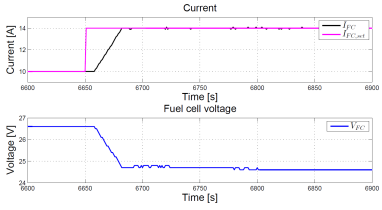

Figure 9: Fuel cell voltage during a load change

If a fuel cell is starved of hydrogen, the voltage will drop. There is no sign of this happening in this case.
The efficiency from the higher heating value system efficiency is plotted in Table 1.

Current [A]	Relative change %
10	+20.2
14	+7.1
16	-6.8

Table 1: Higher heating value to electricity efficiency at different fuel cell currents

The efficiency is higher at both 10 and 14 [A] using the ANFIS predictor. This is because the fuel flow is lower at these operating points using the ANFIS predictors than with the standard controller. The opposite is the case at 16 [A] but here the stoichiometry using the standard control is dropping towards the lower stoichiometry limit.

Conclusion

In this work the problem of controlling the stoichiometry of a Reformed Methanol Fuel Cell system is presented and a solution based on an ANFIS model is proposed. The ANFIS models are trained using experimental data obtained using a gas analyzer. The method has been tested experimentally in a Serenus H3-350 module. The method is capable of controlling the fuel cell anode stoichiometry both in steady state and during transients.
The efficiency at the lower operating points is higher using the ANFIS fuel predictor but it is lower at the high operating point because of the higher constant stoichiometry

Future Work

The ANFIS models can be improved by performing long term gas measurements and including reformer catalyst degradation as an input.
Models of the mass flow of CO_2, CO and the methanol which passes unreformed through the reformer have also been developed and used in a dynamic model of the Serenus H3-350 module.
These models could also be incorporated in a diagnostic system in connection with a fuel cell model to catch incipient faults before the system is harmed.

www.et.aau.dk *kju@et.aau.dk

Poster B

Initial Performance Analysis of a Methanol Steam Reformer

Kristian Kjær Justesen

The poster has been presented at the
European Technical School on Hydrogen and Fuel Cells 2014

Initial Performance Analysis of a Methanol Steam Reformer

Kristian Kjær Justesen

Dept. of Energy Technology, Aalborg University, Denmark

kju@et.aau.dk

AALBORG UNIVERSITY
DENMARK

AALBORG UNIVERSITY
DENMARK

Introduction

PEM Fuel Cells are receiving increasing attention because of their ability to provide electricity from a fuel without harmful emissions. It is, however, difficult and energy consuming to store and transport gaseous hydrogen for fuel. It is therefore of interest to use a liquid fuel as a carrier for the hydrogen.

One suitable fuel is methanol (CH_3OH) which can be reformed, using the steam reforming process, into primarily hydrogen (H_2) and carbon dioxide (CO_2) according to **[1]**:

$$CH_3OH + H_2O \rightarrow 3H_2 + CO_2$$

The Danish company Serenergy® makes an integrated 350 W HTPEM fuel cell and reformer module called the Serenus H3 350. **Figure 1** shows a picture of this module.

Figure 1: Picture of a Serenus H3 350 module from Serenergy ® **[2]**.

The module consists of a fuel tank, which holds a mixture of methanol and water. An evaporator, which is powered by the excess heat from the fuel cell, reform gas and system exhaust. A reformer, where the steam reforming process takes place. A high temperature PEM fuel cell, where about 75% of the H_2 in the fuel used to produce electricity. The remaining H_2 is passed to a burner, which supplies the process heat for the reformer. **Figure 2** shows a concept diagram of the H3 350 module.

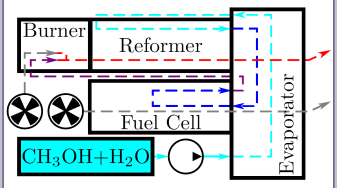

Figure 2: Concept diagram of a Serenus H3 350 system from Serenergy ®. Cyan lines are the fuel, blue lines are the reformed gas, purple lines are the anode exhaust and red is the exhaust.

As well as the steam reforming process , two other reactions take place in the reformer. One is the methanol decomposition process:

$$CH_3OH \rightarrow 2H_2 + CO$$

Which has the undesirable property, that it adds carbon monoxide (CO) to the reform gas. The other reaction is the water gas shift, which removes some of the CO from the gas:

$$CO + H_2O \rightarrow H_2 + CO_2$$

CO is harmful to the efficiency and durability of PEM fuel cells and it is therefore interesting to investigate, how much CO is produced under different operating conditions.

When a fuel cell is operated on reform gas, there has to be a constant flow of fuel through the fuel cell and a certain H_2 over stoichiometry. It is therefore also interesting to investigate how much of the methanol in the fuel is actually reformed into H_2.

The focus of this work is therefore to make a series of identification experiments that can serve as a guide when modeling and operating the H3 350 module.

Results

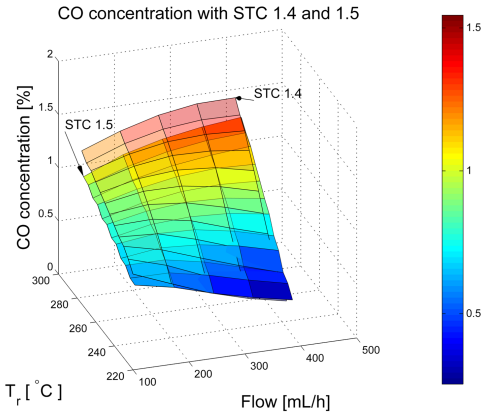

Figure 4: Surface plot of the CO concentration in the experiment.

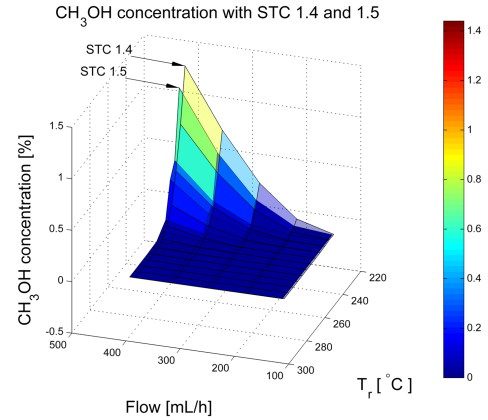

Figure 5: Surface plot of the CH_3OH concentration in the experiment.

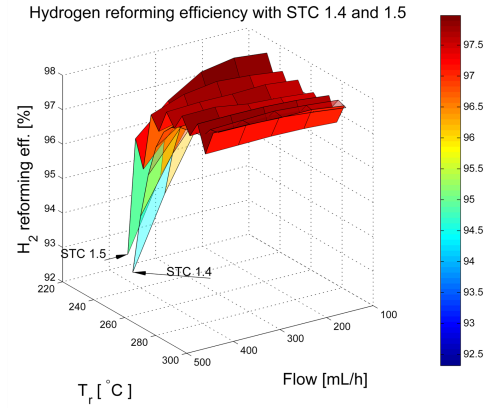

Figure 6: Surface plot of the H_2 reforming efficiency in the experiment.

Made for:

H_2FC

European Technical School on Hydrogen and Fuel Cells 2014

Experiment

For the experiment, the fuel cell in a H3 350 module is replaced with a gas analyzer, which can measure the percentage of H_2, CO_2, CO and methanol in the reformed gas.

The fuel cell cathode air for the evaporator is now supplied by a mass flow controller and a heater, which mimics the air flow at the active operating point.

The fuel cell anode exhaust, which supplies H_2 for the burner, is replaced with a mass flow controller. **Figure 3** shows this setup.

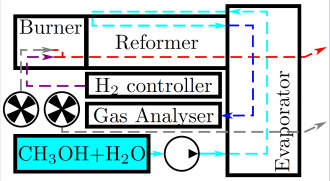

Figure 3: Concept diagram of the experimental setup.

It is chosen to evaluate the reformers performance at operating points corresponding to a fuel cell current of 5, 7.5, 10.5, 13.25, and 16 A which spans the rated operating range. An anode stoichiometry of 1.35 is chosen on the recommendation of the manufacturer. The experiment is repeated for reformer temperatures between 235 and 285 °C in 5 degree steps. the setup is left in steady state for 30 minutes for each step.

The experiment is done with two different methanol/water relationships, also called steam to carbon ration (STC). First STC 1.5 and then STC 1.4.

After the experiment the average value of the gas composition is calculated for each operating point.

Figure 4 shows the concentration of carbon monoxide in % of the volume flow. **Figure 5** shows the methanol slip in % of the volume flow. **Figure 6** shows the calculated H_2 reforming efficiency in % of full and perfect reforming.

Discussion and future work

Figure 4 shows that higher reformer temperature gives a higher CO concentration and that a higher STC gives a lower CO concentration.

Figure 5 shows that a lower reformer temperature gives a higher methanol slip at large flows. And that the methanol slip is smaller with STC 1.5. This tendency is mirror by the hydrogen reforming efficiency in **Figure 6** where low temperatures and high flow gives a low efficiency.

This means that there will be an optimal operating temperature, which is dependent on the fuel flow. This temperature can be calculated on the basis of these experiments.

The experiments will also be used to develop models of the gas composition, which can be used in a dynamic model of the entire module as in **[3]** and **[4]** or be used online to ensure that the minimum anode stoichiometry is met.

Long term experiments which will include catalyst degradation are underway, as well as an experiment with STC 1.6, to see if the positive tendency with increasing STC continues.

References

[1] J.C. Amphlett et al. Hydrogen production by steam reforming of methanol for polymer electrolyte fuel cells. . International Journal of Hydrogen Energy 19 Issue 2 (1994) 131 - 137

[2] Serengy A/S. www.serenergy.com

[3] Justesen et al. Gas composition modeling in a reformed Methanol Fuel Cell system using adaptive Neuro-Fuzzy Inference Systems. International Journal of Hydrogen Energy 38 (2013) 10577 - 10584

[4] Justesen et al. Dynamic Modeling of a Reformed Methanol Fuel Cell System Using Empirical Data and Adaptive Neuro-Fuzzy Inference System Models. JOURNAL OFFUEL CELL SCIENCE AND TECHNOLOGY 11(2)

Poster C

Modeling of a HTPEM Fuel Cell using Adaptive Neuro-Fuzzy Inference Systems

Kristian Kjær Justesen, Søren Juhl Andreasen, Simon Lennart Sahlin

The poster has been presented at the
Carisma 2014 Conference in Cape Town

Modeling of a HTPEM Fuel Cell using Adaptive Neuro-Fuzzy Inference Systems

Kristian Kjær Justesen* - Søren Juhl Andreasen - Simon Lennart Sahlin

Dept. of Energy Technology, Aalborg University, Denmark

*kju@et.aau.dk

AALBORG UNIVERSITY
DENMARK

AALBORG UNIVERSITY
DENMARK

Introduction

HTPEM fuel cells can with great benefit be used in systems with fuel reformers, because they have a high tolerance towards carbon monoxide in the anode gas. Their performance is, however, affected by the presence of carbon monoxide. This effect is dependent on the fuel cell temperature, with the effect being smaller at high temperatures and larger at low temperatures. It is important to model this effect, when choosing optimal operating points for the fuel cell and fuel reformer, or constructing larger system models.

It can, however, be difficult to construct simple, fast evaluating models of the fuel cells performance, which works on a specific fuel cell, at a certain state of degradation. This work presents a method to do this, based on Adaptive Neuro-Fuzzy Inference Systems (ANFIS) trained on experimental data[1].

In this case the factors which are expected to influence the fuel cell voltage are the fuel cell temperature, the CO content of the anode gas and the fuel cell current density. Figure 1 shows a diagram of the ANFIS model structure employed in this work.

The model structure is split up into 5 layers. The first layer is the fuzzyfication layer, where the inputs are converted to fuzzy variables, which are numbers between 0 and 1. The conversion is done using a series of membership functions. Here the output of the membership functions can be interpreted as "to which degree are the inputs high or low." The membership functions used in this work are bell-shaped. These are used because they give smooth transition between functions. The equation for the first of the six membership functions in figure 1 is:

$$O_{1,i} = \frac{1}{1 + \left| \frac{T_{FC} - c_i}{a_i} \right|^{2b_i}}$$

Here $O_{1,i}$ is the degree of membership, the subscript i is the function number and a_i, b_i and c_i are adaptive premise parameters, which are optimized using gradient decent methods during the training of the system. More membership functions increases the ability to model non-linear systems, but also increases complexity and calculation time.

The next layer contains the calculation of the firing levels of the fuzzy rules, each represented by a circle called a node or a neuron. For the top rule firing level means: To which degree is T_{FC} AND x_{CO} AND I_{FC} high.

The next layer is the normalization layer. Here the sum of the firing levels of all the rules is normalized to be 1.

The second to last layer contains the output calculation, where the contribution of each rule to the output of the model is calculated. This is done using this equation.

$$O_{3,i} = \bar{w}_i \cdot (o_i \cdot T_{FC} + p_i \cdot x_{CO} + q_i \cdot I_{FC} + r_i)$$

Where $\bar{w}_i$is the normalized firing level of the rule and o_i, p_i, q_i and r_i are adaptive consequent parameters optimized using least squares regression during the training of the system.

The last layer contains the summation of the contributions.

Results

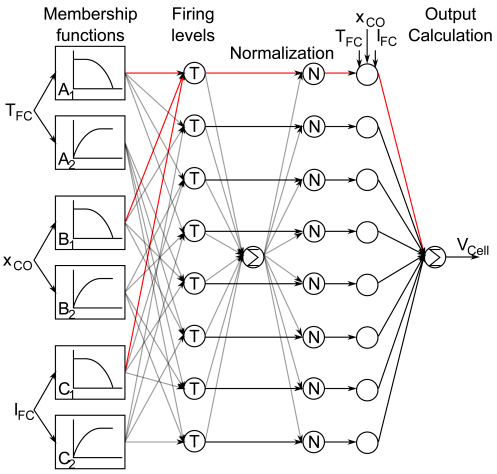

Figure 1: Diagram of the ANFIS structure used in this work.

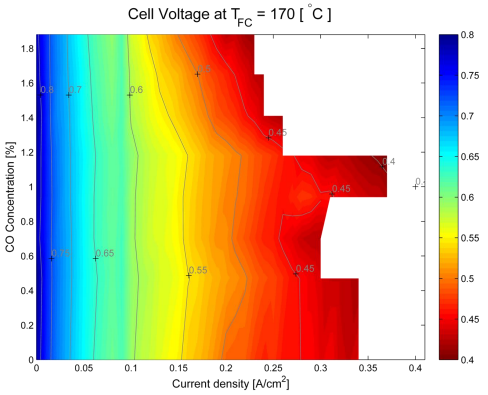

Figure 2: Surface plot of the fuel cell voltage in the experiment.

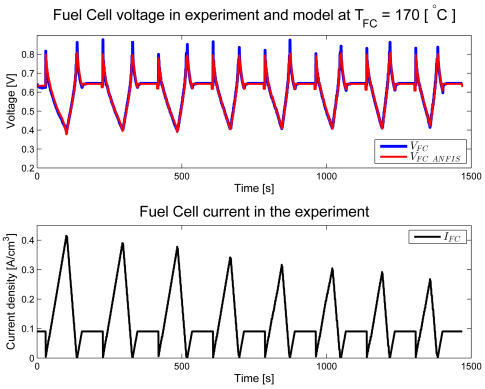

Figure 3: Plot of the fuel cell voltage and current in experiment and model.

Made for:

CARISMA2014
CAPE TOWN, SOUTH AFRICA | 2014

Experiment

To be able to train the ANFIS model it is necessary to have an identification experiment, which spans the likely operating range of the fuel cell. In this work, a 14 cell stack, which is a shortened version of a Serenergy S 165L-25, is used. The cell is in an advanced state of degradation, but this doesn't prevent a proof of concept. Figure 4 shows a picture of this fuel cell stack.

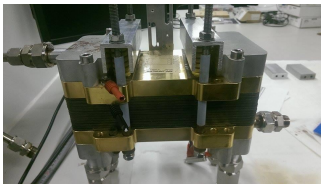

Figure 4: Picture of the fuel cell stack used in this work.

The fuel cell stack is mounted in a Greenlight G200 test station, which can supply an anode gas of the desired composition and temperature as well as the cooling oil, which controls the temperature of the fuel cell.

The maximum expected CO concentration, based on reformer experiments, is 1.9 % so the experiment is performed at 8 equally spaced concentrations from 0 to 1.9. The maximum rated current density is 0.6 $[A/cm^2]$ and the minimum allowable cell voltage is 0.4 $[V]$. The stop condition for the experiment will be that of these parameters, which is reached first. The experiment is performed for fuel cell temperatures of 160, 165 and 170 [°C].

Results and conclusion

A surface plot of the fuel cell voltage at a fuel cell temperature of 170 [°C], which is representative of the other temperatures, can be seen in Figure 2. This shows, that at higher current densities the CO concentration has a larger influence than at low concentrations.

The ANFIS models are trained in Matlab and the optimal number of membership functions is found to be 2, which gives a mean absolute error of 0.9%. Adding further complexity to the model is found to give no significant advantage.

Figure 3 shows the fuel cell voltage at a fuel cell temperature of 170 [°C] from the experiment and the model, as well as the current density. Again this plot is representative of the performance at 160 and 165 [°C].

It is concluded that a model of this type can be precise and useful for system optimization and modeling

Future work

To extend the usefulness of the model degradation in the form of the number of operating hours of the fuel cell could be added to the model.

References

[1] Roger Jang Jyh-Sing. ANFIS: adaptive-network-based fuzzy inference system. IEEE Transactions on Systems, Man, and Cybernetics 1993;23:665e85.